Discovery of a Potent Dual Inhibitor of Acetylcholinesterase and Butyrylcholinesterase with Antioxidant Activity that Alleviates Alzheimer-like Pathology in Old APP/PS1 Mice

Discovery of a potent dual inhibitor of acetylcholinesterase and butyrylcholinesterase with antioxidant activity that alleviates Alzheimer-like pathology in old APP/PS1 mice

Elisabet Viayna,[1,▽] Nicolas Coquelle,[2,3▽] Monika Cieslikiewicz-Bouet,[4] Pedro Cisternas,[5] Carolina A. Oliva,[5] Elena Sánchez-López,[6,7] Miren Ettcheto,[7,8,9] Manuela Bartolini,[10] Angela De Simone,[11] Mattia Ricchini,[1] Marisa Rendina,[1] Mégane Pons,[4] Omidreza Firuzi,[12] Belén Pérez,[13] Luciano Saso,[14] Vincenza Andrisano,[15] Florian Nachon,[16] Xavier Brazzolotto,[16] Maria Luisa García,[6,7] Antoni Camins,[7,8] Israel Silman,[17] Ludovic Jean,[4] Nibaldo C. Inestrosa,[,5,18] Jacques-Philippe Colletier,*[,2] Pierre-Yves Renard,*[,4] and Diego Muñoz-Torrero*[,1]*

[1] Laboratory of Medicinal Chemistry (CSIC Associated Unit), Faculty of Pharmacy and Food Sciences, and Institute of Biomedicine (IBUB), University of Barcelona, Av. Joan XXIII 27-31, E-08028, Barcelona, Spain

[2] Institut de Biologie Structurale, Université Grenoble Alpes, CEA, CNRS UMR 5075, F-38054 Grenoble, France

[3] Large Scale Structures Group, Institut Laue-Langevin, F-38042 Grenoble Cedex 9, France

[4] Normandie University, UNIROUEN, INSA Rouen, CNRS, COBRA (UMR 6014), 76000 Rouen, France

[5] Center of Aging and Regeneration UC (CARE-UC), Departamento de Biología Celular y Molecular, Facultad de Ciencias Biológicas, Pontificia Universidad Católica de Chile, Av. Libertador Bernardo O'Higgins 340, P.O. Box 114, 8331150-Santiago, Chile

[6] Department of Pharmacy, Pharmaceutical Technology and Physical Chemistry, Faculty of Pharmacy and Food Sciences, and Institute of Nanoscience and Nanotechnology (IN2UB), University of Barcelona, Av. Joan XXIII 27-31, E-08028, Barcelona, Spain

[7] Biomedical Research Networking Centre in Neurodegenerative Diseases (CIBERNED), Institute of Health Carlos III, E-28031, Madrid, Spain

[8] Department of Pharmacology, Toxicology and Therapeutic Chemistry, Faculty of Pharmacy and Food Sciences, and Institute of Neuroscience, University of Barcelona, Av. Joan XXIII 27-31, E-08028, Barcelona, Spain

[9] Department of Biochemistry and Biotechnology, Faculty of Medicine and Health Sciences, University Rovira i Virgili, E-43201, Reus, Spain

[10] Department of Pharmacy and Biotechnology, Alma Mater Studiorum University of Bologna, Via Belmeloro 6, I-40126, Bologna, Italy

[11] Department of Drug Science and Technology, University of Turin, I-10125 Torino, Italy

[12] Medicinal and Natural Products Chemistry Research Center, Shiraz University of Medical Sciences, PO Box 3288, 71345 Shiraz, Iran

[13] Department of Pharmacology, Therapeutics and Toxicology, Autonomous University of Barcelona, E-08193, Bellaterra, Barcelona, Spain

[14] Department of Physiology and Pharmacology “Vittorio Erspamer”, Sapienza University of Rome, P.le Aldo Moro 5, 00185 Rome, Italy

[15] Department for Life Quality Studies, University of Bologna, Corso d’Augusto 237, I-47921-Rimini, Italy

[16] Département de Toxicologie et Risques Chimiques, Institut de Recherche Biomédicale des Armées BP73, 91993 Brétigny sur Orge, France

[17] Department of Neurobiology, Weizmann Institute of Science, 76100 Rehovot, Israel

[18] Centro de Excelencia en Biomedicina de Magallanes (CEBIMA), Universidad de Magallanes, 6200000 Punta Arenas, Chile

ABSTRACT: Combination of the scaffolds of the cholinesterase inhibitor huprine Y and the antioxidant capsaicin results in compounds with nanomolar potencies toward human acetylcholinesterase (AChE) and butyrylcholinesterase (BChE) that retain or improve the antioxidant properties of capsaicin. Crystal structures of their complexes with AChE and BChE revealed the molecular basis for their high potency. Brain penetration was confirmed by biodistribution studies in C57BL6 mice, with one compound (**5i**) displaying better brain/plasma ratio than donepezil. Chronic treatment of 10 month-old APP/PS1 mice with **5i** (2 mg/kg, ip, 3 times per week, 4 weeks) rescued learning and memory impairments, as measured by 3 different behavioral tests, delayed the Alzheimer-like pathology progression, as suggested by a significantly reduced Aβ42/Aβ40 ratio in hippocampus, improved basal synaptic efficacy, and significantly reduced hippocampal oxidative stress and neuroinflammation. Compound **5i** emerges as an interesting anti-Alzheimer lead with beneficial effects on cognitive symptoms and on some underlying disease mechanisms.

INTRODUCTION

Alzheimer's disease (AD) is the most common form of senile dementia. Its efficient management remains one of our most urgent unmet medical needs due to its ever-increasing prevalence, mortality, and economic burden.[1] The two main histopathological hallmarks of AD are the intra- and extra-cellular deposition of the microtubule-associated protein tau and of the β-amyloid peptide (Aβ), into paired helical filaments (PHFs) and amyloid plaques, respectively. Oxidative stress has been also suggested to play a pivotal role in the early stages of AD,[2] as it increases deposition of both Aβ and tau.[3] Accordingly, a number of efforts to curb the progression of AD have focused on the development of drugs reducing oxidative stress, clearing toxic Aβ fibrils and oligomers, or inhibiting the enzyme β-secretase (BACE-1), the first of two enzymes involved in the proteolytic cleavage of the amyloid precursor protein (APP) leading to Aβ production.[4,5] Recent failures of these drug candidates in late-stage clinical trials[1,4,6] have led to the hypothesis that that neither Aβ production and deposition[7] nor oxidative stress[8] should be taken as individual targets. Rather, action on a given target should be combined with further action on other key targets in AD.

The current therapeutic arsenal against AD comprises four drugs that ameliorate the symptoms and decrease the rate of cognitive decline, for a period of 6–12 months, but none of these are disease-modifying agents. One of these drugs antagonizes the glutamate NMDA receptor, while the others compensate for the central cholinergic deficit of AD patients by inhibiting brain acetylcholinesterase (AChE).[9] AChE, the enzyme that catalyses the breakdown of acetylcholine (ACh) in the central (CNS) and peripheral nervous systems, is characterized by a 20-Å deep gorge near the bottom of which sits the catalytic triad (Ser200–His440–Glu327, *Torpedo californica* AChE (*Tc*AChE) numbering), flanked by choline- and acyl-binding pockets. The

decreased ACh levels in the brains of AD patients that arise as a consequence of a marked decline in the cholinergic system in regions in charge of cognitive functions (e.g., the enthorhinal cortex and the temporal lobe) provides the rationale underlying the use of AChE inhibitors in the symptomatic treatment of AD. Moreover, both PHFs[10] and neuritic plaques[11] display strong cholinesterase activity, stemming from the presence of AChE and its close homologue, butyrylcholinesterase (BChE). AChE brain levels remain at best constant during the progression of AD,[12] while BChE activity increases by 180% and also locates in neuritic plaques.[13] The presence of cholinesterases (ChEs) in the plaques renders the latter more cytotoxic,[14] but the underlying mechanism of this increased toxicity remains uncertain. It was shown that AChE accelerates the deposition of Aβ,[15] by a mechanism involving a tryptophan residue located in its peripheral anionic site (PAS)[16] (Trp279 and Trp286 in *Tc*AChE and human AChE (hAChE), respectively) and the formation of a stable complex that is more toxic to neurons.[14] Hence, many efforts to develop anticholinesterase agents for AD therapy have focused on dual binding site AChE inhibitors,[17] spanning the active site gorge and interacting at both the catalytic anionic site (CAS) and the PAS, in order to inhibit both ACh hydrolysis and AChE-induced Aβ-aggregation. The fact that BChE activity is characteristic of neuritic plaques and increases with disease progression has prompted the re-examination of the candidacy of BChE as a valuable target or co-target for the treatment of AD, which shares the same overall fold of AChE (including a 20-Å deep active-site gorge), but lacks a tryptophan at the PAS.[18] Highly potent selective inhibitors that specifically target either AChE or BChE are available,[19–21] but molecules that target both enzymes with similar high efficacy are scarce,[22,23] due to differences in the architectures of their active-site gorges.[24] Such molecules would be highly desirable, since they could tackle, from the very outset, the progressive increase in BChE activity in the brains of AD patients, while

efficiently inhibiting AChE. Although inadequate in many respects, inhibition of the ChEs remains one of the very few means of transiently delaying AD progression.

A possible way to extend the therapeutic range of ChE inhibitors, thereby producing a more significant reduction in AD symptoms, is to combine their anticholinesterase action with other activities within a single drug molecule, thus generating multi-target directed ligands (MTDL), which feature a number of advantages over drug combinations, such as the lack of drug–drug interactions and simpler development, manufacturing, and intellectual property issues, among others.[25–28] Such compounds should not only inhibit ChE activity, but also promote other actions, such as inhibition of Aβ production (*e.g.*, through inhibition of BACE-1) and self-aggregation, or antioxidant activities.[29-36] In practice, such MTDLs are usually designed by covalently linking a known ChE inhibitor to a second pharmacophoric moiety that can afford additional biological actions arising from the modulation of another key target in AD pathophysiology, such as oxidative stress, among others.[37-40]

Capsaicin (**1**, Figure 1) is the major bioactive compound in chili peppers. Clinically, it is used mainly in pain management. However, its prominent antioxidant properties have also attracted much attention. Indeed, due to its ability to scavenge reactive oxygen species (ROS), to increase the activity and expression of antioxidant enzymes, and to inhibit protein oxidation and lipid peroxidation, it has been proposed as a protective agent for use in oxidative-stress-related diseases, such as AD.[41-45] Indeed, in vivo studies have shown that capsaicin improves synaptic function by enhancing long-term potentiation (LTP), a cellular mechanism responsible for learning and memory, in the CA1 area of hippocampus, and reduces oxidative stress and neuroinflammation, exerting beneficial effects on synaptic and cognitive functions in mice, and in middle-aged and elderly people.[46-51]

We postulated that combination of a capsaicin moiety with a ChE inhibitor pharmacophore could result in hybrid compounds with the potential to address several major pathologies associated with AD, namely cholinergic deficit, oxidative stress, neuroinflammation, synaptic dysfunction, and cognitive impairment. Here, we report the design, synthesis, in vitro evaluation, structural characterization, biodistribution, and in vivo efficacy of a new series of MTDLs, which are based on capsaicin and huprine Y (**2**, Figure 1), a potent ChE inhibitor developed by our group.[52–55] Accordingly, we set out to investigate whether huprine–capsaicin (HC) hybrids might serve as valuable MTDLs, preserving the affinity of huprine Y for human AChE and BChE, together with the beneficial properties of capsaicin against synaptic dysfunction, oxidative stress, and neuroinflammation. We further examined whether our compounds would also inhibit BACE-1, since we have found that such inhibitory activity is displayed by several families of huprine-based hybrids.[56–58] Furthermore, we performed extensive structural characterization of the complexes of *Tc*AChE and human BChE (hBChE) with selected HC hybrids, so as to reveal the molecular basis for their AChE-over-BChE selectivity, and to open up new avenues for design of both selective and dual AChE and BChE inhibitors. The brain permeability of all the compounds was first assessed in vitro, and then confirmed in vivo by biodistribution studies in C57BL6 mice for two selected compounds. Finally, in vivo chronic efficacy studies were performed with the two selected hybrids in double transgenic APP/PS1 mice to assess their impact on amyloid pathology, synaptic plasticity, oxidative stress, neuroinflammation, and cognition, and, hence, their beneficial effects on disease progression and symptomatology.

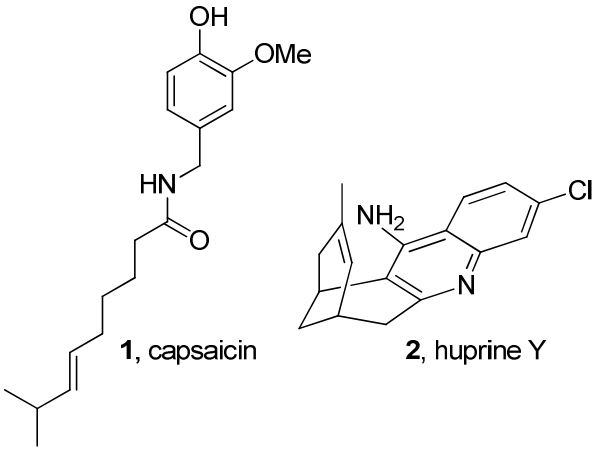

Figure 1. Structures of capsaicin and huprine Y.

RESULTS AND DISCUSSION

Design. The novel HC hybrids were designed by connecting the exocyclic amino group at position 12 of huprine Y with an *N*-(4-hydroxy-3-methoxybenzyl) alkanamide (hybrids **5a**-**e**, Scheme 1) or alkenamide (hybrids **5g**,**h**, Scheme 3) moiety derived from capsaicin. With the intention of allowing the capsaicin-like *N*-(4-hydroxy-3-methoxybenzyl)carboxamide moiety of HC hybrids to establish interactions both with the PAS of AChE and within the large catalytic site of BACE-1, various oligomethylene spacers were considered, having 7-12 atoms between the nitrogen atom at position 12 of the huprine moiety and the aromatic ring of the capsaicin moiety. We also designed the benzamide **5f** (Scheme 2) with the aim of promoting hydrophobic interactions with the aromatic residues lining the active-site gorge of AChE, again by substitution on position 12 of the huprine unit. Since attachment of a triazolylbutyl substituent at position 9 of huprine was recently reported as a means of obtaining highly potent AChE inhibitors,[59,60] we designed the HC hybrid **5i** (Scheme 4), in which the *N*-(4-hydroxy-3-methoxybenzyl)carboxamide moiety of capsaicin was linked, through a triazolylbutyl tether, to

huprine position 9. Compounds synthesized by derivatization at positions 12 and 9 of the huprine scaffold are hereafter referred to as 12-HC and 9-HC hybrids, respectively.

Chemistry. 12-HC hybrids of the alkanamide and benzamide series (**5a**–**e**, **5f**) were synthesized through a two-step sequence from racemic nitriles **3a**–**e** and **3f**[56] and commercially available amine **4** (Schemes 1 and 2). Saponification of nitriles **3a**–**e** and **3f**, followed by amide coupling by reaction of amine **4** with the mixed anhydrides formed from the resulting carboxylic acids and ethyl chloroformate, afforded the target hybrids **5a**–**e** and **5f** in low to moderate overall yields (9–44%). Benzamide **5f** was synthesized with a higher overall yield (76%) by using the O-triisopropylsislyl-protected amine **6**[61] instead of **4** for the amide coupling reaction, followed by deprotection with tetrabutylammonium fluoride (Scheme 2).

Scheme 1. Synthesis of the HC Hybrids 5a–e[a]

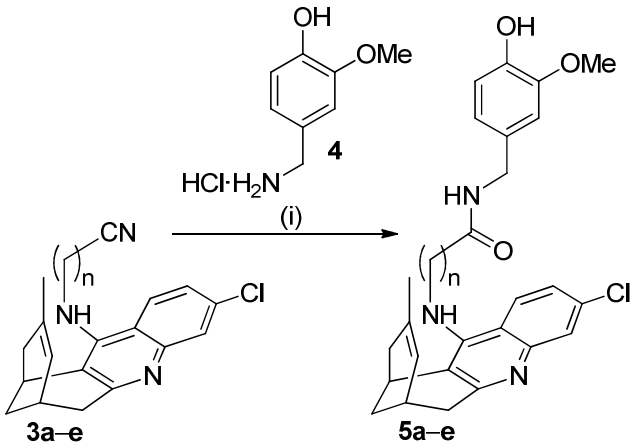

[a]Reagents and conditions: (i) 1) **3a**–**e**, 40% methanolic KOH, reflux, 3 h; then H_2O, reflux, overnight; 0.5 N HCl/Et_2O; 2) crude carboxylic acid (1 equiv), $ClCO_2Et$ (1 equiv), Et_3N (5 equiv), CH_2Cl_2, 0 ºC, 30 min; then, **4**·HCl (1 equiv), CH_2Cl_2, rt, 3 days, 18% (**5a**), 38% (**5b**), 44% (**5c**), 17% (**5d**), 9% (**5e**) overall.

Scheme 2. Synthesis of the HC Hybrid 5f[a]

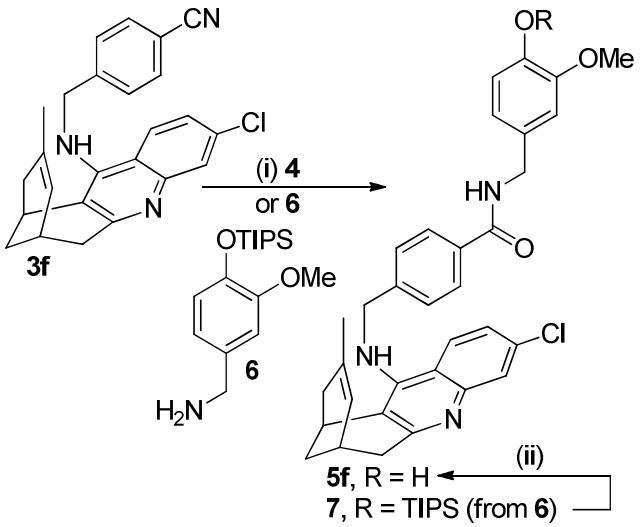

[a]Reagents and conditions: (i) 1) **3f**, 40% methanolic KOH, reflux, 3 h; then H_2O, reflux, overnight; 0.5 N HCl/Et_2O; 2) crude carboxylic acid (1 equiv), $ClCO_2Et$ (1 equiv), Et_3N (5 equiv), CH_2Cl_2, 0 ºC, 30 min; then, **4**·HCl (1 equiv) or **6** (1 equiv), CH_2Cl_2, rt, 3 days, 33% (**5f**, from **3f** and **4**), 81% (**7**, from **3f** and **6**) overall; (ii) 1 M TBAF/THF, THF, rt, 4 h, 94% (76% overall yield of **5f** via **7**).

Synthesis of the 12-HC hybrids of the alkenamide series (**5g**,**h**), which feature the carbon–carbon double bond of the side chain of capsaicin, was less straightforward. Attempts to synthesize them via the formation of mixed anhydrides were unsuccessful, as cross metathesis between 6-heptenenitrile and allyl bromide in the presence of 2nd generation Grubbs catalyst did not yield the required, and commercially non-available, 8-bromo-6-octenenitrile. In contrast, 8-bromo-6-octenoic acid was obtained in excellent yield (96%, *E*/*Z* 4:1), but did not react with huprine Y in the presence of NaOH in DMSO, hence precluding obtention of the huprine-based alkenoic acid. Therefore, we envisaged an alternative synthetic sequence, based on the cross metathesis reaction between the capsaicin-based alkene **9** and racemic 12-alkenylhuprines **10g**,**h** (Scheme 3).

Scheme 3. Synthesis of the HC Hybrids 5g,h[a]

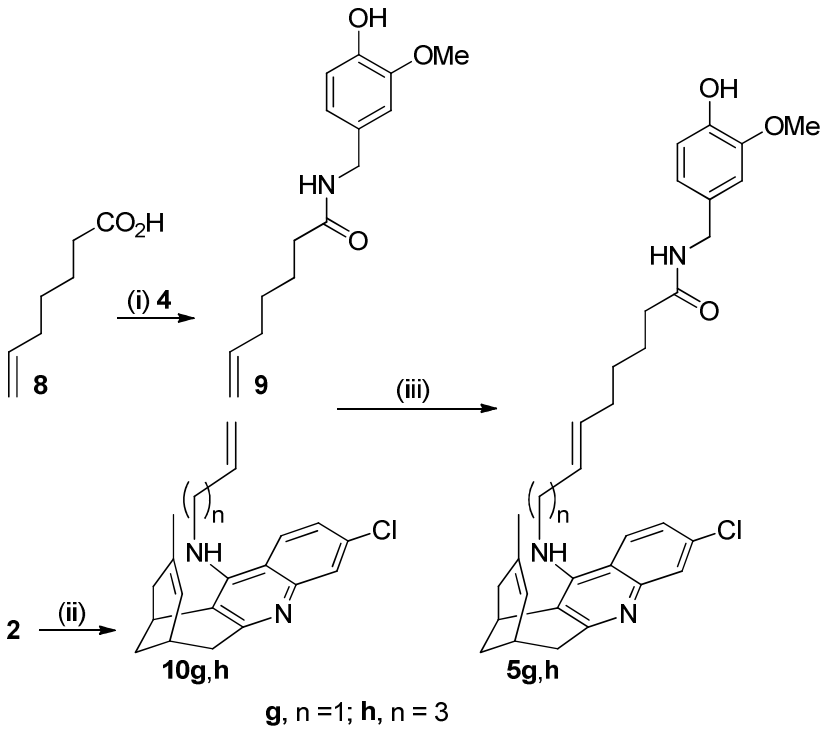

[a]Reagents and conditions: (i) 1) **8** (1 equiv), $ClCO_2Et$ (1 equiv), Et_3N (2.2 equiv), CH_2Cl_2, 0 ºC, 30 min; then, **4**·HCl (1 equiv), CH_2Cl_2, rt, 3 days; 2) sat. aq. $NaHCO_3$, MeOH, H_2O, rt, overnight, 78%; (ii) KOH or NaOH (1.6 equiv), 4 Å molecular sieves, DMSO, rt, 2 h; then allyl bromide (1 equiv) or 5-bromo-1-pentene (1.1 equiv), DMSO, rt, overnight, 55% (**10g**), 27% (**10h**); (iii) **10g**,**h** (1 equiv), **9** (1.2–1.8 equiv), *p*-benzoquinone (0.1 equiv), Grubbs-Hoveyda II generation catalyst (0.05 equiv), reflux, 3 days, 9% (**5g**), 7% (**5h**).

First, we prepared alkenamide **9** by treatment of commercially available 6-heptenoic acid, **8**, with ethyl chloroformate in the presence of Et_3N, and subsequent reaction of the resulting mixed anhydride with amine **4**. A small amount of byproduct was formed, that arose from the additional acylation of **4** on its hydroxyl group. Direct treatment of the mixture with saturated aqueous $NaHCO_3$ in MeOH at rt allowed chemoselective hydrolysis of the ester group of the byproduct, affording alkenamide **9** in 78% yield. Alkenylhuprines **10g** and **10h**[62] were then synthesized in

moderate yields by alkylation of racemic huprine Y with allyl bromide and 5-bromo-1-pentene, respectively, using either KOH or NaOH as a base in DMSO at room temperature. Finally, cross metathesis of alkene **9** with alkenylhuprines **10g** and **10h** was performed in the presence of 5 mol% 2nd generation Grubbs-Hoveyda catalyst in refluxing CH_2Cl_2, using 10 mol% *p*-benzoquinone to prevent olefin isomerization.[63] A tedious silica gel column chromatography purification allowed us to obtain alkenamide hybrids **5g** and **5h** as pure (*E*)-diastereoisomers, albeit in low yields (9% and 7%, respectively).

For the synthesis of the 9-HC hybrid **5i**, featuring the *N*-(4-hydroxy-3-methoxybenzyl)carboxamide moiety of capsaicin linked through a triazolylbutyl tether on position 9 of huprine, we first attempted a copper-catalyzed azide–alkyne cycloaddition (CuAAC) of an O-protected capsaicin-based 3-butynamide to the previously reported racemic 9-azidobutylhuprine **13**[60,64] (Scheme 4). Use of an O-TIPS-protected capsaicin-based 3-butynamide, generated by coupling amine **6** with 3-butynoic acid, led to an inseparable 25:75 mixture of the desired 3-butynamide and its 2,3-butadienamide isomerization product. Fortunately, the amount of the isomerization byproduct was much lower (12%) when the O-TBDMS-protected amine **11**[65] was used instead of **6**. The byproduct and the desired 3-butynamide **12** could be separated by silica gel column chromatography, affording the latter in 36% yield. The CuAAC reaction of 3-butynamide **12** and azide **13** in acetonitrile yielded the O-TBDMS-protected hybrid **14**, which after acidic deprotection led to the target 9-HC hybrid **5i** in good yield (58% over two steps).

Scheme 4. Synthesis of the HC Hybrid 5i[a]

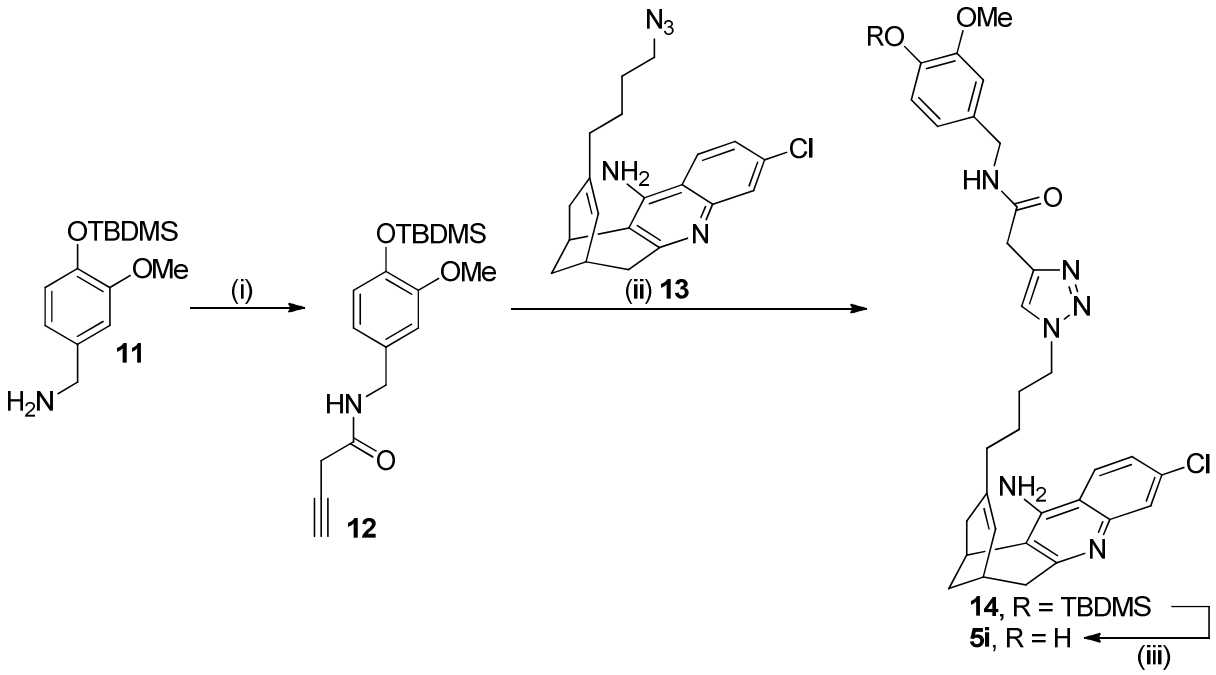

[a]Reagents and conditions: (i) **11** (1 equiv), 3-butynoic acid (1 equiv), EDC·HCl (1 equiv), CH_2Cl_2, rt, 2 h, 36%; (ii) **13** (1 equiv), **12** (1.2 equiv), CuI (1 equiv), CH_3CN, rt, 12 h, 80%; (iii) camphorsulfonic acid (0.02 equiv), CH_2Cl_2/MeOH 80:20, rt, 24 h, 73%.

Purity of the Compounds. The hybrids **5a**–**5h** were transformed into the corresponding hydrochloride salts for their chemical characterization and biological profiling. Hybrid **5i** was characterized and tested as the free base. The analytical samples of all the tested compounds possessed a purity > 95%, according to NMR spectra with full assignments and elemental analyses and/or HPLC-UV/HRMS measurements (for more details see the Experimental Section and Supporting Information).

Biological Activities of the HC Hybrids

In Vitro Inhibition of hAChE and hBChE. We first set out to determine whether the HC hybrids were active against human ChEs. To this end, we used the method of Ellman et al.,[66] with capsaicin and racemic huprine Y as negative and positive controls, respectively (Table 1).

Table 1. Inhibitory Activities of the HC Hybrids and Reference Compounds against Human AChE, BChE, and BACE-1, Antioxidant Activity, and PAMPA-BBB Permeabilities

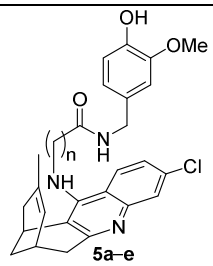

5a–e

a, n = 4; **b**, n = 5; **c**, n = 6; **d**, n = 7; **e**, n = 8

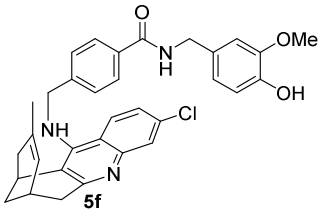

5f

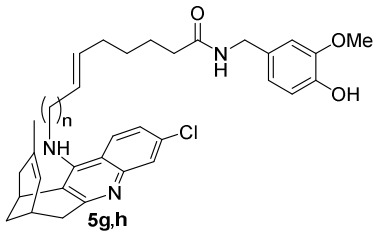

5g,h

g, n = 1; **h**, n = 3

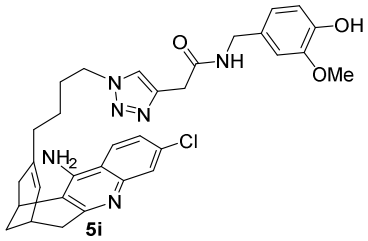

5i

compd	hAChE IC_{50} (nM)[a]	hBChE IC_{50} (nM)[a]	selectivity ratio[b]	hBACE-1 % inhibition @1 μM[c]	DPPH IC_{50} (μM)[d]	PAMPA-BBB permeability[e]
5a	5.48 ± 0.28	52.2 ± 1.3	9.5	55.6 ± 20.3	68.5 ± 8.2	11.5 ± 1.1 (CNS+)
5b	4.35 ± 0.18	70.0 ± 4.9	16.1	34.3 ± 17.2	62.6 ± 11.6	14.9 ± 1.2 (CNS+)
5c	0.77 ± 0.06	30.6 ± 1.7	39.7	7.4 ± 3.2	55.4 ± 2.3	17.2 ± 1.0 (CNS+)
5d	1.94 ± 0.15	51.8 ± 3.0	26.7	3.6 ± 1.5	70.8 ± 20.8	20.1 ± 1.1 (CNS+)
5e	2.94 ± 0.16	36.1 ± 2.2	12.3	23.7 ± 8.8	64.6 ± 8.6	21.8 ± 1.3 (CNS+)
5f	24.9 ± 1.9	290 ± 19	11.6	na[f]	71.4 ± 15.5	14.3 ± 0.3 (CNS+)
5g	4.41 ± 0.17	78.1 ± 2.9	17.7	na[f]	31.7 ± 8.7	16.8 ± 0.1 (CNS+)
5h	5.64 ± 0.30	53.1 ± 2.4	9.4	21.6 ± 6.2	54.6 ± 12.5	22.3 ± 1.1 (CNS+)
5i	1.06 ± 0.26	7.3 ± 0.6	6.9	na[f]	92.0 ± 12.4	8.8 ± 1.3 (CNS+)

1	>200,000	na[g]		na[f]	50.3 ± 8.3	10.3 ± 1.2 (CNS+)
2[h]	1.07 ± 0.05	181 ± 15	169.2	na[i]	nd[j]	23.8 ± 2.7 (CNS+)

[a]IC_{50} values (nM) for inhibition of human recombinant AChE or BChE from human serum. Values are expressed as mean ± standard error of the mean (SEM) of at least two experiments, each performed in duplicate/triplicate. [b]AChE-over-BChE selectivity ratio = IC_{50} hBChE/IC_{50} hAChE. [c]% inhibition of human recombinant BACE-1 with inhibitor at 1 μM. Values are expressed as mean ± standard deviation (SD) of two independent experiments, each performed in triplicate. [d]IC_{50} inhibitory concentration (μM) for DPPH radical scavenging activity. Values are expressed as mean ± SD of three experiments, each performed in duplicate. [e]Permeability values (P_e, 10^{-6} cm s^{-1}) from the PAMPA-BBB assay. Values are expressed as mean ± SD of three experiments, each performed in triplicate. [f]Not active. [g]na = not active; 20% inhibition at 100 μM. [h]Data from ref. 56 under the same experimental conditions, unless otherwise indicated. [i]14% inhibition at 5 μM. [j]Not determined.

In agreement with previous reports,[67] we found that capsaicin was inactive against both hAChE and hBChE, whereas huprine Y is a potent inhibitor of both enzymes, with an AChE-over-BChE selectivity ratio of 169. All HC hybrids **5a**–**i** retained the high potency of the parent huprine Y against hAChE and hBChE and displayed a reduced AChE-over-BChE selectivity ratio (6.9–39.7).

Compounds **5a**–**5e** are 12-HC hybrids that differ only in the length of the alkane chain linking the capsaicin-amide and huprine moieties (7−11 atoms). A hexamethylene linker, and, hence, a total tether length of 9 atoms between the nitrogen atom at position 12 of the huprine moiety and the aromatic ring of the capsaicin moiety, is optimal for the inhibition of both hAChE and hBChE (Table 1), yielding a compound, **5c**, that surpassed the nanomolar potency of huprine Y. The effect of linker length was more pronounced for hAChE than for hBChE, resulting in a decreased AChE-over-BChE selectivity ratio for compounds featuring a shorter (**5a**, **5b**) or longer (**5d**, **5e**) linker than **5c**. Interestingly, compounds **5c** and **5e** displayed similar potency against hBChE, but not against hAChE. Compound **5f**, which features a benzamide linker, was the least potent of all the HC hybrids, while compounds **5g** and **5h**, characterized by an

alkenamide linker of 10 and 12 atoms in total, respectively, displayed a lower potency against both hAChE and hBChE than their closest alkanamide counterparts, *i.e.* compounds **5d** (10 atoms) and **5e** (11 atoms). Thus, biochemical data suggest that a flexible, saturated linker is best suited to inhibit ChEs. The observation that compounds **5e** and **5h**, which feature a linker of 11 and 12 atoms, respectively, bind to hBChE with higher affinity than their 10-atom counterparts (**5d** and **5g**) suggests that a linker length >11 atoms may allow binding to another subsite at the rim of the hBChE active-site gorge. Compound **5i**, the 9-HC hybrid, displayed the lowest AChE-over-BChE selectivity ratio of all the HC hybrids. Unlike for the other compounds, this decrease in selectivity ratio does not stem from a decreased potency against hAChE, but rather from an increased hBChE inhibitory activity. Importantly, compound **5i** is the first huprine-based inhibitor displaying one-digit nanomolar inhibitory activity against both hBChE (IC_{50} = 7.3 nM, i.e. 25-fold more potent than the parent huprine Y) and hAChE (IC_{50} = 1.06 nM, i.e., the same as that of huprine Y).

Kinetic Studies of AChE Inhibition and Propidium Displacement Studies. In the light of the subnanomolar inhibition of hAChE by compound **5c**, we investigated its mode of inhibition by use of Lineweaver–Burk and Cornish–Bowden plots. The interception of the lines in the Lineweaver–Burk plot above the x-axis (Figure 2, left) suggests a mixed-type inhibition of hAChE by **5c**. The mixed-type mechanism was further confirmed by the Cornish–Bowden plot (S/*v* *vs* [I]).[68] The inhibition constant (K_i) and the dissociation constant for the enzyme–substrate–inhibitor complex (K'_i) of hybrid **5c** were estimated to be 0.68 nM and 0.94 nM, respectively. The similarity between the K_i and K'_i values is suggestive of dual tight binding at the two binding sites, i.e., CAS and PAS. To verify this hypothesis, we confirmed the interaction of **5c** with the PAS through displacement studies using propidium iodide, a specific PAS ligand

(K_D = 0.70 μM), as a probe and electric eel (*Ee*)AChE. Back-titration experiments with increasing concentrations of hybrid **5c** showed a concentration-dependent decrease in the fluorescence intensity associated with the propidium–AChE complex, suggesting that **5c** can effectively displace propidium from the AChE's PAS (Figure 2, right).[69,70] We found a low micromolar affinity of **5c** for the PAS of *Ee*AChE (K_D = 3.59 μM), confirming that hybrid **5c** can interact with the PAS of AChE. On the basis of the putative orientation of the HC hybrids within AChE, with the capsaicin moiety pointing toward AChE's PAS (as confirmed by crystallographic studies, see below), capsaicin was also assayed to evaluate its ability to displace propidium. Unfortunately, in the conditions used for such assay, spectral interference due to the intrinsic fluorescence of capsaicin was significant and precluded the accurate determination of its affinity for PAS. Nevertheless, from data acquired at the lowest tested concentrations (4–16 μM), at which spectral interference was limited, some qualitative considerations could be made, allowing us to state that also capsaicin is able to bind AChE's PAS, albeit in a weaker manner than **5c** (decrease of fluorescence intensity by **5c** and capsaicin both tested at 2/1 ratio over propidium = 23% and 11%, respectively).

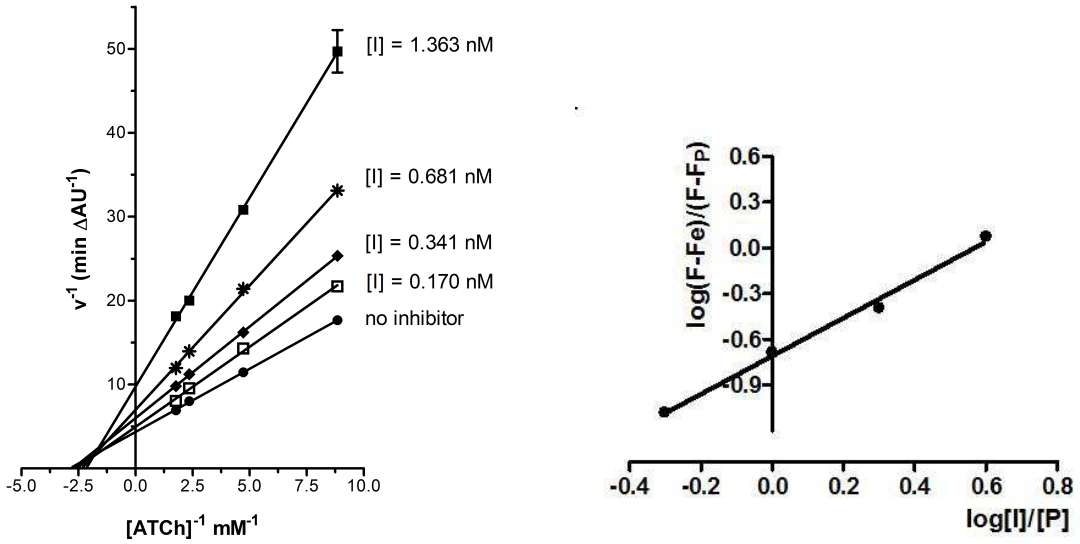

Figure 2. Left: Kinetic measurements to characterize the mode of inhibition of AChE by **5c**. Lineweaver–Burk reciprocal plots show the variation of the AChE initial velocity rate with increasing substrate concentrations (acetylthiocholine (ATCh), 0.11–0.57 mM) in the absence and presence of increasing concentrations of **5c** (0.17–1.36 nM). Lines were derived from a weighted least-squares analysis of the data points. The mechanism of inhibition was assessed by two independent experiments, each performed in triplicate. Right: Determination of the K_D value for **5c** binding to PAS from the antilog of the Y-intercept value.[69] Experimental conditions: 2.0 μM *Ee*AChE, 8.0 μM propidium, 1.0 mM Tris HCl, pH 8.0; P stands for propidium iodide and I stands for the tested inhibitor; Fe is the initial fluorescence intensity when enzyme sites are saturated with P, F_P is the fluorescence intensity when propidium is completely displaced from the enzyme, and F denotes the fluorescence intensity after adding a determined amount of displacing agent during the titration experiment. Data are the average of three independent experiments.

Structural Characterization of hAChE and hBChE Complexes with HC Hybrids. The crystal structure of the complex of **5i** (9-HC hybrid) with hBChE, as well as those of the complexes of **5b**, **5c**, **5d**, **5f**, **5h** (12-HC hybrids) and **5i** (9-HC hybrid) with *Tc*AChE were determined (Figures 3–5). Data were collected from crystals soaked for 12 h in mother liquor supplemented with a 1 mM solution of a racemic mixture of the selected compounds. Further details regarding structure determination and refinement are listed in Table S1 of the Supporting Information and in the Experimental Section.

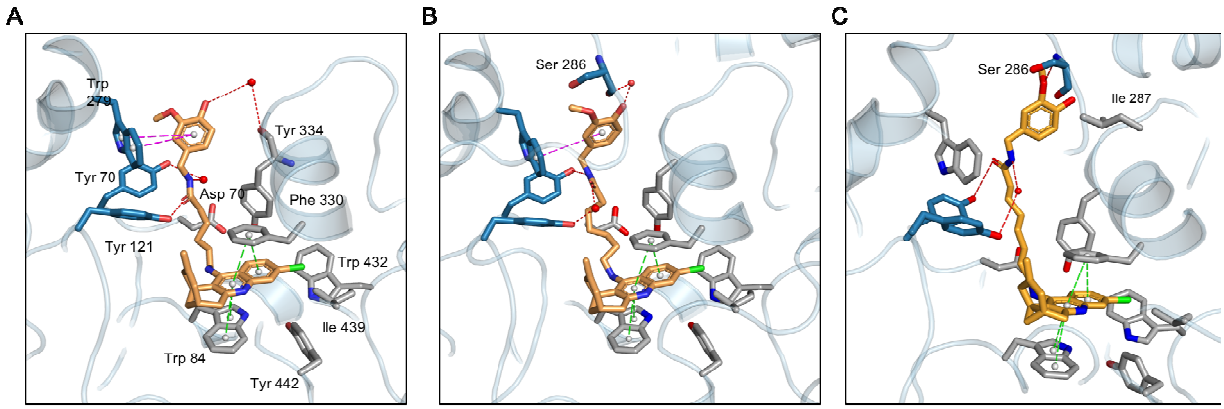

Figure 3. Crystal structures of complexes with *Tc*AChE of HC hybrids **5b** (A), **5c** (B), and **5d** (C). Compounds (light orange) and key residues of *Tc*AChE (blue/grey) are shown as sticks. The protein backbone is represented as a light blue cartoon. The type of interaction is color-coded as follows: *Tc*AChE residues involved in hydrophobic interactions are colored grey, parallel and perpendicular π-stacking interactions are represented as green and magenta sticks between interacting aromatic centers (modeled as white spheres), and hydrogen bonds are represented as red dashes, with amino acid residues involved colored blue.

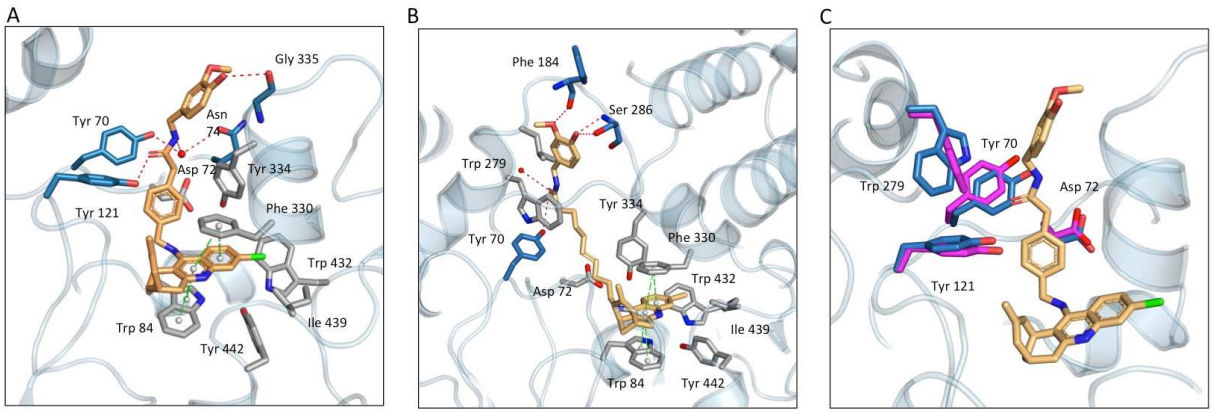

Figure 4. Crystal structure of complexes with *Tc*AChE of HC hybrids **5f** (A) and **5h** (B). Residues and interactions are color-coded as in Figure 3. (C) Gorge restructuration upon binding of **5f**. The *Tc*AChE backbone is shown in blue cartoon format, and compound **5f** as light orange sticks. Residues that change conformation upon binding of **5f** are shown as sticks, with the native conformation shown in blue, and the **5f**-bound conformation in magenta.

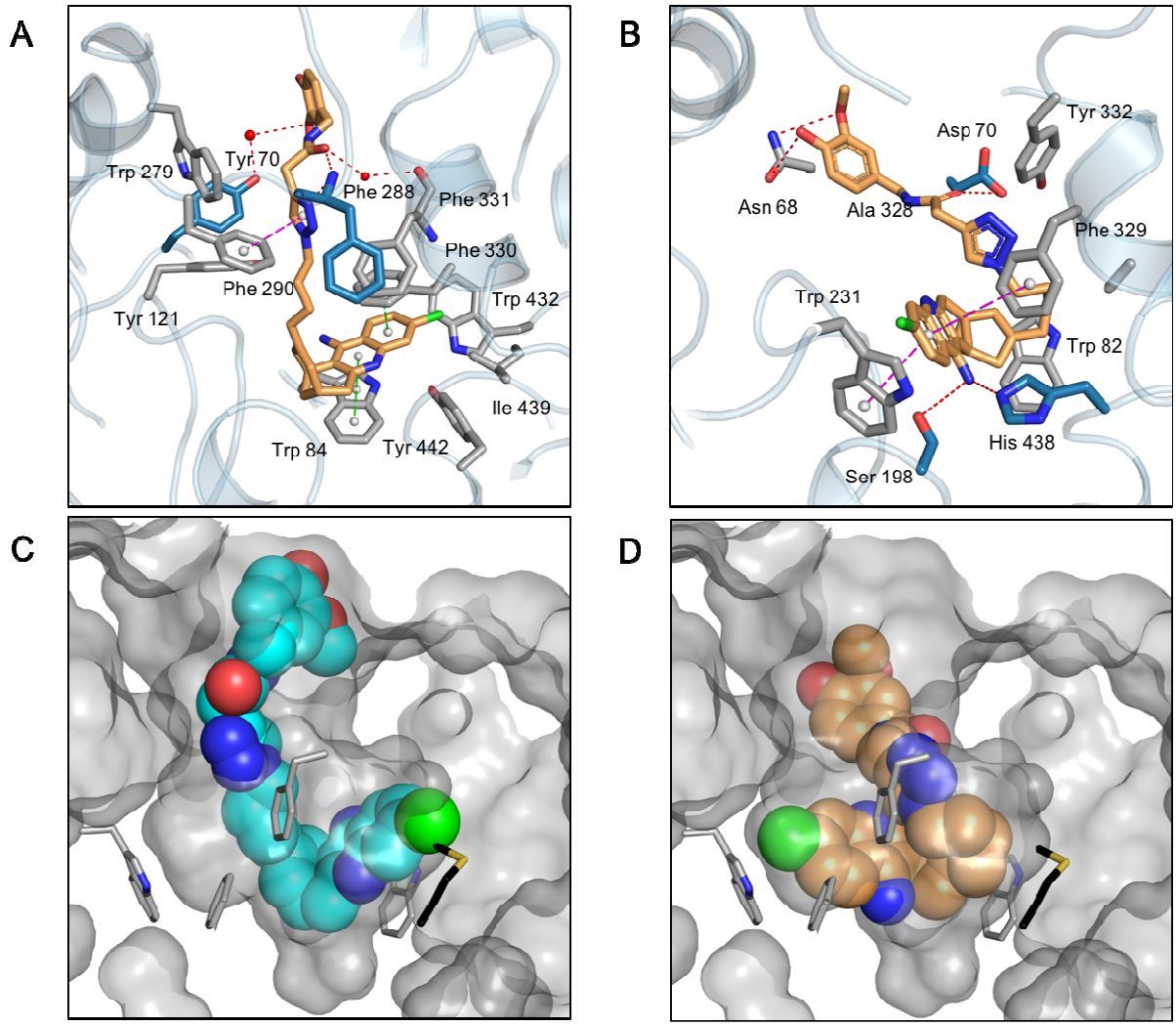

Figure 5. Crystal structures of **5i**–*Tc*AChE (A) and **5i**–hBChE complexes (B). Residues and interactions are color-coded as in Figure 3. (C, D) Surface representations of the hBChE active-site gorge, with key residues shown as grey sticks. The conformation of compound **5i** observed in the crystal structure of its complex with *Tc*AChE was modeled into the hBChE active-site gorge (after superimposition of the two structures). Compound **5i** is shown as cyan spheres (scaled to match the Van der Waals radius). This representation clearly shows that the chlorine atom of the huprine Y moiety cannot fit into the hBChE active-site gorge, due to steric hindrance by Met437 (black stick). (D) Observed binding mode for **5i** in its complex with hBChE.

The crystal structures of the complexes with *Tc*AChE of compounds **5b**, **5c**, **5d**, **5f**, **5h** (12-HC hybrids) and **5i (**9-HC hybrid) reveal that the huprine moieties of the specific enantiomers with the (7*S*,11*S*)-configuration (eutomers in this structural class for AChE inhibition) bind at the bottom of the gorge, in the choline-binding pocket, in an orientation similar to that of the parent huprines (huprines W, X, Y) and of previously reported huprine derivatives (Figure 3).[24,60,71] Briefly, the aromatic system π-stacks to Trp84, while the chlorine atom fits into a hydrophobic groove contributed to by Phe330, Tyr334, Trp432, Met437, and Ile439. The linker of the 12-HC hybrids and of the 9-HC hybrid **5i** traces up to the PAS, orientating toward different sides of the aromatic side gorge – those adjacent to the choline-binding pocket or to the acyl-binding pocket of the active site, respectively. Compounds featuring an alkanamide or a benzamide linker (**5b**–**5d**, **5f**) all benefit from a H-bond interaction of their amide oxygen with either Tyr121(OH) (**5b**, **5f**) or Tyr70(OH) (**5c**, **5d**) (Figures 3 and 4 and Table S2 of the Supporting Information). At the PAS, none of these compounds interacts by parallel π-stacking; rather, the capsaicin hydroxyl and ether oxygens establish H-bonds with residues at the PAS (**5d**, **5f, 5h**) or with waters H-bonded to them (**5b**, **5c**) (Figures 3 and 4 and Table S2 of the Supporting Information). The capsaicin moiety of compounds **5b** and **5c** is engaged in perpendicular π-stacking with the PAS residue Trp279 (Figures 3A and 3B). The observation of a more perpendicular stacking of the capsaicin moiety of **5c** (89º vs 65º for compounds **5c** and **5b**, respectively) may explain why it displays the highest affinity for hAChE of all the HC hybrids. Compound **5d**, the second best hAChE inhibitor in the 12-HC series, displays two conformations at the PAS, but since one involves a non-physiologically relevant symmetry-related molecule (Table S2 of the Supporting Information – alternate conformation A), it can be safely discarded as irrelevant to the mode of binding in solution. In the representative conformation (i.e., alternate conformation B), the

hydroxyl and ether oxygen in the capsaicin moiety of **5d** are H-bonded to Gly335(O) and Ser286(N) (Figure 3C). Compound **5f**, endowed with a similar linker length, but a more rigid structure, fails to adapt to the native active-site gorge structure and its binding is accompanied by concomitant conformational changes in Tyr121, in the gorge, and Tyr70, Asp72, and Trp279 at the PAS (Figure 4C). These observations likely explain the 32-fold decreased potency of **5f** toward AChE, as compared to **5c** (Table 1). We speculate that the increased linker rigidity in **5g** and **5h** also explains their slighltly reduced potencies as compared to **5d** and **5e**, respectively. Nevertheless, we expect **5g** binds in a mode similar to that of **5d**, i.e., with its capsaicin moiety interacting with Gly335(O) and Ser286(N) (Figure 3C). Likewise, compound **5e** should display a binding mode similar to that of **5h**, whose capsaicin moiety completely plugs the entrance of the active-site gorge, fitting into a groove contributed by residues 282–289 (Table S2 of the Supporting Information).

As mentioned above, compound **5i** binds to the active site of *Tc*AChE similarly to the 12-HC compounds, but lays on the side of the gorge adjacent to the acyl-binding pocket rather than on that adjacent to the choline-binding pocket (Figure 5A). As observed earlier in the structure of a complex of a 9-triazolylbutyl derivative of huprine with hAChE,[60] the triazole ring π-stacks perpendicular to Phe290 side chain and a H-bond forms between a triazole nitrogen of **5i** and Phe288(N) (Phe295(N) in hAChE). In addition, the amide nitrogen atom of **5i** H-bonds both to Ser286(N) and to a structural water, which itself is H-bonded to Phe331(O). Finally, a water bridge is formed *via* water 78 between the ether oxygen of the capsaicin moiety of **5i** and Tyr121(OH). Taken together, these observations rationalize the high affinity of **5i** for hAChE and explain its higher affinity than **5d**, an alkanamide-based 12-HC compound with a similar linker length.

No structure was obtained of a complex with hBChE of a 12-HC hybrid due to loss of diffraction. This is in line with the previous report that the absence of a sufficiently deep hydrophobic groove at the bottom of the choline-binding pocket hampers binding of huprine (and thus also of huprine derivatives) to hBChE.[24] This groove is contributed by Phe330 (Tyr337), Trp432 (Trp439), Met436 (Met443), Ile439 (Pro446), and Tyr442 (Tyr449) in *Tc*AChE (hAChE), and by Ala328, Trp430, Met434, Met437 and Tyr440 in hBChE. The replacement of Ile439 (Pro446) in *Tc*AChE (hAChE) by a methionine in hBChE (Met437) offers an explanation as to why this groove cannot accommodate the chlorine atom of huprines while maintaining a native conformation, as it had been previously suggested for tacrine derivatives on the basis of docking studies.[24,72,73] The loss of diffraction upon soaking of hBChE crystals with 12-HC derivatives may, therefore, be due to an incompatibility between the large conformational changes that occur upon binding of these compounds and the preservation of crystal contacts. The structure of the **5f**/*Tc*AChE complex indeed demonstrates that binding of huprine derivatives may require large conformational changes in active-site gorge residues. Those induced by binding of the 12-HC hybrids in hBChE are presumably of a greater magnitude, since they disrupt crystal-packing interactions.

Nonetheless, the structure of the **5i**/hBChE complex was determined, revealing a hitherto unobserved binding mode for huprines and their derivatives with ChEs. As observed for a previously reported huprine/hBChE complex,[74] the chlorine atom of huprine is in the acyl-binding pocket, at 4.0 and 4.1 Å, respectively, from Leu286(O) (Phe288 in *Tc*AChE) and Trp231(NE1) (Trp233 in *Tc*AChE), with the aromatic system π-stacked against Phe329 (Phe331 in *Tc*AChE) and Trp231 (Trp233 in *Tc*AChE), but by contrast, the amine on position 12 fits between Ser198(O) and His438(NE2) (Figure 5B), effectively disrupting the catalytic triad.

Thus, the huprine unit is upside down compared to its position in the previous huprine/hBChE complex, and additionally rotated by 90° as compared to complexes of huprines and huprine derivatives with AChEs. This difference arises from the presence of a bromide anion in the earlier huprine/hBChE complex at the position occupied by the primary amino group of **5i**. The cyclohexene ring of huprine stacks over Trp82 and the linker contorts itself in the hydrophobic groove of the choline-binding pocket, resulting in interactions (i) of the triazole ring with the aromatic ring of Tyr332 (Tyr334 in *Tc*AChE), (ii) of the amide oxygen with Asp70 (Asp72 in *Tc*AChE), and (iii) of the capsaicin hydroxyl and ether oxygen with Asn68(OD1) and (ND2), respectively (Figure 5B and Table S2 of the Supporting Information). Differences in *Tc*AChE vs hBChE active-site gorge architecture at the PAS (Tyr70, Trp279 vs Asn68, Ala277), in the acyl-binding pocket (Phe288, Phe290, Phe330, and Val400 vs Leu286, Val288, Ala328, and Phe398) and in the choline-binding pocket (Ile439 vs Met437) suggest that the binding mode observed in the **5i**/hBChE complex would not occur in the corresponding *Tc*AChE complex, nor, by analogy, in the hAChE complex.

In Vitro Antioxidant Activity and hBACE-1 Inhibition. Suitably designed huprine derivatives have already shown to be valuable anti-Alzheimer MTDLs, allowing not only AChE and BChE inhibition, but also inhibition of BACE-1.[56-58] For the latter activity, molecular dynamics simulations have suggested that the huprine moiety, protonated in the acidic endosomal compartments where BACE-1 localizes, can establish a salt bridge with the two aspartate residues of the enzyme catalytic dyad, whereas a second pharmacophore containing a hydrogen bond acceptor group might interact at a transient secondary binding site, at the edge of the large catalytic site.[75] The resulting dual site binding within hBACE-1 would account for the

high inhibitory activity of some huprine-based hybrids, which display IC_{50} values reaching into the nanomolar range.[56] On the basis of these findings and of the structures of the HC hybrids, we hypothesized that their capsaicin moiety might bind at the secondary site in BACE-1, just as it bound at the secondary binding site of AChE, viz., at the PAS. Accordingly, apart from the antioxidant activity of the HC hybrids supposedly imparted by their capsaicin moiety, we also examined their capacity to inhibit BACE-1.

The in vitro antioxidant activity of the HC hybrids was assessed by an easy and commonly used method, which is based on the ability of antioxidant compounds to donate a hydrogen atom to scavenging the 2,2-diphenyl-1-picrylhydrazyl (DPPH) free radical.[76] We found that all the compounds retained the antioxidant activity of parent capsaicin in the DPPH assay, displaying very similar IC_{50} values, which demonstrated that hybridization did not result in a loss of function. Indeed, compound **5g**, of the alkenamide series, was even slightly more potent than both capsaicin itself and the rest of compounds of the series.

Regarding hBACE-1 inhibition, all compounds in the alkanamide series were found to be active. Of these, the most active was **5a** (55.6% inhibition at 1 μM) and a negative correlation was observed between linker length and inhibition of hBACE-1, up to 10 atoms. Compound **5e** was, nevertheless, more active than compounds **5c** and **5d** suggesting, again, that an 11-atom linker might permit binding to a second subsite of the large BACE-1 active site. Indeed, compound **5h**, of the alkenamide series, with a linker length similar to that of **5e**, was equipotent to **5e**. Compounds **5f**, **5g**, and **5i** were not active against hBACE-1 at the tested concentration (1 μM).

In Vitro Brain Permeation. As a preliminary assessment of the ability of the novel compounds to enter the brain, where they should exert their effects, their permeabilities were determined using the well-established parallel artificial membrane permeation assay for blood–brain barrier (PAMPA-BBB).[77] All compounds had permeabilities (P_e) well above the cutoff value for good brain permeation (CNS+: P_e (10^{-6} cm s^{-1}) > 5.1), suggesting that they would be able to reach their molecular targets in the brains of both AD patients and animal models. The CNS+ propensity increased with linker length, which indicates that an increased lipophilicity fosters the BBB crossing. In support of this hypothesis, compound **5i**, which features a hydrophilic triazole ring in the linker, displayed the lowest P_e value, even though still being clearly CNS+.

Biodistribution Studies in C57BL6 Mice. The in vitro biological profiling of the novel HC hybrids put hybrids **5c** and **5i** forward as promising anti-Alzheimer MTDLs, by virtue of their highly potent inhibitory activity on hAChE and hBChE, combined to decent antioxidant activity and favorable in vitro brain permeability. Indeed, **5c** and **5i** emerged as the two most potent hAChE inhibitors (IC_{50} = 0.77 nM and 1.06 nM, respectively) and BChE inhibitors (IC_{50} = 30.6 nM and 7.3 nM, respectively) of the series, and retained the antioxidant activity of the parent capsaicin, even though the latter activity, in the micromolar range, was not balanced relative to the highly potent anticholinesterase activities, which might challenge their ability to simultaneously elicit all these activities in vivo.

Before advancing the lead HC hybrids to in vivo efficacy studies, we decided to confirm their ability to penetrate the brain in vivo and to assess their potential presence in other important organs. We performed biodistribution studies in wild type (C57BL6) mice. Instead of a single dose, we mimicked a chronic treatment by applying the same dosing protocol that was to be

followed in the subsequent in vivo chronic efficacy studies (i.e., same dose, administration route, and frequency of administration and for enough time as to enable the tested compounds to reach levels in organs corresponding to a chronic treatment). Briefly, compounds **5c** and **5i** were administered intraperitoneally (i.p.) to C57BL6 mice at a dose of 2 mg/kg three times a week for two weeks. The anti-Alzheimer drug donepezil was used as a reference compound. Four hours after injection of the last dose of **5c**, **5i**, or donepezil, the animals were sacrificed and their organs (brain, kidneys, liver, lungs) and plasma were collected for quantification of the compounds' levels by HPLC/MS/MS (Figure 6).

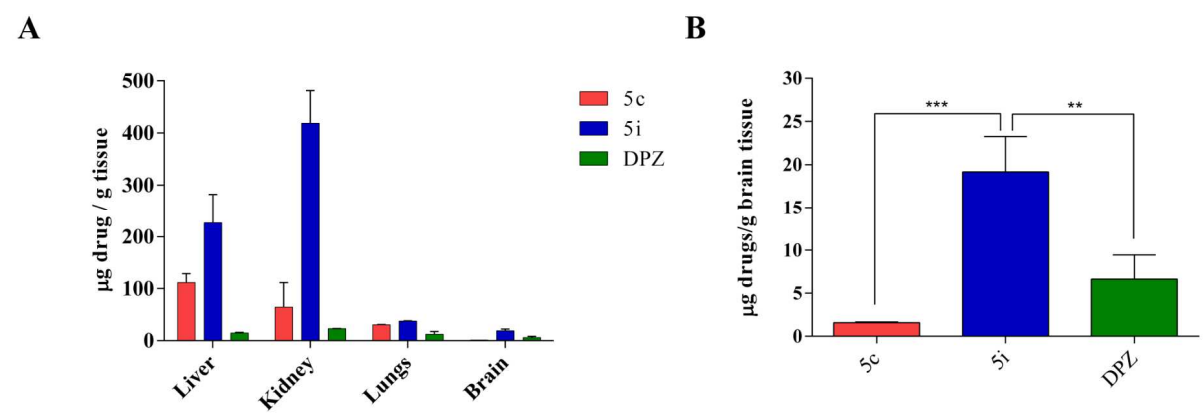

Figure 6. (A) In vivo distribution of compounds **5c** and **5i** and of the reference drug, donepezil (DPZ), to various organs in 6-month-old C57BL6 mice. (B) Comparison of brain levels of **5c**, **5i**, and donepezil. Data were analyzed using one-way analysis of variance (ANOVA), followed by Tukey's post hoc test; ** $p < 0.01$; *** $p < 0.001$ were considered significant differences.

Four hours after injection of the last dose of **5c** and **5i**, these compounds were found to be mainly distributed to the kidneys and the liver, but importantly, both of them were also detected in the brains of C57BL6 mice (Figure 6A and Table S4 of the Supporting Information). Indeed, **5c** and

5i were present in the brains at concentrations of 1.58 and 18.88 μg/g brain tissue, respectively, which were higher than those found in plasma (<3 ng/mL (detection limit) and 35.58 ng/mL, respectively). Thus, both compounds have a favorable brain/plasma ratio. Of note, compound **5i** attained a higher brain concentration ($p < 0.01$; Figure 6B and Table S4 of the Supporting Information) and a lower plasma level than donepezil (6.13 μg donepezil/g brain tissue and 6.46 μg donepezil/mL in plasma, respectively), thus displaying a better brain/plasma ratio than the anti-Alzheimer reference drug at that particular time point. Irrespective of the fact that different amounts of the tested compounds and donepezil could have been found at other time points as a result of their different distribution or half-lives, these results unambiguously confirmed the penetration of the target compounds into the brain and encouraged us to perform chronic in vivo efficacy studies with a transgenic mouse model of AD.

Chronic In Vivo Efficacy Studies

Behavioral Studies. After confirming the brain penetration of compounds **5c** and **5i** in wild type mice, we performed chronic efficacy studies in a well-established animal model of AD, namely double transgenic APPswe/PSEN1dE9 (APP/PS1) mice. Animals of two different ages were used in our study: one group aged 5 months (young mice) at the beginning of the study, when the Alzheimer-like pathology starts developing, and a second group aged 10 months (old mice), with already well-established pathology. Young and old transgenic animals were treated by i.p. injection of either **5c** or **5i** at a dose of 2 mg/kg with saline solution as vehicle, or only vehicle (control group), three times per week, for 4 weeks. Thus, at the end of the treatment young and old animals were 6- and 11-month-old, respectively. All the animals of the six experimental

groups finished the treatment successfully, remaining healthy in terms of weight, lipid and hepatic parameters, and by visual inspection.

To study the effects of **5c** and **5i** on cognitive functions we performed several tests, namely the large open-field (LOF), novel object recognition (NOR), novel object localization (NOL), and memory flexibility tests. Initially, despite the apparent healthy status of the treated mice, we wanted to additionally rule out movement or stress problems due to treatment. To this end, the general behavior and the locomotor activity of treated and control mice was studied using the LOF test. This test measures the time spent by the animal moving along the field and the number of times that the animal crosses the central area of a transparent cage. No significant change among groups was observed, thereby confirming that treatment with **5c** and **5i** did not alter the general behavior of the animals, both young and old (one-way ANOVA, $p < 0.05$, followed by appropriate post hoc testing) (Figure 7). Thus, the basal status of the treated animals did not affect their performance in the subsequent behavioral tests, in which the effects of the compounds on memory and learning functions were assessed.

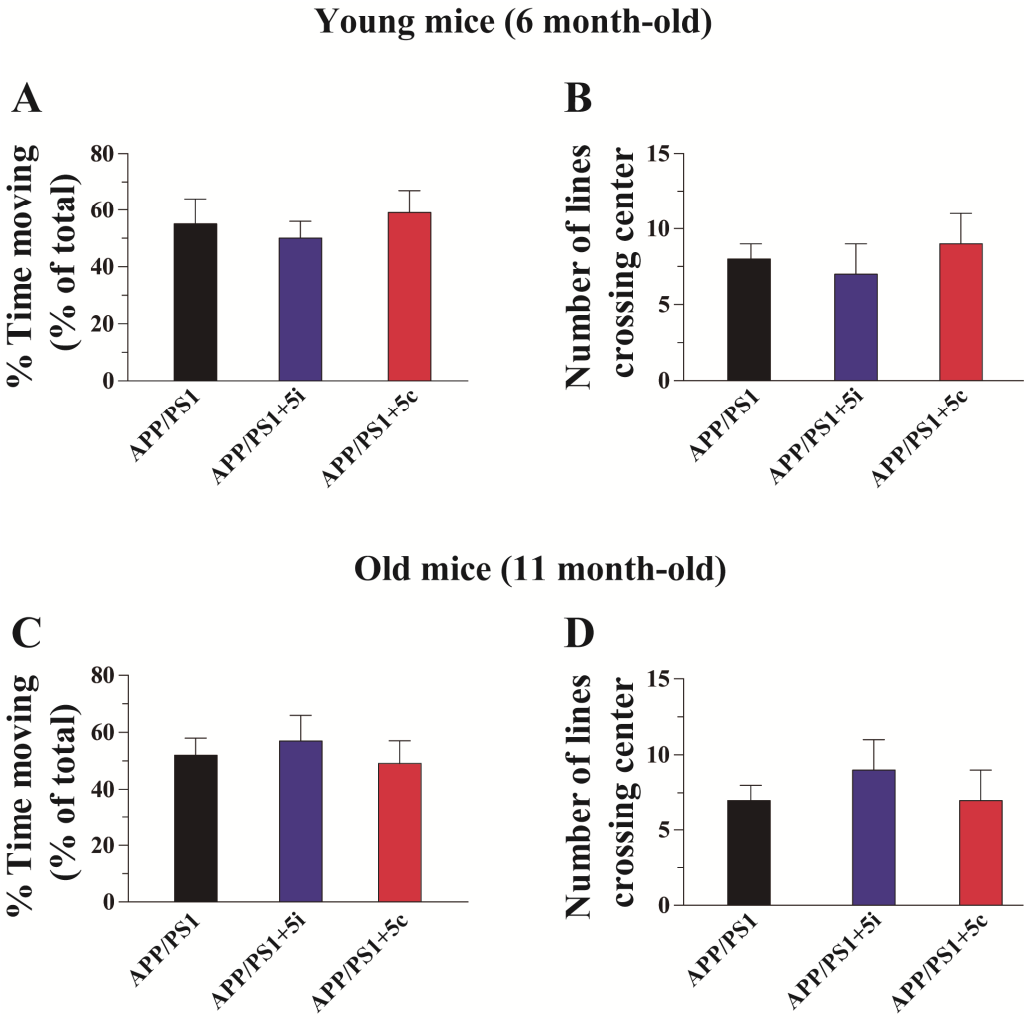

Figure 7. Time spent moving and number of crossings by (A, B) young and (C, D) old male APP/PS1 mice treated with vehicle, **5c**, and **5i** in the LOF test. Data are expressed as mean values ± SEM of n = 7 animals in each group. Data were analyzed by one-way ANOVA, followed by Bonferroni's post hoc test; $p \leq 0.05$ was considered the threshold for statistical significance with 95% confidence interval (CI).

We then explored whether administration of **5c** and **5i** to young and old transgenic animals might delay or rescue their cognitive impairment. To evaluate memory, we performed

the NOR and NOL tests, which are both associated with hippocampal function. Briefly, after habituation to the experimental cages, transgenic mice were allowed to explore a platform containing two identical objects at specific locations. Afterwards, one of the familiar objects was first moved to a different place within the platform (NOL), and then one of the familiar objects was replaced by a new one (NOR). The preference for each object shown by the mice exposed to these two consecutive changes was registered and an object preference index was determined by dividing the time spent exploring the relocated/novel object by the total time spent exploring both objects. Thus, a lower preference index when comparing different animal groups is indicative of cognitive impairment, and viceversa, a higher preference index is associated with cognitive enhancement.

We did not observe significant changes in the preference index of young transgenic mice treated with **5c** or **5i** relative to the control group (Figure 8A, B). However, in the group of old APP/PS1 mice treated with compound **5i** we observed a significant increase in the preference index relative to vehicle-treated transgenic mice, both in the NOR and NOL tests (one-way ANOVA, $p < 0.05$, followed by appropriate post hoc testing) (Figure 8C, D). Thus, administration of compound **5i** significantly enhanced learning and memory in old APP/PS1 mice.

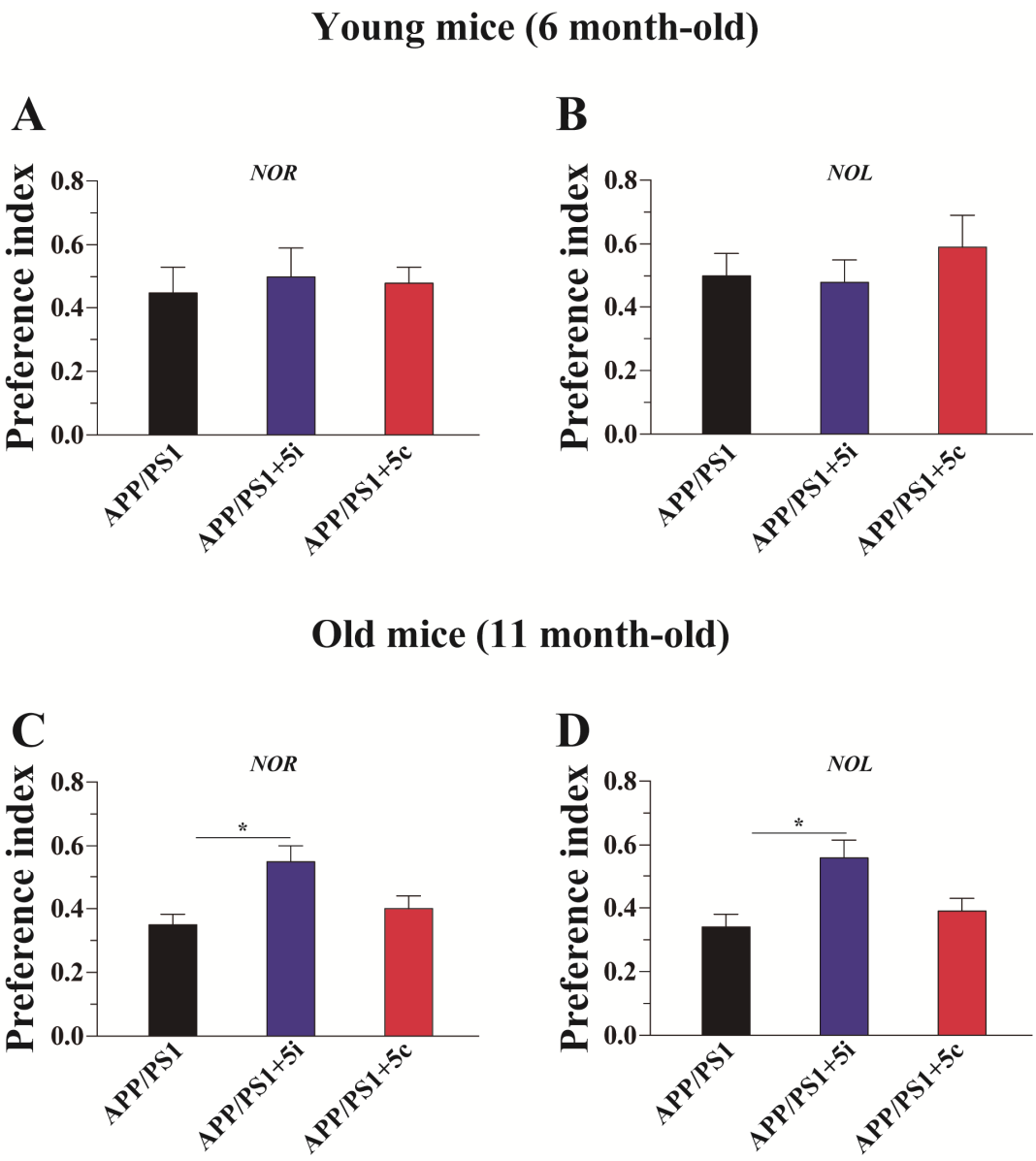

Figure 8. Preference indices in the NOR and NOL tests with (A, B) young and (C, D) old male APP/PS1 mice treated with vehicle, **5c**, and **5i**. Data are expressed as mean values ± SEM of n = 7 animals in each group. Data were analyzed by one-way ANOVA, followed by Bonferroni's post hoc test; *$p \leq 0.05$ was considered the threshold for statistical significance with 95% CI.

Next, we performed a highly sensitive memory flexibility test to assess learning and memory performance,[78] based on the ability of mice to find a hidden platform within a pool, similarly to the Morris Water Maze. In the case of young transgenic mice, we did not observe significant differences among groups (Figure 9A). However, some differences were found when comparing the performance of the different groups of old transgenic mice already on the first trial day, with the **5i**-treated APP/PS1 mice needing 13 trials to reach criterion, whereas **5c**- and vehicle-treated mice needed 14 trials. After 4 days of testing, old APP/PS1 mice treated with vehicle or compound **5c** needed 13 trials to reach criterion, whereas those treated with compound **5i** needed only 7 trials, showing that the treatment with **5i** significantly delayed the cognitive decline that affected memory/learning of old transgenic mice (one-way ANOVA, $p < 0.05$, followed by appropriate post hoc testing) (Figure 9B).

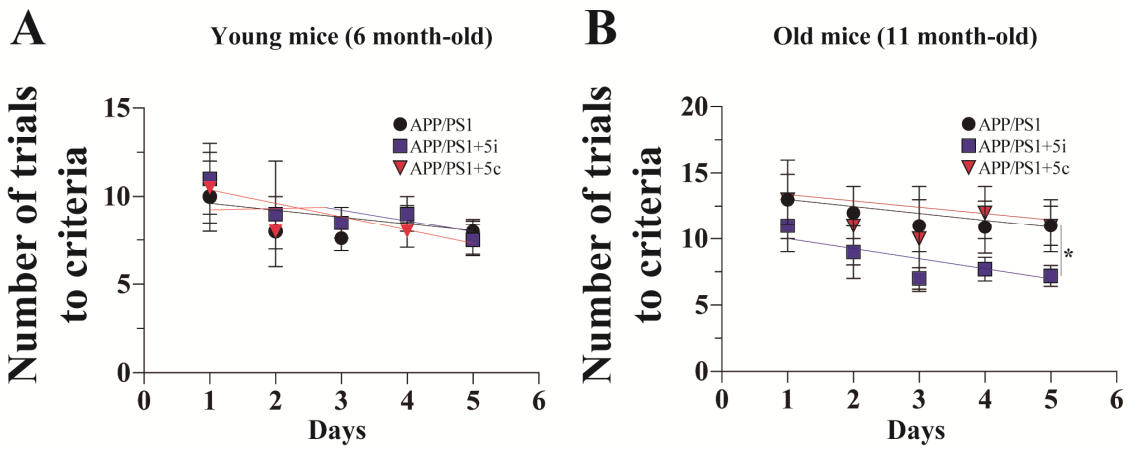

Figure 9. Number of trials to reach criterion in the memory flexibility test in (A) young and (B) old male APP/PS1 mice treated with vehicle, **5c**, and **5i**. Data are expressed as mean values ± SEM of n = 7 animals in each group. Data were analyzed by one-way ANOVA, followed by Bonferroni's post hoc test; *$p \leq 0.05$ was considered the threshold for statistical significance with 95% CI.

Thus, compound **5i** significantly enhanced learning and memory in old APP/PS1 mice in all the performed tests (NOR, NOL, and memory flexibility), while neither **5i** nor **5c** were effective in young transgenic mice.

Effects on Hippocampal β-Amyloid Levels. After the behavioral studies had been completed, the brains of control and treated transgenic mice were collected for analyses. A specific ELISA assay kit was used to evaluate the levels of Aβ40 and Aβ42 in the hippocampus of young and old APP/PS1 mice treated with vehicle, **5c** or **5i**. Similar hippocampal levels of both Aβ40 and Aβ42 were found in young transgenic mice treated with **5c** or **5i** compared with vehicle-treated mice (Figure 10A–C and Table S6 of the Supporting Information). Actually, a positive tendency, albeit statistically nonsignificant, toward increased Aβ40 and decreased Aβ42 levels, and, hence toward a reduced Aβ42/Aβ40 ratio, was found in APP/PS1 mice treated with **5i** relative to the control group. Interestingly, the beneficial effects of **5i** on β-amyloid levels did reach statistical significance in old transgenic mice. Indeed, a significant increase (2.1-fold) in the levels of Aβ40, the less aggregation-prone and less toxic Aβ form, was observed in the hippocampus of old APP/PS1 mice treated with **5i** (18.4 ± 1.24 pg/mL), compared with vehicle-treated control mice (8.65 ± 0.44 pg/mL) (Figure 10D and Table S6 of the Supporting Information), whereas the levels of the more neurotoxic Aβ42 remained unaffected by the treatment (62.6 ± 3.68 pg/mL in APP/PS1 mice treated with **5i** vs 69.0 ± 4.54 pg/mL in vehicle-treated APP/PS1 mice, Figure 10E). Thus, treatment of 11-month-old transgenic mice with compound **5i** led to a significant decrease in the Aβ42/Aβ40 ratio (3.42 ± 0.36 in APP/PS1 mice treated with **5i** vs 7.99 ± 0.60 in vehicle-treated APP/PS1 mice, Figure 10F and Table S6 of the Supporting Information), which

is an important marker of the progression of AD, with this reduced ratio being indicative of a delaying effect on disease progression.

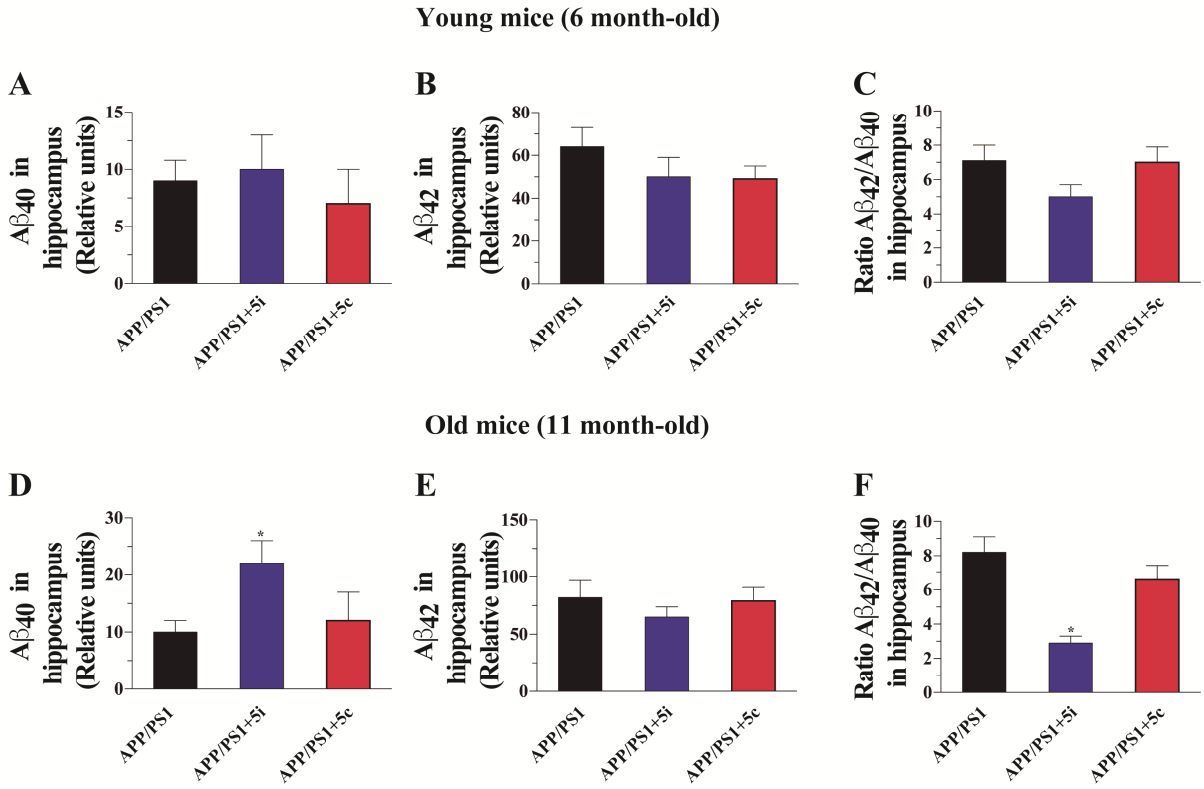

Figure 10. Hippocampal levels of Aβ40, Aβ42, and Aβ42/Aβ40 ratio in (A–C) young and (D–F) old male APP/PS1 mice treated with vehicle, **5c**, or **5i**. Data are expressed as mean values ± SEM of n = 7 animals in each group. Data were analyzed by one-way ANOVA, followed by Bonferroni's post hoc test; *p ≤ 0.05 was considered the threshold for statistical significance with 95% CI.

Electrophysiological Studies. Effects on Basal Activity and Synaptic Plasticity in APP/PS1 Mice Treated with 5c or 5i. Among the alterations that are described for AD patients and

animal models, synaptic anomalies appear long before amyloid plaques and neuronal death can be detected.[79,80] Several AD models have been used to investigate the relationship between synaptic dysfunction and age.[81] A reduction in long-term synaptic potentiation, with no alteration in basal transmisision have been reported in several variants of the APP/PS1 mouse model.[82] To elucidate the effects of treatment with compounds **5c** and **5i** on synaptic transmission and plasticity mechanisms, we performed electrophysiological experiments in brain slices obtained from young double transgenic mice that had been treated for 4 weeks with either **5c**, **5i**, or saline (control). We stimulated the collateral axons at the CA3 area of hippocampus and recorded the evoked field excitatory postsynaptic potentials (fEPSPs) at the level of the CA1 region. First, we analyzed the paired pulse facilitation (PPF), which is a presynaptic form of plasticity indicative of short-term plasticity, with the purpose of measuring the probability of release at presynaptic terminals. To do this, we evoked two EPSPs (R1 and R2) separated by time intervals of 10–200 ms. The ratio R2/R1 is the facilitation index, which measures the probability of vesicle release at the presynaptic terminal by effect of the level of accumulated calcium: an index larger than 1 indicates that R2 is larger than R1, showing that more synaptic vesicles are released in the second pulse due to the accumulation of intracellular calcium (Figure 11A). This is called facilitation and demonstrates that a synapse has low probability of vesicle release in the first pulse. The longer the time interval between the two pulses, the lower the ratio, indicating that the calcium that entered during R1 had more time to be cleared before R2. In our case, there is a significant difference between treatments, with these differences being more evident at the first interval (at 10 ms stimulus interval). Treatment with **5i** increased the probability of vesicle release in the first pulse, reducing the facilitation, as compared to vehicle- and **5c**-treated animals (Figure 11A, index at 10 ms time interval: control: 3.18 ± 0.8 ms;

transgenic (Tg) ± **5i**: 1.93 ± 0.03 ms; Tg ± **5c**: 3.44 ± 0.6 ms; two-way AVOVA followed by Bonferroni's post-hoc test, Tg + **5i** vs Tg + **5c**, *p < 0.05). Thus, **5i** transforms a synapse with low release probability into a high release probability synapse. Next, by applying increasing levels of current intensities, we obtained an input–output relationship that determined the maximum capacity of the system to evoke responses when an increasing stimulus is applied (Figure 11B). The plots of the fEPSP slope against stimulus amplitude (Figure 11C) shows no difference between the curves, indicating that treatment with **5c** or **5i** does not affect the basal synaptic activity of young transgenic mice (Figure 11C, values at the maximum current intensity: Tg control = 0.269 ± 0.072 mV/ms; Tg + **5i** = 0.296 ± 0.089 mV/ms; Tg + **5c** = 0.262 ± 0.096 mV/ms; p = 0.713). We also built the input–output relationship with the fiber volley (FV) amplitudes, and despite that two-way ANOVA analysis suggested differences among treatments, post-hoc analysis showed that the differences between treated animals and the control group were not significant (Figure 11D, values at the maximum current intensity: Tg control = 0.719 ± 0.175 mV/ms; Tg + **5i** = 0.738 ± 0.243 mV/ms; Tg + **5c** = 0.399 ± 0.111 mV/ms; p = 0.088). These data indicate that the treatment with **5c** and **5i** does not affect the number of axons recruited, and thus the excitability during basal synaptic transmission in young transgenic mice.

Then, we studied how effective was the correlation between the axonal recruitment and the evoked response. To do that, we built a plot from FV amplitudes and EPSP slopes. We applied linear regression and then compared the slopes obtained for the three experimental conditions (Figure 11E). A significant positive correlation between FV amplitude and fEPSP slopes was obtained in all three cases and showed that the three groups differ significantly from each other (Figure 11E, see also Supporting Information for more details). Thus, in young transgenic mice treatment with both **5c** amd **5i** improved the efficacy of synaptic transmission

per activated axon; indeed, both compounds increased the effectiveness in basal transmission relative to vehicle-treated animals, with **5c** exerting a stronger effect than **5i**.

As it has been extensively studied, APP/PS1 mice show deficient generation of synaptic plasticity in the form of hippocampal long-term potentiation (LTP).[83−85] We therefore evaluated whether the chronic treatment of APP/PS1 mice with **5c** or **5i** could affect LTP in young transgenic mice (Figure 11F). To that end, we first obtained stable recording for at least 15 min and then applied a theta burst stimulation (TBS) protocol to induce LTP. After that, the recording for more than 1 h was compared to the basal time before TBS to quantify the amount of LTP generated, which was shown as the relative change (Figure 11F). Some examples of the evoked fEPSP before and after LTP induction are shown in Figure 11F, inset. The graph shows that all three experimental groups can generate a significant amount of LTP, taking into account that these are transgenic animals and that at this age they start to display some synaptic deficiencies. However, young transgenic mice treated with both **5i** or **5c** displayed significantly higher LTP compared to the transgenic control group (average of the last 10 min (gray area): Tg control: 134.1 ± 13.1%; Tg + **5i**: 397.3 ± 23.7%; Tg + **5c**: 275.6 ± 61.5% of baseline; one-way ANOVA followed by Bonferroni's post-hoc test, ***$p < 0.001$). These results indicate that treatment with both **5i** and **5c** significantly affects the postsynaptic mechanisms involved in LTP in young transgenic mice, improving plasticity.

Furthermore, to determine whether these differences in the level of LTP response were due to the status of the synapses before and after LTP induction in the three treatment groups, we plotted the input–output function before and after LTP induction (Figure 11G). To do this, we averaged the FV amplitudes and the fEPSP slopes of all the experiments used to calculate LTP. We then plotted these measurements of FV amplitude and slopes both before (Figure 11G, open

symbols within circle) and after TBS (Figure 11G, closed symbols). The recordings were stable with time, because the amplitude of FV did not change before and after LTP induction, which indicates that the same presynaptic fibers are being recruited and that the differences seen are due only to postsynaptic effects (for more details see the Supporting Information). We then determined whether the correlation of FV amplitudes with fEPSP slopes was significantly different across the groups and found that all the correlations were statistically significant (for more details see the Supporting Information). Interestingly, the treatment with compounds **5c** and **5i** reduced the number of recruited axons (lower FV amplitudes), compared to control, to produce almost the same evoked response during basal activity. In all cases, after TBS or during LTP induction, the correlation in all three groups significantly increased after the induction of LTP, especially in mice treated with the compounds. The correlation 'r' in all three groups increased after the induction of LTP, especially in the mice groups treated with the compounds, becoming significantly different among groups. Taken together, these data indicate that in young animals both treatments led to a structural change that made synaptic transmission more efficient, with these changes influencing the postsynaptic mechanisms that induce plasticity.

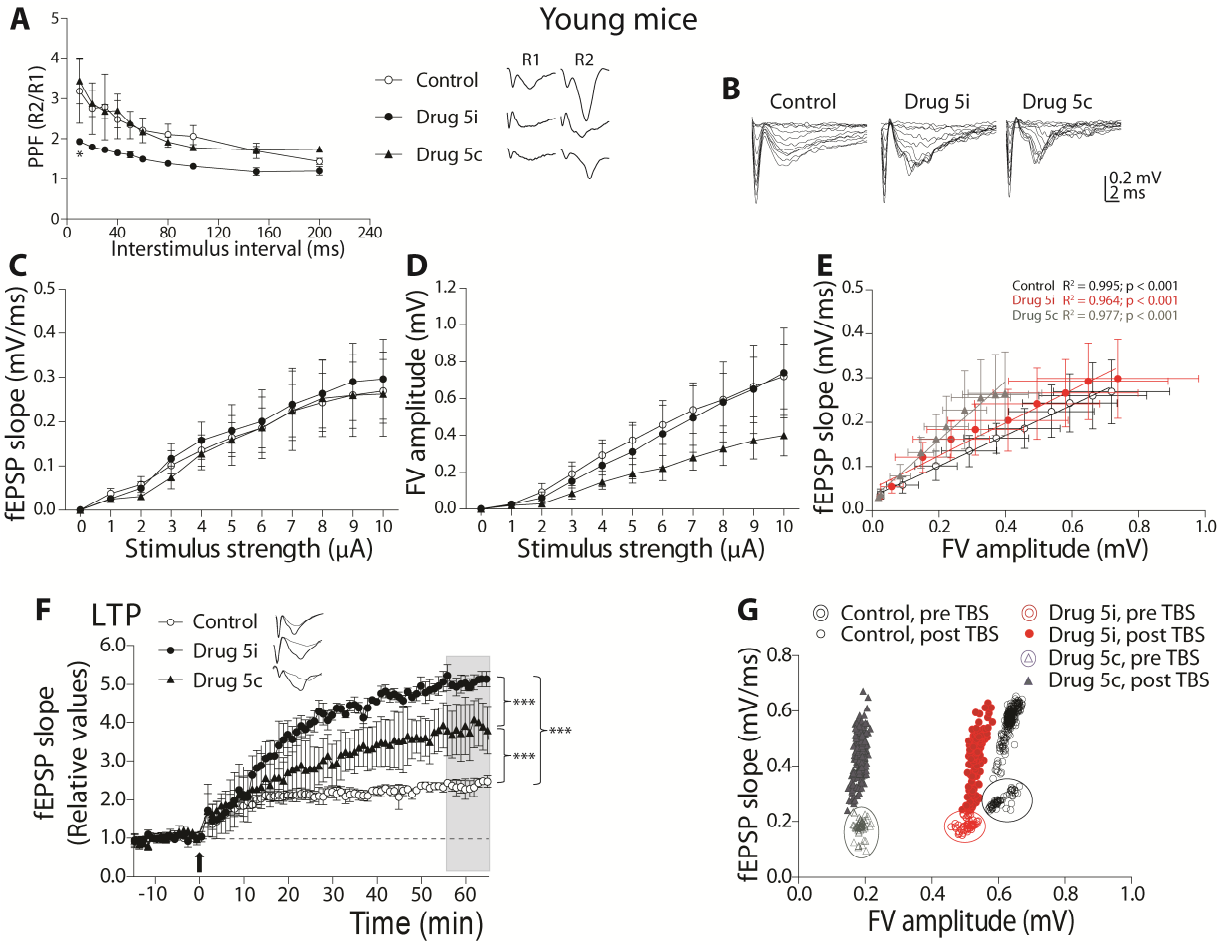

Figure 11. Synaptic transmission efficacy and plasticity mechanisms are affected in young male APP/PS1 mice treated with compounds **5c** and **5i**. (A) The PPF plot shows the ratio of the second versus the first fEPSP slope (R2/R1), recorded at different time intervals (10, 20, 30, 50, 60, 80, 100, 150, and 200 ms), showing that only at the beginning short-term plasticity was different in **5i**-treated animals compared with vehicle- and **5c**-treated mice. Tg control (open circles), Tg + **5i** (black circles) and Tg + **5c** (black triangles). Representative traces of two evoked fEPSPs separated by 20 ms (inset). (B) Representative traces of postsynaptic potentials evoked by increasing stimulus intensities (µA). Input–output curves of both fEPSP slope (C) and fiber volley amplitude (D) against stimulus intensity. (E) The correlations between FV amplitude and

fEPSP slope were adjusted by linear regressions and found to significantly differ from each other. (F) LTP plot, where fEPSPs slopes after TBS (arrow) were normalized to slopes during basal time. (G) Correlation plot between FV amplitudes and fEPSP slopes of three groups, before TBS (pre-TBS, open symbols within circle) and after TBS (post-TBS, solid symbols); all comparisons were found significant among groups. Data represent the mean ± SEM from 9 slices out of 3 Tg control mice, 9 slices out of 3 Tg + **5i** mice, and 9 slices out of 3 Tg + **5c** mice. Analysis by one-way or two-way ANOVA, followed by Bonferroni's post hoc test, *$p < 0.05$, **$p < 0.01$, ***$p < 0.001$.

To assess the effects of **5c** and **5i** on basal activity and synaptic plasticity of 11-month-old APP/PS1 mice, we performed the same experiments and analyses previously described for the young mice. Thus, we analyzed the PPF curve, which, as previously mentioned, is a presynaptic form of plasticity indicative of short-term plasticity (Figure 12A). In old transgenic mice, no significant difference was found among the groups, indicating that calcium-dependent vesicle release was not affected by treatment with either **5c** or **5i** as compared to control (Figure 12A, index at 10 ms time interval: Tg control: 2.05 ± 0.2 ms; Tg ± **5i**: 1.96 ± 0.02 ms; Tg ± **5c**: 2.32 ± 0.1 ms; two-way ANOVA, $p = 0.097$). Next, the input–output relationship was built in the three cases (Figure 12B) and plotted with the fEPSP slopes (Figure 12C) and the fiber volley (Figure 12D). Interestingly, the plots of the fEPSP slopes against the stimulus amplitude showed that the control curve was significantly lower and different from the other two, indicating that the treatment with both **5c** and **5i** did affect basal synaptic activity in old transgenic mice (Figure 12C, values at the maximum current intensity: Tg control = 0.293 ± 0.105 mV/ms; Tg + **5i** = 0.652 ± 0.107 mV/ms; Tg + **5c** = 0.545 ± 0.083 mV/ms; two-way ANOVA followed by

Bonferroni's post-hoc test, *p < 0.05, **p < 0.01, ***p < 0.001). In contrast, the FV input–output plot showed no significant difference among the groups (Figure 12D, values at the maximum current intensity: Tg control = 0.826 ± 0.169 mV; Tg + **5i** = 1.039 ± 0.245 mV; Tg + **5c** = 0.808 ± 0.069 mV; two-way ANOVA followed by Bonferroni's post-hoc test, p = 0.088). Unlike what was observed in young mice, old APP/PS1 mice treated with compounds **5i** and **5c** showed an enhanced basal synaptic transmission, without the number of axons recruited being affected.

We also plotted the correlation between FV amplitude and fEPSP slopes obtained in the input–output protocol. We adjusted the plots by linear regression and then compared them under the three experimental conditions (Figure 12E). There was a positive correlation between FV amplitude and fEPSP slopes in all the three conditions (Figure 12E, for details see the Supporting Information). Also, the analysis between regressions revealed significant differences across them. The analyses indicated that in the old APP/PS1 mice treatment with either **5i** or **5c** improved the strength of synaptic transmission per activated axon compared to the control, thus increasing the efficacy of basal transmission.

Next, we evaluated the effect of **5i** and **5c** on LTP in old transgenic mice. Some representative traces of evoked fEPSPs before and after LTP induction are shown in Figure 12F, inset. The plot shows that in all three experimental groups some degree of LTP can be generated, but that there are no significant differences among the groups (average of the last 10 min (gray area), Tg control: 83.9 ± 21.1%; Tg + **5i**: 111.0 ± 45.0%; Tg + **5c**: 124.3 ± 16.8% of baseline; one-way ANOVA, followed by Bonferroni's post-hoc test: p = 0.25). Thus, in the old animals neither **5c** nor **5i** significantly improved the postsynaptic mechanisms involved in LTP.

As we had done for the young mice, we compared the synaptic status of the old transgenic mice, during induction of long-term plasticity, under the same three conditions. We plotted the input–output function with the average measurements of FV amplitude and slopes, before and after TBS (Figure 12G). Unlike what was found in young mice, in old animals both the FV amplitude and the evoked response values for the control and the **5i**-treated group were similar and differed from the **5c**-treated group (see the Supporting Information). Thus, the effects of **5i** in old mice were different from those found in young mice. In contract, the effects of **5c** on synaptic activity of old mice were more similar to those exerted by this compound in young animals. Thus, **5c** can change the effectiveness of synaptic transmission between FV amplitude and fEPSP slope before and after LTP induction, even though it does not affect the mechanisms to induce LTP.

Taken together, the electrophysiological measurements show that treatment with both **5c** and **5i** affects synaptic transmission. Indeed, both compounds improve the efficacy of basal synaptic transmission, with no change in the presynaptic calcium-dependent release mechanism, in either young or old animals. Other mechanisms could be involved in producing the effects observed, such as changes in the number of vesicles or at the active sites. Changes in quantal amplitude may also contribute, by increasing postsynaptic receptors levels. Regarding plasticity phenomena, both **5i** and **5c** improved long-term plasticity in young but not in old mice, suggesting that changes at the level of LTP induced by these compounds can provide a protective mechanism to preserve synaptic plasticity and brain connectivity in young circuits. We cannot, however, rule out the possibility that the old mice might respond to a more prolonged treatment regime.

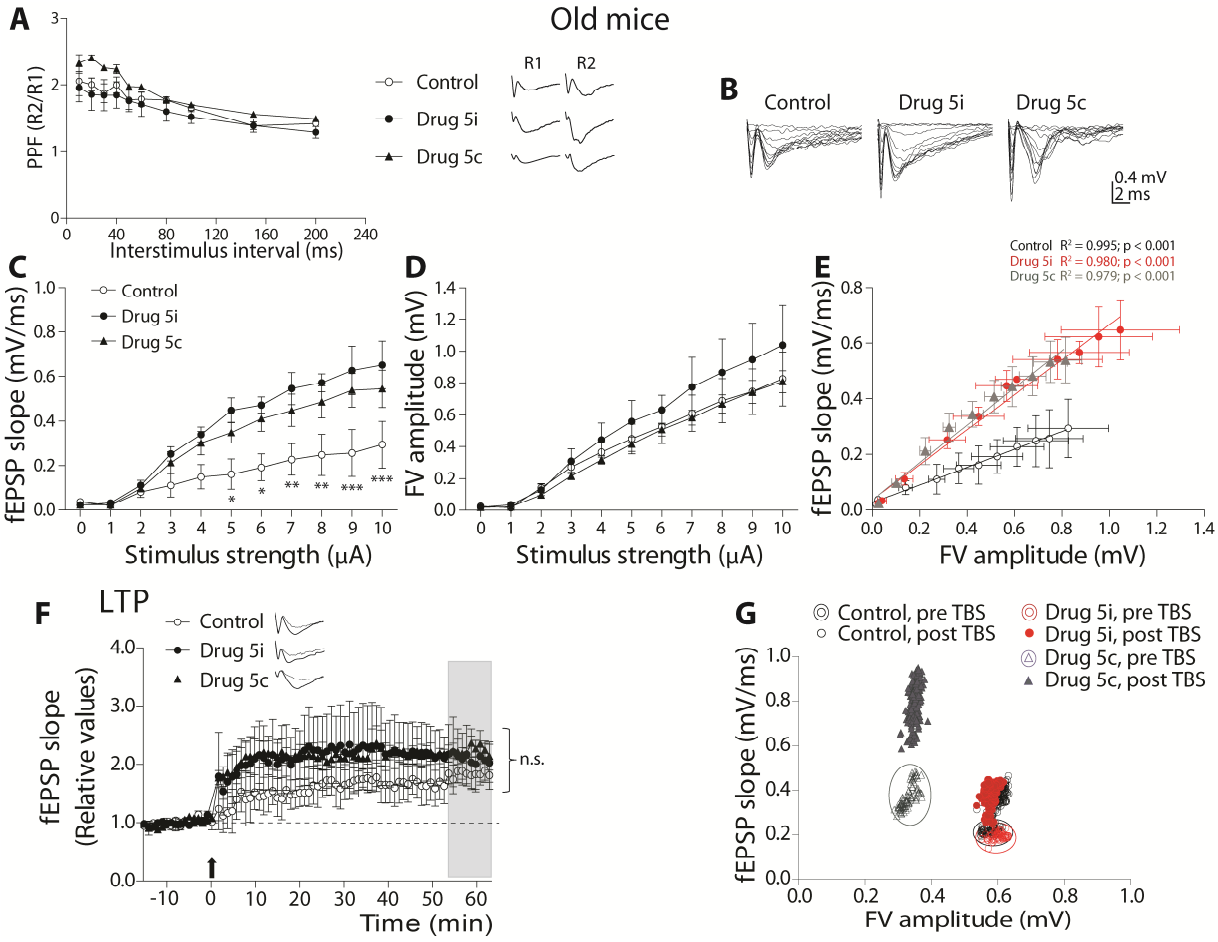

Figure 12. Synaptic transmission efficacy but not plasticity mechanisms are affected in old male APP/PS1 mice treated with compounds **5i** and **5c**. (A) The PPF plot shows the ratio of the second versus the first fEPSP slopes (R2/R1), recorded at various time intervals (10, 20, 30, 50, 60, 80, 100, 150, and 200 ms), showing that short-term plasticity was not significantly changed by treatment with **5i** or **5c**. Tg control (open circles), Tg + **5i** (black circles) and Tg + **5c** (black triangles). Representative traces of two evoked fEPSPs separated by 20 ms (inset). (B) Representative traces of postsynaptic potentials evoked by increasing stimulus intensities (µA). Their input–output curves of both fEPSP slope (C) and fiber volley amplitude (D) against stimulus intensity. (E) The correlations between FV amplitude and fEPSP slope were adjusted by linear regression and revealed that both **5i** and **5c** differ from the control. (F) LTP plot, where

fEPSPs slope after TBS (arrow) were normalized to slopes during basal time. (G) Correlation plot between FV amplitudes and fEPSP slopes of three groups, before TBS (pre-TBS, open symbols within circle) and after TBS (post-TBS, solid symbols); control and Tg + **5i** do not differ from each other, but both differ from Tg + **5c**. Data represent the mean ± SEM from 9 slices out of 3 Tg control mice, 9 slices out of 3 Tg + **5i** mice, and 9 slices out of 3 Tg + **5c** mice. Analysis by two-way ANOVA, followed by Bonferroni's post hoc test, *$p < 0.05$, **$p < 0.01$, ***$p < 0.001$.

Effects on the Levels of Oxidative Stress and Neuroinflammation Markers in Hippocampus of APP/PS1 Mice

To determine if chronic treatment of APP/PS1 mice with compounds **5i** and **5c** induced beneficial effects against oxidative stress, we measured the levels of 4-hydroxy-2-nonenal (4-HNE). Plasma membrane integrity is essential for neuronal signaling. 4-HNE is a reactive α,β-unsaturated aldehyde arising from lipid peroxidation that serves as a marker of plasma membrane oxidative damage.[86] No differences in hippocampal levels of 4-HNE were found among young APP/PS1 mice treated with vehicle, **5i**, or **5c** (Figure 13A,C). However, in old APP/PS1 mice **5c** and **5i** induced a significant decrease in the hippocampal levels of 4-HNE compared with the control group (Figure 13B,D). These results suggest that chronic administration of both **5c** and **5i** rescues old APP/PS1 mice from the oxidative stress characteristic of their Alzheimer-like pathology. Thus, notwithstanding the fact that the antioxidant activity measured in vitro for **5c** and **5i** is not well balanced with their anticholinesterase potencies, an antioxidant effect of these compounds is eventually operating in

vivo, even though alternative mechanisms other than a direct antioxidant effect cannot be ruled out.

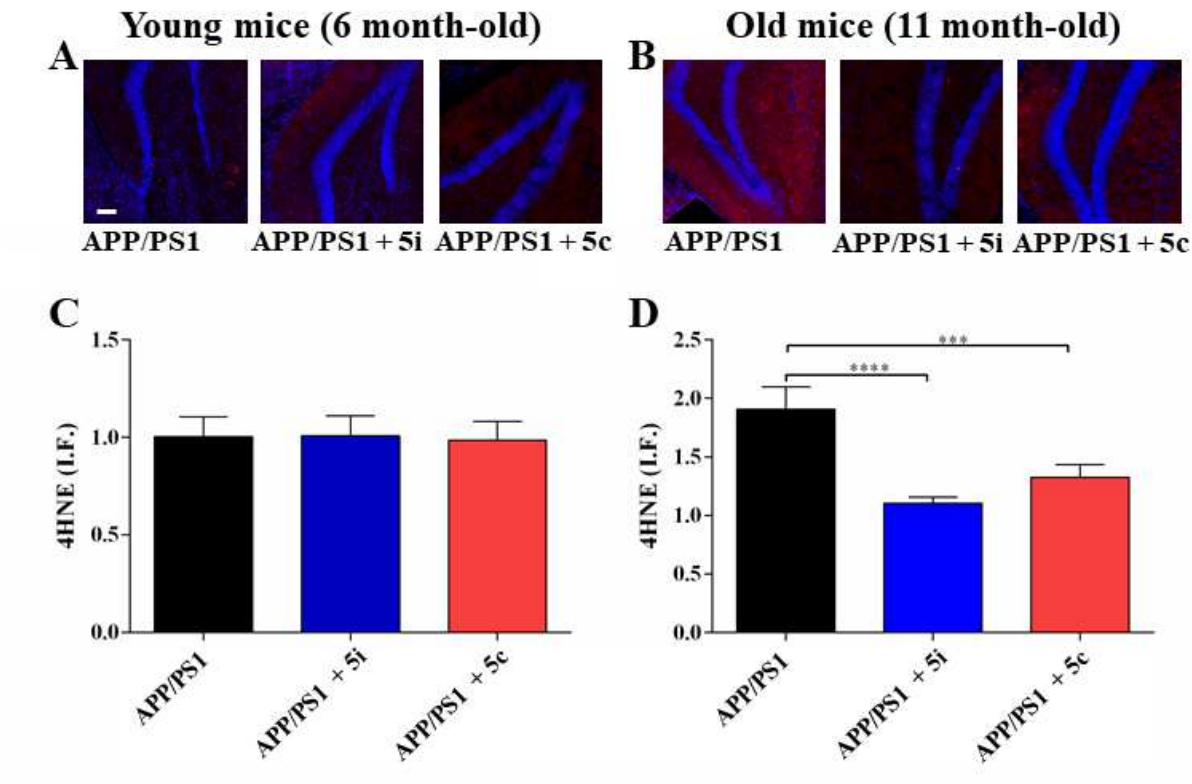

Figure 13. Representative immunofluorescence of the hippocampal levels of 4-HNE (4-HNE, red; nuclear stain Hoechst, blue) in (A, C) young and (B, D) old male APP/PS1 mice treated with vehicle, **5i**, or **5c**. Data are expressed as mean values ± SEM of n = 4 animals per group. Data were analyzed statistically by one-way ANOVA followed by Bonferroni's post hoc test. ***p < 0.001; ****p < 0.0001. Scale bar: 100 μm.

Next, we measured the levels of glial fibrillary acidic protein (GFAP), a well-known marker of astrogliosis, a reactive inflammatory state of astrocytes in response to neurodegeneration during

AD progression.[87] GFAP levels were significantly reduced in young APP/PS1 mice treated with **5c**, but not with **5i**, relative to vehicle-treated animals (Figure 14A,C). Chronic treatment of old APP/PS1 mice with both **5c** and **5i** led to a significant decrease in hippocampal levels of GFAP compared with vehicle-treated animals, with **5i** exerting a more pronounced effect (Figure 14B,D). Thus, chronic treatment with **5i** and **5c** alleviated neuroinflammation in the hippocampus of APP/PS1 mice, especially in the old animals.

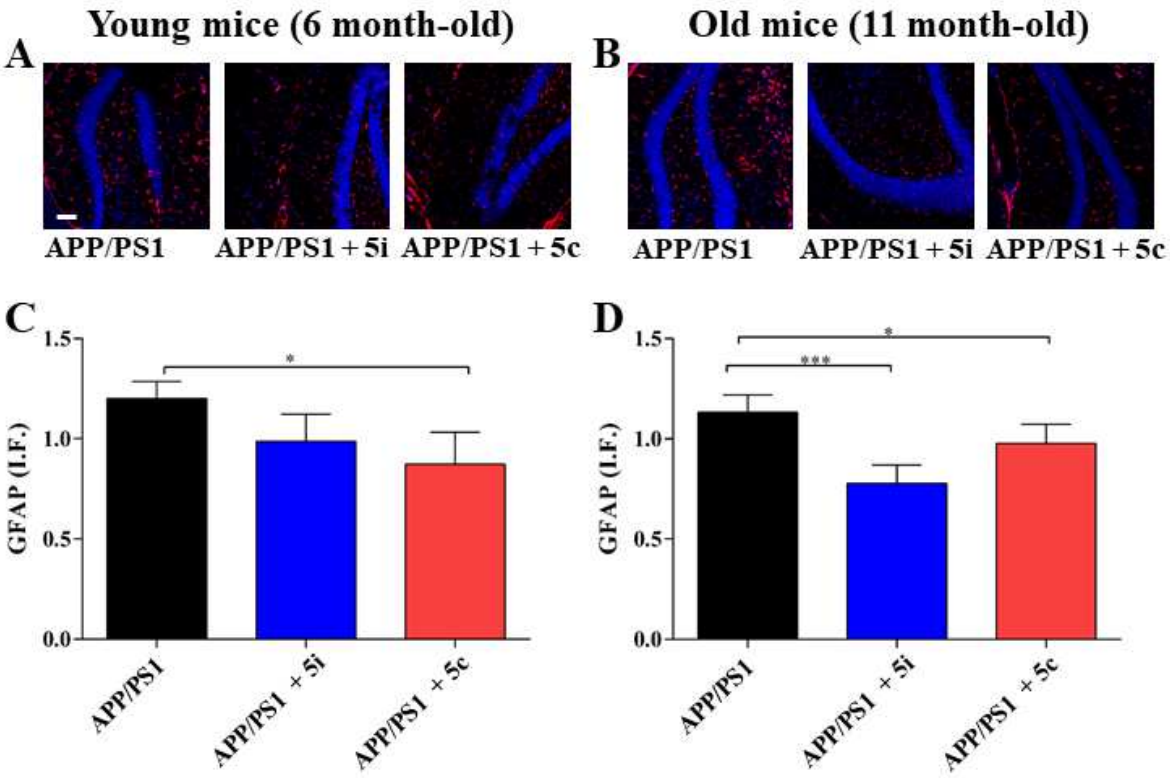

Figure 14. Representative immunofluorescence of the hippocampal levels of GFAP (GFAP, red; nuclear stain Hoechst, blue) in (A, C) young and (B, D) old male APP/PS1 mice treated with vehicle, **5i**, or **5c**. Data are expressed as mean values ± SEM of n = 4 animals per group. Data

were analyzed statistically by one-way ANOVA followed by Bonferroni's post hoc test. *$p < 0.05$; ***$p < 0.001$. Scale bar: 100 μm.

CONCLUSIONS

The difficult-to-refute argument that complex multifactorial diseases, such as AD, may be more efficiently tackled with therapeutic regimes that simultaneously hit several key targets or pathological events has spurred very intensive research on MTDLs. Suitably designed huprine derivatives have already shown to be valuable MTDLs for the treatment of AD, allowing not only AChE and BChE inhibition, but also modulation of other targets, such as BACE-1, oxidative stress, and tau pathology.[56–58,62] Capsaicin has been shown to be endowed with a set of activities of high value in the context of AD treatment, including beneficial effects in vivo against oxidative stress and neuroinflammation,[41–45] and enhancement of hippocampal LTP and synaptic function, which eventually lead to improved cognition.[46-49] Based on these premises, we hipothesized that combination of the scaffolds of capsaicin and a huprine might result in hybrid compounds with the potential to address several major pathologies associated with AD, namely cholinergic deficit, oxidative stress, neuroinflammation, synaptic dysfunction, and cognitive impairment. HC hybrids were generated by introduction of a variety of linkers (alkanamide, alkenamide, and benzamide) at position 12 of the huprine scaffold or a triazolylbutyl linker at position 9. All compounds retained the in vitro beneficial activities of the two parent moieties, i.e., they potently inhibited both AChE and BChE, and showed antioxidative activities comparable to those of capsaicin, demonstrating that derivatization does not result in a loss of function.

The observation that all 12-HC compounds are potent hBChE inhibitors shows that they are able to bind efficiently to hBChE, although presumably in a non-native conformation that differs

from the canonical binding mode of huprines in complexes with *Tc*AChE substantially enough to eliminate crystal packing interactions. In the 12-HC series, compound **5c** stands out, displaying subnanomolar inhibitory activity against hAChE, a reduced AChE-over-BChE selectivity ratio of 40, relative to the parent huprine Y (selectivity ratio = 169), antioxidant properties comparable to those of the parent capsacin, moderate BACE-1 inhibition, and a strong predicted permeability across the BBB.

While compounds derivatized on position 12 were, in general, active against BACE-1, derivatization at position 9 resulted in a compound, **5i**, which was inactive against BACE-1, but displayed comparably high affinity for hAChE and hBChE. With an AChE-over-BChE selectivity ratio of 6.9, **5i** presents a 25-fold improvement in affinity for hBChE, with respect to the parent huprine Y. The structure of its complex with hBChE rationalised this observation, revealing a completely new binding mode, in which the chorine atom of the huprine moiety fits in the acyl- instead of the choline-binding pocket, while its primary amino group is stabilized between the catalytic serine (Ser198 in hBChE) and histidine (His438 in hBChE), effectively disrupting the triad. Since derivatization at position 12 involves the amino group, this peculiar binding mode is inaccessible to compounds of the 12-HC series. Interestingly, binding of **5i** to BChE exploits all the differences in active-site gorge architecture between hAChE and hBChE, i.e., differences in the acyl- and choline-binding pocket of the CAS, and at the PAS. It is, therefore, unlikely that this binding mode would occur in AChE. Indeed, the structures of six HC hybrid–*Tc*AChE complexes (including **5i**) revealed the canonical binding mode, i.e., with the chlorine atom fitting into the choline-binding pocket and the amine facing the upper part of the gorge. Derivatization at position 9 of huprines thus emerges as a viable option for overcoming the AChE-over-BChE specificity of huprine derivatives and could be further exploited to

produce BChE-specific MTDLs, e.g., by further functionalization of the triazole linker. Since hBChE activity increases and co-localizes with plaques and neurofibrillary tangles in the brains of AD patients,[88] hBChE-specific inhibitors could prove to be valuable tools for both treatment and diagnosis of AD. Nonetheless, a compound such as **5i**, which displays similar affinity for hAChE and hBChE, could already prove beneficial in the clinic, allowing simultaneous inhibition of the two enzymes involved in cholinergic breakdown by use of a single, highly potent compound.

The good brain permeability of the novel compounds, measured in vitro by the PAMPA-BBB assay, was confirmed for compounds **5c** and **5i** by biodistribution studies in wild-type mice, using the same dosing protocol that was later used for the in vivo efficacy studies. Despite the apparent higher polarity and lower PAMPA-BBB permeability of hybrid **5i**, its brain concentration and brain/plasma ratio were significantly higher than those of both **5c** and the reference anti-AD drug donepezil.

Chronic administration of **5c** and **5i** (2 mg/kg, ip, 3 times per week, 4 weeks) to 5- and 10-month-old APP/PS1 mice was well tolerated, with all the animals remaining healthy at the end of the treatment, according to weight, lipid and hepatic parameters, and by visual inspection. Moreover, chronic treatment did not induce locomotor or stress problems, as found in LOF tests, thereby ruling out potential interferences of the basal status of the animals when assessing the effects of the compounds on learning and memory in the subsequent behavioral assays.

Neither **5c** nor **5i** exerted beneficial effects in young transgenic mice as compared with the vehicle-treated group. Only in electrophysiological studies were positive effects found, with both compounds increasing the effectiveness of basal synaptic transmission relative to vehicle-treated animals and both increasing LTP, as well, thereby improving synaptic plasticity. In addition, **5c**

was found to significantly reduce the neuroinflammation marker GFAP in the hippocampus of young transgenic mice, compared with the control group.

The beneficial in vivo effects were much more prominent in the old APP/PS1 mice, especially for **5i**. This compound significantly enhanced learning and memory of the old transgenic mice, compared to the control group, in three behavioral tests (NOR, NOL, and the memory flexibility tests). Furthermore, **5i** significantly increased the hippocampal levels of the less neurotoxic Aβ40 (2.1-fold relative to vehicle-treated mice), while leaving unaltered the levels of the more aggregation-prone and neurotoxic Aβ42. Thus, **5i**-treatment led to a significant decrease of the Aβ42/Aβ40 ratio, which is a marker of AD progression, with this reduced ratio being indicative of a delayed disease progression, and, hence, of a disease-modifying effect. In addition, it was found that **5i** significantly increased the strength of synaptic transmission, without affecting LTP, in contrast to its effects in young mice. The beneficial effect on basal synaptic efficacy was also found in old mice treated with **5c**. Finally, chronic treatment with both **5i** and **5c** significantly reduced hippocampal levels of the oxidative stress marker 4-HNE and the neuroinflammation (astrogliosis) marker GFAP, with **5i** exerting a more pronounced effect on both markers.

Likely, the very strong hAChE and hBChE inhibitory activity of **5i**, as well as other modes of action due to the presence of the capsaicin moiety, account for its cognition-enhancing effect. The in vivo effects of **5i** on several underlying disease mechanisms, especially its beneficial effects on synaptic function, oxidative stress, and neuroinflammation, might also result from the presence of the capsaicin scaffold in its structure. Indeed, capsaicin has been reported to improve synaptic and cognitive functions and to reduce oxidative stress and neuroinflammation, by activation of transient receptor potential vanillin 1 (TRPV1).[50,51] This mechanism might be also

underlying the disease-modifying effects exerted by compound **5i**, which emerges as a promising new anti-Alzheimer lead compound.

EXPERIMENTAL SECTION

Chemistry. Melting points were determined in open capillary tubes with a MFB 595010M Gallenkamp melting point apparatus. 400 MHz ^{1}H/101 MHz ^{13}C NMR were recorded on a Varian Mercury 400 spectrometer, 200 MHz ^{1}H NMR and 300 MHz ^{1}H/75 MHz ^{13}C NMR were recorded on a Bruker 200 or 300 MHz spectrometer. The chemical shifts are reported in ppm (δ scale) and coupling constants are reported in Hertz (Hz). Assignments given for the NMR spectra of the new compounds were made by comparison with the NMR data of hybrids **5b**, **5f**, **5g**, **5i**, **7**, and **14** as model compounds, which in turn, were assigned on the basis of DEPT, COSY ^{1}H/^{1}H (standard procedures), and COSY ^{1}H/^{13}C (gHSQC and gHMBC sequences) experiments. The *syn* (*anti*) notation of the protons at position 13 of the huprine moiety of the hybrids means that the corresponding proton at position 13 is on the same (different) side of the quinoline moiety with respect to the cyclohexene ring. IR spectra were run on a Perkin-Elmer Spectrum RX I spectrophotometer. Absorption values are expressed as wavenumbers (cm^{-1}); only significant absorption bands are given. Column chromatography was performed on silica gel 60 AC.C (40−60 mesh, SDS, ref 2000027). Thin-layer chromatography was performed with aluminum-backed sheets with silica gel 60 F_{254} (Merck, ref 1.05554), and spots were visualized with UV light and 1% aqueous $KMnO_4$. Elemental analyses were carried out at the Mycroanalysis Service of the IIQAB (CSIC, Barcelona, Spain) with a Carlo Erba 1106 analyzer. HPLC purity measurements were performed with a Thermo Scientific Surveyor Plus instrument equipped with a PDA detector (Method A, acetonitrile/H_2O (0.10% TFA), flow rate 1 mL/min,

det. 254–330 nm). HRMS were obtained with LC/MSD TOF Agilent Technologies or Varian MAT 311 spectrometers, using an electrospray source. The analytical samples of the HC hybrids that were subjected to pharmacological evaluation possess a purity ≥95% as indicated by their elemental analyses or HPLC measurements.

5-[(3-Chloro-6,7,10,11-tetrahydro-9-methyl-7,11-methanocycloocta[*b*]quinolin-12-yl)amino]-*N*-(4-hydroxy-3-methoxybenzyl)pentanamide (5a). A solution of nitrile **3a** (1.43 g, 3.91 mmol) in MeOH (5 mL) was treated with a 40% solution of KOH in MeOH (10 mL) and the mixture was stirred under reflux for 3 h and treated with H_2O (16 mL). The reaction mixture was stirred under reflux overnight, cooled to rt, and evaporated under reduced pressure. The resulting residue was treated with HCl/Et_2O (0.5 N, 156 mL) and concentrated under reduced pressure to give the carboxylic acid, in the form of its hydrochloride salt (6.00 g), as a white solid that was used in the next step without further purification.

A suspension of crude carboxylic acid (3.00 g) in anhydrous CH_2Cl_2 (20 mL) was cooled to 0 °C in an ice bath and treated dropwise with freshly distilled Et_3N (1.32 mL, 958 mg, 9.47 mmol) and $ClCO_2Et$ (0.18 mL, 204 mg, 1.90 mmol). The resulting suspension was stirred at 0 °C for 30 min and then treated with amine **4** (360 mg, 1.90 mmol). The reaction mixture was stirred at rt for 3 days, diluted with 10% aq. Na_2CO_3 (60 mL) and extracted with CH_2Cl_2 (2 × 40 mL). The combined organic extracts were dried over anhydrous Na_2SO_4 and evaporated under reduced pressure to give a yellow solid (740 mg), which was purified by column chromatography (40–60 μm silica gel, CH_2Cl_2/MeOH/50% aq. NH_4OH mixtures, gradient elution). On elution with CH_2Cl_2/MeOH/50% aq. NH_4OH 99:1:0.2, hybrid **5a** (180 mg, 18% overall yield from **3a**) was isolated; R_f 0.19 (CH_2Cl_2/MeOH/50% aq. NH_4OH 9:1:0.05).

A solution of **5a** (180 mg, 0.35 mmol) in CH_2Cl_2 (6 mL) was filtered through a 0.2 μm PTFE filter, treated with methanolic HCl (0.43 N, 2.42 mL), and evaporated under reduced pressure. The resulting solid was washed with pentane (3 × 2 mL) to give, after drying at 65 ºC/2 Torr for 48 h, **5a**·HCl (176 mg) as a beige solid: mp 132–133 °C; IR (KBr) *ν* 3500–2500 (max at 3250, 3061, 3012, 2925, 2857, 2801, O–H, N–H, N^+–H, and C–H st), 1632, 1584, 1514 (C=O, Ar–C–C, and Ar–C–N st) cm^{-1}; ^1H NMR (400 MHz, CD_3OD) *δ* 1.56 (s, 3H, 9'-CH_3), 1.77 (tt, *J* = 7.2 Hz, *J'* = 6.8 Hz, 2H, 3-H_2), superimposed in part 1.88 (tt, *J* = *J'* = 7.2 Hz, 2H, 4-H_2), 1.90 (br d, *J* = 18.0 Hz, 1H, 10'-H_{endo}), superimposed in part 1.92 (dm, *J* = 11.2 Hz, 1H, 13'-H_{syn}), 2.06 (dm, *J* = 11.2 Hz, 1H, 13'-H_{anti}), 2.34 (t, *J* = 6.8 Hz, 2H, 2-H_2), 2.54 (dd, *J* = 18.0 Hz, *J'* = 5.2 Hz 1H, 10'-H_{exo}), 2.75 (m, 1H, 7'-H), 2.87 (br d, *J* = 18.0 Hz, 1H, 6'-H_{endo}), 3.19 (dd, *J* = 18.0 Hz, *J'* = 5.2 Hz, 1H, 6'-H_{exo}), 3.44 (m, 1H, 11'-H), 3.76 (s, 3H, 3"-OCH_3), 3.95 (t, *J* = 7.6 Hz, 2H, 5-H_2), 4.23 (br d, *J* = 4.0 Hz, 2H, CONHCH_2), 4.85 (s, NH, $^+$NH, OH), 5.56 (br d, *J* = 4.8 Hz, 1H, 8'-H), 6.61 (d, *J* = 8.0 Hz, 1H, 5"-H), 6.66 (br d, *J* = 8.0 Hz, 1H, 6"-H), 6.80 (s, 1H, 2"-H), 7.48 (br d, *J* = 9.2 Hz, 1H, 2'-H), 7.74 (br s, 1H, 4'-H), 8.30 (d, *J* = 9.2 Hz, 1H, 1'-H), 8.39 (t, *J* = 4.0 Hz, 1H, CONHCH$_2$); ^{13}C NMR (100.6 MHz, CD_3OD) *δ* 23.5 (CH_3, 9'-CH_3), 23.8 (CH_2, C3), 27.2 (CH, C11'), 27.8 (CH, C7'), 29.3 (CH_2, C13'), 30.7 (CH_2, C4), 36.0 (CH_2, C6'), 36.1 (2CH_2, C2, C10'), 43.9 (CH_2, major rotamer CONHCH_2), 44.1 (CH_2, minor rotamer CONHCH_2), 49.1 (CH_2, C5), 56.3 (CH_3, 3"-OCH_3), 112.4 (CH, C2"), 115.5 (C, C12a'), 116.0 (CH, C5"), 117.6 (C, C11a'), 119.1 (CH, C4'), 121.3 (CH, C6"), 125.1 (CH, C8'), 126.7 (CH, C2'), 129.3 (CH, C1'), 131.5 (C, C1"), 134.6 (C, C9'), 140.0 (C, C3'), 140.9 (C, C4a'), 146.7 (C, C4"), 148.8 (C, C3"), 151.2 (C, C5a'), 156.7 (C, C12'), 175.26 (C, major rotamer C1), 175.35 (C, minor rotamer C1); HRMS (ESI) calcd for ($C_{30}H_{34}{}^{35}ClN_3O_3$ + H^+): 520.2361, found 520.2357. Anal. ($C_{30}H_{34}ClN_3O_3$·HCl·3/4H_2O) C, H, N.

6-[(3-Chloro-6,7,10,11-tetrahydro-9-methyl-7,11-methanocycloocta[*b*]quinolin-12-yl)amino]-*N*-(4-hydroxy-3-methoxybenzyl)hexanamide (5b). It was prepared as described for **5a**. From nitrile **3b** (1.60 g, 4.21 mmol) crude carboxylic acid (6.61 g) was obtained as a white solid, which was used in the next step without further purification. From this crude carboxylic acid (6.26 g) and amine **4** (757 mg, 3.99 mmol), a yellowish solid residue (2.00 g) was obtained and purified by column chromatography (40–60 μm silica gel, CH_2Cl_2/MeOH/50% aq. NH_4OH mixtures, gradient elution). On elution with CH_2Cl_2/MeOH/50% aq. NH_4OH 98.5:1.5:0.2, hybrid **5b** (800 mg, 38% overall yield from **3b**) was obtained; R_f 0.20 (CH_2Cl_2/MeOH/50% aq. NH_4OH 9:1:0.05).

5b·HCl: mp 134–135 °C; IR (KBr) *ν* 3500–2500 (max at 3233, 3054, 3012, 2924, 2855, 2791, O–H, N–H, N^+–H, and C–H st), 1632, 1601, 1583, 1569, 1513 (C=O, Ar–C–C, and Ar–C–N st) cm^{-1}; ^1H NMR (400 MHz, CD_3OD) δ 1.46 (tt, $J = J' = 7.6$ Hz, 2H, 4-H_2), 1.57 (s, 3H, 9'-CH_3), 1.71 (tt, $J = J' = 7.6$ Hz, 2H, 3-H_2), 1.87 (tt, $J = J' = 7.6$ Hz, 2H, 5-H_2), 1.91 (br d, $J = 18.0$ Hz, 1H, 10'-H_{endo}), superimposed in part 1.93 (dm, $J = 12.4$ Hz, 1H, 13'-H_{syn}), 2.06 (dm, $J = 12.4$ Hz, 1H, 13'-H_{anti}), 2.27 (t, $J = 7.6$ Hz, 2H, 2-H_2), 2.54 (dd, $J = 18.0$ Hz, $J' = 4.8$ Hz, 1H, 10'-H_{exo}), 2.75 (m, 1H, 7'-H), 2.86 (br d, $J = 18.0$ Hz, 1H, 6'-H_{endo}), 3.19 (dd, $J = 18.0$ Hz, $J' = 5.6$ Hz, 1H, 6'-H_{exo}), 3.43 (m, 1H, 11'-H), 3.80 (s, 3H, 3"-OCH_3), 3.94 (t, $J = 7.2$ Hz, 2H, 6-H_2), 4.24 (d, $J = 6.0$ Hz) and 4.25 (d, $J = 4.4$ Hz) (2H, rotamers of CONHCH_2), 4.85 (s, NH, $^+$NH, OH), 5.57 (br d, $J = 4.8$ Hz, 1H, 8'-H), 6.67 (d, $J = 8.0$ Hz, 1H, 5"-H), 6.69 (dd, $J = 8.0$ Hz, $J' = 1.6$ Hz, 1H, 6"-H), 6.84 (br s, 1H, 2"-H), 7.53 (dd, $J = 9.2$ Hz, $J' = 2.0$ Hz, 1H, 2'-H), 7.76 (d, $J = 2.0$ Hz, 1H, 4'-H), superimposed in part 8.30 (t, $J = 4.4$ Hz) and 8.33 (t, $J = 6.0$ Hz) (1H, rotamers of CON*H*CH_2), 8.35 (d, $J = 9.2$ Hz, 1H, 1'-H); ^{13}C NMR (100.6 MHz, CD_3OD) δ 23.5 (CH_3, 9'-CH_3), 26.4 (CH_2, C3), 27.3 (CH_2 + CH, C4, C11'), 27.8 (CH, C7'), 29.3 (CH_2, C13'),

30.9 (CH_2, C5), 36.0 (CH_2, C6'), 36.1 (CH_2, C10'), 36.7 (CH_2, major rotamer C2), 36.8 (CH_2, minor rotamer C2), 43.9 (CH_2, major rotamer CONH*C*H2), 44.1 (CH_2, minor rotamer CONH*C*H2), 49.5 (CH_2, C6), 56.4 (CH_3, 3''-OCH_3), 112.5 (CH, C2''), 115.7 (C, C12a'), 116.1 (CH, C5''), 117.6 (C, C11a'), 119.1 (CH, C4'), 121.3 (CH, C6''), 125.1 (CH, C8'), 126.7 (CH, C2'), 129.4 (CH, C1'), 131.5 (C, C1''), 134.6 (C, C9'), 140.2 (C, C3'), 140.9 (C, C4a'), 146.8 (C, C4''), 148.9 (C, C3''), 151.2 (C, C5a'), 156.8 (C, C12'), 175.6 (C, major rotamer C1), 175.7 (C, minor rotamer C1); HRMS (ESI) calcd for ($C_{31}H_{36}{}^{35}ClN_3O_3$ + H^+): 534.2518, found 534.2527. Anal. ($C_{31}H_{36}ClN_3O_3 \cdot HCl \cdot 1/2H_2O$) C, H, N.

7-[(3-Chloro-6,7,10,11-tetrahydro-9-methyl-7,11-methanocycloocta[*b*]quinolin-12-yl)amino]-*N*-(4-hydroxy-3-methoxybenzyl)heptanamide (5c). It was prepared as described for **5a**. From nitrile **3c** (800 mg, 2.03 mmol) crude carboxylic acid (3.43 g) was obtained as a white solid, which was used in the next step without further purification. From this crude carboxylic acid (3.43 g) and amine **4** (385 mg, 2.03 mmol), a yellowish solid residue (1.09 g) was obtained and purified by column chromatography (40–60 μm silica gel, CH_2Cl_2/MeOH/50% aq. NH_4OH mixtures, gradient elution). On elution with CH_2Cl_2/MeOH/50% aq. NH_4OH 99:1:0.2, hybrid **5c** (490 mg, 44% overall yield from **3c**) was obtained; R_f 0.24 (CH_2Cl_2/MeOH/50% aq. NH_4OH 9:1:0.05).

5c·HCl: mp 133–135 °C; IR (KBr) ν 3500–2500 (max at 3233, 3057, 3007, 2925, 2854, 2785, O–H, N–H, N^+–H, and C–H st), 1630, 1599, 1583, 1566, 1513 (C=O, Ar–C–C, and Ar–C–N st) cm^{-1}; ^1H NMR (400 MHz, CD_3OD) δ 1.36–1.48 (complex signal, 4H, 4-H_2, 5-H_2), 1.58 (s, 3H, 9'-CH_3), 1.65 (tt, $J = J' = 7.2$ Hz, 2H, 3-H_2), 1.84 (tt, $J = J' = 6.8$ Hz, 2H, 6-H_2), 1.92 (br d, J = 18.0 Hz, 1H, 10'-H_{endo}), superimposed in part 1.95 (dm, J = 12.8 Hz, 1H, 13'-H_{syn}), 2.08 (dm, J = 12.8 Hz, 1H, 13'-H_{anti}), 2.23 (t, J = 7.2 Hz, 2H, 2-H_2), 2.55 (dd, J = 18.0 Hz, J' = 4.4 Hz, 1H,

10'-H_{exo}), 2.77 (m, 1H, 7'-H), 2.86 (br d, J = 18.0 Hz, 1H, 6'-H_{endo}), 3.20 (dd, J = 18.0 Hz, J' = 5.6 Hz, 1H, 6'-H_{exo}), 3.44 (m, 1H, 11'-H), 3.81 (s, 3H, 3"-OCH_3), 3.93 (br t, J = 6.8 Hz, 2H, 7-H_2), 4.24 (d, J = 5.6 Hz, 2H, CONHCH_2), 4.85 (s, NH, $^+$NH, OH), 5.58 (br d, J = 4.4 Hz, 1H, 8'-H), 6.68 (d, J = 8.0 Hz, 1H, 5"-H), 6.70 (br d, J = 8.0 Hz, 1H, 6"-H), 6.84 (br s, 1H, 2"-H), 7.54 (dd, J = 9.2 Hz, J' = 2.0 Hz, 1H, 2'-H), 7.75 (d, J = 2.0 Hz, 1H, 4'-H), 8.30 (t, J = 5.6 Hz, 1H, CONHCH$_2$), 8.35 (d, J = 9.2 Hz, 1H, 1'-H); ^{13}C NMR (100.6 MHz, CD_3OD) δ 23.5 (CH_3, 9'-CH_3), 26.8 (CH_2, C3), 27.3 (CH, C11'), 27.5 (CH_2, C4), 27.9 (CH, C7'), 29.3 (CH_2, C13'), 29.6 (CH_2, C5), 31.0 (CH_2, C6), 36.0 (CH_2, C6'), 36.1 (CH_2, C10'), 36.9 (CH_2, C2), 43.9 (CH_2, major rotamer CONHCH2), 44.1 (CH_2, minor rotamer CONHCH2), 49.6 (CH_2, C7), 56.4 (CH_3, 3"-OCH_3), 112.6 (CH, C2"), 115.7 (C, C12a'), 116.1 (CH, C5"), 117.6 (C, C11a'), 119.2 (CH, C4'), 121.4 (CH, C6"), 125.1 (CH, C8'), 126.7 (CH, C2'), 129.4 (CH, C1'), 131.6 (C, C1"), 134.6 (C, C9'), 140.2 (C, C3'), 141.0 (C, C4a'), 146.8 (C, C4"), 148.9 (C, C3"), 151.2 (C, C5a'), 156.9 (C, C12'), 175.8 (C, major rotamer C1), 175.9 (C, minor rotamer C1); HRMS (ESI) calcd for ($C_{32}H_{38}{}^{35}ClN_3O_3$ + H^+): 548.2674, found 548.2677. Anal. ($C_{32}H_{38}ClN_3O_3 \cdot HCl \cdot 3/4H_2O$) C, H, N.

8-[(3-Chloro-6,7,10,11-tetrahydro-9-methyl-7,11-methanocycloocta[*b*]quinolin-12-yl)amino]-*N*-(4-hydroxy-3-methoxybenzyl)octanamide (5d). It was prepared as described for **5a**. From nitrile **3d** (540 g, 1.32 mmol) crude carboxylic acid (2.32 g) was obtained as a white solid, which was used in the next step without further purification. From crude carboxylic acid (2.00 g) and amine **4** (216 mg, 1.14 mmol), a yellowish solid residue (0.75 g) was obtained and purified by column chromatography (40–60 μm silica gel, CH_2Cl_2/MeOH/50% aq. NH_4OH mixtures, gradient elution). On elution with CH_2Cl_2/MeOH/50% aq. NH_4OH 99.5:0.5:0.2, hybrid **5d** (110 mg, 17% overall yield from **3d**) was obtained; R_f 0.29 (CH_2Cl_2/MeOH/50% aq. NH_4OH 9:1:0.05).

5d·HCl: mp 126–127 °C; IR (KBr) *v* 3500–2500 (max at 3253, 3056, 3012, 2927, 2854, 2790, O–H, N–H, N^+–H, and C–H st), 1630, 1583, 1514 (C=O, Ar–C–C, and Ar–C–N st) cm^{-1}; ^1H NMR (400 MHz, CD_3OD) δ 1.29–1.45 (complex signal, 6H, 4-H_2, 5-H_2, 6-H_2), 1.58 (s, 3H, 9'-CH_3), 1.62 (tt, $J = J' = 7.2$ Hz, 2H, 3-H_2), 1.83 (tt, $J = J' = 7.2$ Hz, 2H, 7-H_2), 1.92 (br d, $J = 18.0$ Hz, 1H, 10'-H_{endo}), superimposed in part 1.94 (dm, $J = 12.4$ Hz, 1H, 13'-H_{syn}), 2.08 (dm, $J = 12.4$ Hz, 1H, 13'-H_{anti}), 2.21 (t, $J = 7.2$ Hz, 2H, 2-H_2), 2.54 (dd, $J = 18.0$ Hz, $J' = 4.0$ Hz, 1H, 10'-H_{exo}), 2.76 (m, 1H, 7'-H), 2.85 (dm, $J = 18.0$ Hz, 1H, 6'-H_{endo}), 3.20 (dd, $J = 18.0$ Hz, $J' = 5.6$ Hz, 1H, 6'-H_{exo}), 3.44 (m, 1H, 11'-H), 3.82 (s, 3H, 3"-OCH_3), 3.95 (br t, $J = 7.2$ Hz, 2H, 8-H_2), 4.25 (d, $J = 4.4$ Hz, 2H, CONHCH_2), 4.85 (s, NH, $^+$NH, OH), 5.58 (br d, $J = 4.4$ Hz, 1H, 8'-H), 6.69–6.71 (complex signal, 2H, 5"-H, 6"-H), 6.85 (br s, 1H, 2"-H), 7.55 (dd, $J = 9.2$ Hz, $J' = 2.0$ Hz, 1H, 2'-H), 7.75 (d, $J = 2.0$ Hz, 1H, 4'-H), 8.29 (br t, $J = 4.4$ Hz, 1H, CON*H*CH_2), 8.37 (d, $J = 9.2$ Hz, 1H, 1'-H); ^{13}C NMR (100.6 MHz, CD_3OD) δ 23.5 (CH_3, 9'-CH_3), 26.8 (CH_2, C3), 27.3 (CH, C11'), 27.6 (CH_2, C4), 27.9 (CH, C7'), 29.3 (CH_2, C13'), 29.9 (CH_2), 30.0 (CH_2) (C5, C6), 31.1 (CH_2, C7), 36.06 (CH_2, C6'), 36.10 (CH_2, C10'), 37.0 (CH_2, C2), 43.9 (CH_2, CONH*C*H2), 49.6 (CH_2, C8), 56.4 (CH_3, 3"-OCH_3), 112.5 (CH, C2"), 115.7 (C, C12a'), 116.1 (CH, C5"), 117.6 (C, C11a'), 119.2 (CH, C4'), 121.4 (CH, C6"), 125.1 (CH, C8'), 126.7 (CH, C2'), 129.4 (CH, C1'), 131.6 (C, C1"), 134.6 (C, C9'), 140.2 (C, C3'), 141.0 (C, C4a'), 146.8 (C, C4"), 149.0 (C, C3"), 151.3 (C, C5a'), 156.9 (C, C12'), 175.9 (C, C1); HRMS (ESI) calcd for ($C_{33}H_{40}{}^{35}ClN_3O_3 + H^+$): 562.2831, found 562.2828. Anal. ($C_{33}H_{40}ClN_3O_3$·HCl·1/2H_2O) C, H, N.

9-[(3-Chloro-6,7,10,11-tetrahydro-9-methyl-7,11-methanocycloocta[*b*]quinolin-12-yl)amino]-*N*-(4-hydroxy-3-methoxybenzyl)nonanamide (5e). It was prepared as described for **5a**. From nitrile **3e** (400 mg, 0.95 mmol) crude carboxylic acid (1.71 g) was obtained as a white

solid, which was used in the next step without further purification. From crude carboxylic acid (1.55 g) and amine **4** (163 mg, 0.86 mmol), a yellowish solid residue (450 mg) was obtained and purified by column chromatography (40–60 μm silica gel, CH_2Cl_2/MeOH/50% aq. NH_4OH mixtures, gradient elution). On elution with CH_2Cl_2/MeOH/50% aq. NH_4OH 99.5:0.5:0.2, hybrid **5e** (45 mg, 9% overall yield from **3e**) was isolated; R_f 0.33 (CH_2Cl_2/MeOH/50% aq. NH_4OH 9:1:0.05).

5e·HCl: mp 122 –123 °C; IR (KBr) *v* 3500–2500 (max at 3250, 3059, 3002, 2926, 2854, 2795, O–H, N–H, N^+–H, and C–H st), 1630, 1583, 1514 (C=O, Ar–C–C, and Ar–C–N st) cm^{-1}; ^1H NMR (400 MHz, CD_3OD) δ 1.28–1.44 (complex signal, 8H, 4-H_2, 5-H_2, 6-H_2, 7-H_2), 1.58 (s, 3H, 9'-CH_3), superimposed in part 1.61 (tt, $J = J' = 7.2$ Hz, 2H, 3-H_2), 1.84 (tt, $J = J' = 6.8$ Hz, 2H, 8-H_2), 1.94 (br d, $J = 17.2$ Hz, 1H, 10'-H_{endo}), superimposed in part 1.95 (dm, J =12.4 Hz, 1H, 13'-H_{syn}), 2.08 (dm, $J = 12.4$ Hz, 1H, 13'-H_{anti}), 2.21 (t, $J = 7.2$ Hz, 2H, 2-H_2), 2.55 (dd, J = 17.2 Hz, $J' = 4.4$ Hz, 1H, 10'-H_{exo}), 2.77 (m, 1H, 7'-H), 2.86 (dm, $J = 17.6$ Hz, 1H, 6'-H_{endo}), 3.20 (dd, $J = 17.6$ Hz, $J' = 5.6$ Hz, 1H, 6'-H_{exo}), 3.44 (m, 1H, 11'-H), 3.82 (s, 3H, 3"-OCH_3), 3.96 (br t, $J = 6.8$ Hz, 2H, 9-H_2), 4.24 (br s, 2H, CONHCH_2), 4.85 (s, NH, $^+$NH, OH), 5.58 (br d, $J = 4.8$ Hz, 1H, 8'-H), 6.70 (complex signal, 2H, 5"-H, 6"-H), 6.85 (s, 1H, 2"-H), 7.55 (dd, J = 9.2 Hz, $J' = 2.0$ Hz, 1H, 2'-H), 7.75 (d, $J = 2.0$ Hz, 1H, 4'-H), 8.28 (m, 1H, CON*H*CH_2), 8.38 (d, $J = 9.2$ Hz, 1H, 1'-H); ^{13}C NMR (100.6 MHz, CD_3OD) δ 23.5 (CH_3, 9'-CH_3), 27.0 (CH_2, C3), 27.3 (CH, C11'), 27.7 (CH_2, C4), 27.9 (CH, C7'), 29.3 (CH_2, C13'), 30.0 (CH_2), 30.1 (CH_2), 30.2 (CH_2) (C5, C6, C7), 31.2 (CH_2, C8), 36.0 (CH_2, C6'), 36.1 (CH_2, C10'), 37.0 (CH_2, C2), 43.9 (CH_2, CONH*C*H2), 49.7 (CH_2, C9), 56.4 (CH_3, 3"-OCH_3), 112.5 (CH, C2"), 115.7 (C, C12a'), 116.1 (CH, C5"), 117.6 (C, C11a'), 119.1 (CH, C4'), 121.4 (CH, C6"), 125.1 (CH, C8'), 126.7 (CH, C2'), 129.5 (CH, C1'), 131.6 (C, C1"), 134.6 (C, C9'), 140.2 (C, C3'), 141.0 (C,

C4a'), 146.8 (C, C4"), 149.0 (C, C3"), 151.2 (C, C5a'), 156.9 (C, C12'), 175.9 (C, C1); HRMS (ESI) calcd for ($C_{34}H_{42}{}^{35}ClN_3O_3$ + H^+): 576.2987, found 576.2995. Anal. ($C_{34}H_{42}ClN_3O_3 \cdot HCl \cdot 3/4H_2O$) C, H, N.

4-{[(3-Chloro-6,7,10,11-tetrahydro-9-methyl-7,11-methanocycloocta[*b*]quinolin-12-yl)amino]methyl}-*N*-(4-hydroxy-3-methoxybenzyl)benzamide (5f). It was prepared as described for **5a**. From nitrile **3f** (870 g, 2.18 mmol) crude carboxylic acid (3.50 g) was obtained as a white solid, which was used in the next step without further purification. From this crude carboxylic acid (3.50 g) and amine **4** (394 mg, 2.08 mmol), a yellowish solid residue (1.12 g) was obtained and purified by column chromatography (40–60 μm silica gel, CH_2Cl_2/MeOH/50% aq. NH_4OH mixtures, gradient elution). On elution with CH_2Cl_2/MeOH/50% aq. NH_4OH 99.5:0.5:0.2, hybrid **5f** (380 mg, 33% overall yield from **3f**) was obtained; R_f 0.24 (CH_2Cl_2/MeOH/50% aq. NH_4OH 9:1:0.05).

5f·HCl: mp 209–211 °C; IR (KBr) ν 3500–2500 (max at 3229, 3105, 3052, 3002, 2925, 2852, 2790, O–H, N–H, N^+–H, and C–H st), 1635, 1602, 1583, 1560, 1508, 1501 (C=O, Ar–C–C, and Ar–C–N st) cm^{-1}; ^1H NMR (400 MHz, CD_3OD) δ 1.60 (s, 3H, 9'-CH_3), superimposed in part 1.97 (dm, J = 12.8 Hz, 1H, 13'-H_{syn}), 1.98 (br d, J = 17.2 Hz, 1H, 10'-H_{endo}), 2.09 (dm, J = 12.8 Hz, 1H, 13'-H_{anti}), 2.55 (dd, J = 17.2 Hz, J' = 4.4 Hz, 1H, 10'-H_{exo}), 2.78 (m, 1H, 7'-H), 2.91 (br d, J = 17.6 Hz, 1H, 6'-H_{endo}), 3.24 (dd, J = 17.6 Hz, J' = 5.6 Hz, 1H, 6'-H_{exo}), 3.51 (m, 1H, 11'-H), 3.82 (s, 3H, 3"-OCH_3), 4.47 (br d, J = 5.6 Hz, 2H, CONHCH_2), 4.85 (s, NH, $^+$NH, OH), 5.24 (s, 2H, benzamide C4-CH_2NH), 5.59 (br d, J = 4.8 Hz, 1H, 8'-H), 6.72 (d, J = 8.4 Hz, 1H, 5"-H), 6.78 (dd, J = 8.4 Hz, J' = 2.0 Hz, 1H, 6"-H), 6.93 (d, J = 2.0 Hz, 1H, 2"-H), 7.35 (dd, J = 8.8 Hz, J' = 2.0 Hz, 1H, 2'-H), 7.52 [d, J = 8.0 Hz, 2H, benzamide C3(5)-H], 7.76 (d, J = 2.0 Hz, 1H, 4'-H), 7.90 [d, J = 8.0 Hz, 2H, benzamide C2(6)-H], 8.16 (d, J = 8.8 Hz, 1H, 1'-H), 8.89 (t, J = 5.6

Hz, 1H, CON*H*CH_2); ^{13}C NMR (100.6 MHz, CD_3OD) δ 23.5 (CH_3, 9'-CH_3), 27.5 (CH, C11'), 27.9 (CH, C7'), 29.3 (CH_2, C13'), 36.1 (CH_2, C6'), 36.2 (CH_2, C10'), 44.4 (CH_2, CONH*C*H_2), 52.0 (CH_2, benzamide C4-*C*H_2NH), 56.4 (CH_3, 3"-OCH_3), 112.6 (CH, C2"), 115.7 (C, C12a'), 116.1 (CH, C5"), 118.4 (C, C11a'), 119.3 (CH, C4'), 121.4 (CH, C6"), 125.1 (CH, C8'), 126.8 (CH, C2'), 127.8 [2CH, benzamide C3(5)], 129.1 (CH, C1'), 129.2 [2CH, benzamide C2(6)], 131.6 (C, C1"), 134.7 (C, C9'), 135.4 (C, benzamide C1), 140.3 (C, C3'), 140.8 (C, C4a'), 142.5 (C, benzamide C4), 146.9 (C, C4"), 149.0 (C, C3"), 152.0 (C, C5a'), 157.4 (C, C12'), 169.3 (C, *C*ONHCH$_2$); HRMS (ESI) calcd for ($C_{33}H_{32}{}^{35}ClN_3O_3$ + H^+): 554.2205, found 554.2205. Anal. ($C_{33}H_{32}ClN_3O_3 \cdot HCl \cdot 1.5H_2O$) C, H, N.

4-{[(3-Chloro-6,7,10,11-tetrahydro-9-methyl-7,11-methanocycloocta[*b*]quinolin-12-yl)amino]methyl}-*N*-[3-methoxy-4-(triisopropylsilyloxy)benzyl]benzamide (7). Hybrid **7** was prepared as described for **5a**. From nitrile **3f** (658 mg, 1.65 mmol) crude carboxylic acid (3.40 g) was obtained as a white solid, which was used in the next step without further purification. From this crude carboxylic acid (3.30 g) and 3-methoxy-4-(triisopropylsilyloxy)benzylamine, **6**[73] (494 mg, 1.60 mmol), a yellowish solid residue (1.39 g) was obtained and purified by column chromatography (40–60 μm silica gel, CH_2Cl_2/MeOH/50% aq. NH_4OH mixtures, gradient elution). On elution with CH_2Cl_2/MeOH/50% aq. NH_4OH 99.5:0.5:0.2, hybrid **7** (919 mg, 81% overall yield from **3f**) was obtained as a colorless oil; R_f 0.36 (CH_2Cl_2/MeOH/50% aq. NH_4OH 9:1:0.05); IR (KBr) ν 3296 (N–H st), 1640, 1607, 1583, 1553, 1514 (C=O, Ar–C–C, and Ar–C–N st) cm^{-1}; ^{1}H NMR (400 MHz, $CDCl_3$) δ 1.08 [d, J = 7.2 Hz, 18H, OSi[CH(C*H*$_3$)$_2$]$_3$], 1.24 [m, 3H, OSi[C*H*(CH$_3$)$_2$]$_3$], 1.49 (s, 3H, 9'-CH_3), 1.73 (br d, J = 16.8 Hz, 1H 10'-H$_{endo}$) 1.82 (dm, J = 12.4 Hz, 1H, 13'-H$_{syn}$), 1.97 (dm, J = 12.4 Hz, 1H, 13'-H$_{anti}$), 2.45 (dd, J = 16.8 Hz, J' = 4.0 Hz, 1H, 10'-H$_{exo}$), 2.71 (m, 1H, 7'-H), 3.10−3.22 (complex signal, 3H, 6'-H$_{endo}$, 6'-H$_{exo}$, 11'-H), 3.79

(s, 3H, 3”-OCH_3), 4.57 (d, *J* = 5.6 Hz, 2H, CONHCH_2), 4.76 (m, 2H, benzamide C4-CH_2NH), 5.51 (br d, *J* = 5.6 Hz, 1H, 8’-H), 6.45 (br signal, 1H, CONHCH_2), 6.78 (dd, *J* = 8.0 Hz, *J’* = 2.0 Hz, 1H, 6”-H), 6.83 (d, *J* = 8.0 Hz, 1H, 5”-H), 6.85 (d, *J* = 2.0 Hz, 1H, 2”-H), 7.24 (dd, *J* = 8.8 Hz, *J’* = 2.0 Hz, 1H, 2’-H), 7.42 [d, *J* = 8.0 Hz, 2H, benzamide C3(5)-H], 7.81 [d, *J* = 8.0 Hz, 2H, benzamide C2(6)-H], 7.91 (d, *J* = 8.8 Hz, 1H, 1’-H), 8.04 (br s, 1H, 4’-H); ^{13}C NMR (100.6 MHz, $CDCl_3$) δ 13.0 [3CH, OSi[CH(CH_3)$_2$]$_3$], 18.0 [6CH_3, OSi[CH(CH$_3$)$_2$]$_3$], 23.5 (CH_3, 9’-CH_3), 27.7 (CH, C11’), 28.3 (CH, C7’), 29.1 (CH_2, C13’), 37.4 (CH_2, C10’), 40.2 (CH_2, C6’), 44.3 (CH_2, CONHCH$_2$), 54.0 (CH_2, benzamide C4-CH$_2$NH), 55.7 (CH_3, 3”-OCH_3), 112.3 (CH, C2”), 119.3 (C, C12a’), 120.4 (CH, C6”), 120.5 (CH, C5”), 122.7 (C, C11a’), 124.9 (CH, C2’), 125.1 (CH, C1’), 125.7 (CH, C8’), 127.7 [2CH, benzamide C3(5)], 127.8 [2CH, benzamide C2(6)], 128.0 (CH, C4’), 131.1 (C, C1”), 131.7 (C, C9’), 134.2 (C, benzamide C1), 134.3 (C, C3’), 143.0 (C, benzamide C4), 145.3 (C, C4”), 148.7 (C, C4a’), 149.7 (C, C12’), 151.2 (C, C3”), 159.1 (C, C5a’), 166.8 (C, CONHCH$_2$); HRMS (ESI) calcd for ($C_{42}H_{52}{}^{35}ClN_3O_3Si$ + H^+): 710.3539, found 710.3549.

Hybrid 5f by deprotection of 7. A solution of hybrid **7** (520 mg, 0.73 mmol) in anhydrous THF (15 mL) was treated dropwise with TBAF (1 M solution in THF, 1.10 mL, 1.10 mmol) and the reaction mixture was stirred at rt for 4 h, diluted with 10% aq. Na_2CO_3 (70 mL), and extracted with CH_2Cl_2 (2 × 50 mL). The combined organic extracts were washed with H_2O (3 × 70 mL), dried over anhydrous Na_2SO_4, and evaporated under reduced pressure, to give hybrid **5f** (380 mg, 94% yield).

***N*-(4-Hydroxy-3-methoxybenzyl)-6-heptenamide (9).** A solution of 6-heptenoic acid, **8** (0.71 mL, 675 mg, 5.25 mmol), in anhydrous CH_2Cl_2 (10 mL) was cooled to 0 °C in an ice bath, then treated dropwise with freshly distilled Et_3N (1.61 mL, 1.17 g, 11.6 mmol), and $ClCO_2Et$ (0.50

mL, 567 mg, 5.25 mmol). The resulting solution was stirred at 0 °C for 30 min and treated with amine **4** (1.00 g, 5.25 mmol). The reaction mixture was stirred at rt for 3 days, diluted with 10% aq. Na_2CO_3 (60 mL), and extracted with CH_2Cl_2 (3 × 40 mL). The combined organic extracts were washed with H_2O (3 × 60 mL), dried over anhydrous Na_2SO_4, and evaporated under reduced pressure to give a colorless oil (1.53 g), which consisted of a mixture of amide **9** and the corresponding *O*-acylated byproduct in an approximate ratio of 9:1 (^{1}H NMR). This mixture was taken up in MeOH (108 mL), and H_2O (59 mL) and saturated aq. $NaHCO_3$ (80 mL) were added. The resulting mixture was stirred at rt overnight, concentrated under reduced pressure, and extracted with CH_2Cl_2 (3 × 90 mL). The combined organic extracts were washed with H_2O (3 × 150 mL), dried over anhydrous Na_2SO_4, and evaporated under reduced pressure to provide **9** (1.08 g, 78% yield) as a white solid; R_f 0.65 (CH_2Cl_2/MeOH/50% aq. NH_4OH 9:1:0.05); mp 57−59 °C; IR (KBr) ν 3379, 3344, 3076 (O–H and N–H st), 1640, 1601, 1549, 1522 (C=O and Ar–C–C st) cm^{-1}; ^{1}H NMR (400 MHz, $CDCl_3$) δ 1.41 (tt, J = J' = 7.2 Hz, 2H, 4-H_2), 1.66 (tt, J = 7.6 Hz, J' = 7.2 Hz, 2H, 3-H_2), 2.05 (tddd, J = 7.2 Hz, J' = 6.8 Hz, J'' = 1.6 Hz, J''' = 1.2 Hz, 2H, 5-H_2), 2.19 (t, J = 7.6 Hz, 2H, 2-H_2), 3.85 (s, 3H, 3'-OCH_3), 4.33 (d, J = 6.0 Hz, 2H, CONHCH_2), 4.93 (ddt, J = 10.0 Hz, J' = 2.0 Hz, J'' = 1.2 Hz, 1H, 7-H_a), 4.98 (ddt, J = 17.2 Hz, J' = 2.0 Hz, J'' = 1.6 Hz, 1H, 7-H_b), 5.77 (ddt, J = 17.2 Hz, J' = 10.0 Hz, J'' = 6.8 Hz, 1H, 6-H), 5.79 (br s, 1H, CONHCH_2), 6.74 (dd, J = 8.0 Hz, J' = 2.0 Hz, 1H, 6'-H), 6.79 (d, J = 2.0 Hz, 1H, 2'-H), 6.84 (d, J = 8.0 Hz, 1H, 5'-H); ^{13}C NMR (100.6 MHz, $CDCl_3$) δ 25.2 (CH_2, C3), 28.5 (CH_2, C4), 33.4 (CH_2, C5), 36.6 (CH_2, C2), 43.5 (CH_2, CONHCH$_2$), 55.9 (CH_3, 3'-OCH_3), 110.7 (CH, C2'), 114.4 (CH, C5'), 114.7 (CH_2, C7), 120.7 (CH, C6'), 130.3 (C, C1'), 138.4 (CH, C6), 145.1 (C, C4'), 146.7 (C, C3'), 172.7 (C, C1); HRMS (ESI) calcd for ($C_{15}H_{21}NO_3$ + H^+): 264.1594, found 264.1592.

3-Chloro-6,7,10,11-tetrahydro-9-methyl-12-(2-propenylamino)-7,11-methanocycloocta[*b*]quinoline (10g). A suspension of huprine Y, **2** (500 mg, 1.76 mmol), finely powdered KOH (85% purity, 186 mg, 2.82 mmol), and 4 Å molecular sieves in anhydrous DMSO (6 mL) was stirred, heating approximately every 10 min with a heat gun for 1 h and at rt for an additional 1 h, and then treated with allyl bromide (0.15 mL, 213 mg, 1.76 mmol). The reaction mixture was stirred at rt overnight, diluted with 2 N NaOH (15 mL), and extracted with EtOAc (3 × 35 mL). The combined organic extracts were washed with H_2O (3 × 25 mL), dried over anhydrous Na_2SO_4, and evaporated under reduced pressure to give a yellow oil (654 mg), which was purified by column chromatography (40–60 μm silica gel, CH_2Cl_2/MeOH/50% aq. NH_4OH mixtures, gradient elution). On elution with CH_2Cl_2/MeOH/50% aq. NH_4OH 99.5:0.5:0.2 to 99:1:0.2, alkene **10g** (314 mg, 55% yield) was obtained; R_f 0.60 (CH_2Cl_2/MeOH/50% aq. NH_4OH 9:1:0.05).

10g·HCl: mp 228–230 °C; IR (KBr) *v* 3500–2500 (max at 3401, 3215, 3113, 3078, 3051, 3015, 2925, 2903, 2882, 2852, 2703, 2685, N–H, N^+–H, and C–H st), 1634, 1604, 1583, 1562, 1519 (Ar–C–C and Ar–C–N st) cm^{-1}; ^1H NMR (400 MHz, CD_3OD) δ 1.59 (s, 3H, 9-CH_3), 1.94 (br d, J = 17.6 Hz, 1H, 10-H_{endo}), superimposed in part 1.96 (dm, J = 12.8 Hz, 1H, 13-H_{syn}), 2.09 (dm, J = 12.8 Hz, 1H, 13-H_{anti}), 2.55 (dd, J = 17.6 Hz, J' = 4.8 Hz, 1H, 10-H_{exo}), 2.79 (m, 1H, 7-H), 2.88 (dm, J = 18.0 Hz, 1H, 6-H_{endo}), 3.22 (dd, J = 18.0 Hz, J' = 5.2 Hz, 1H, 6-H_{exo}), 3.45 (m, 1H, 11-H), 4.58 (m, 2H, 1'-H_2), 4.85 (s, NH, $^+$NH), superimposed in part 5.39 (ddt, J = 10.4 Hz, J' = 2.0 Hz, J'' = 1.2 Hz, 1H, 3'-H_a), superimposed in part 5.41 (ddt, J = 17.2 Hz, J' = 2.0 Hz, J'' = 1.2 Hz, 1H, 3'-H_b), 5.59 (br d, J = 4.4 Hz, 1H, 8-H), 6.19 (ddt, J = 17.2 Hz, J' = 10.4 Hz, J'' = 4.4 Hz, 1H, 2'-H), 7.51 (dd, J = 9.6 Hz, J' = 2.0 Hz, 1H, 2-H), 7.76 (d, J = 2.0 Hz, 1H, 4-H), 8.36 (d, J = 9.6 Hz, 1H, 1-H); ^{13}C NMR (100.6 MHz, CD_3OD) δ : 23.4 (CH_3, 9-CH_3), 27.4 (CH,

C11), 27.9 (CH, C7), 29.3 (CH_2, C13), 36.1 (CH_2, C6), 36.2 (CH_2, C10), 50.9 (CH_2, C1'), 115.5 (C, C12a), 117.8 (CH_2, C3'), 118.0 (C, C11a), 119.1 (CH, C4), 125.1 (CH, C8), 126.7 (CH, C2), 129.5 (CH, C1), 134.7 (C, C9), 135.1 (CH, C2'), 140.3 (C, C3), 140.9 (C, C4a), 151.5 (C, C5a), 157.4 (C, C12); HRMS (ESI) calcd for ($C_{20}H_{21}{}^{35}ClN_2 + H^+$): 325.1466, found 325.1466.

(*E*)-8-[(3-Chloro-6,7,10,11-tetrahydro-9-methyl-7,11-methanocycloocta[*b*]quinolin-12-yl)amino]-*N*-(4-hydroxy-3-methoxybenzyl)-6-octenamide (5g). To a solution of alkene **10g** (80 mg, 0.25 mmol) in anhydrous CH_2Cl_2 (1.5 mL), alkene **9** (118 mg, 0.45 mmol), *p*-benzoquinone (3 mg, 27.8 µmol), and Grubbs-Hoveyda II generation catalyst (8 mg, 12.8 µmol) were added. The reaction mixture was stirred under reflux for 3 days and purified by column chromatography (40–60 µm silica gel, CH_2Cl_2/MeOH/50% aq. NH_4OH mixtures, gradient elution). On elution with CH_2Cl_2/MeOH/50% aq. NH_4OH 99.5:0.5:0.2, hybrid **5g** (12 mg, 9% yield) was obtained; R_f 0.42 (CH_2Cl_2/MeOH/50% aq. NH_4OH 9:1:0.05).

5g·HCl: mp 135–136 °C; IR (KBr) ν 3500–2500 (max at 3234, 3105, 3056, 3007, 2927, 2863, 2790, O–H, N–H, N^+–H, and C–H st), 1633, 1599, 1583, 1566, 1514 (C=O, Ar–C–C, and Ar–C–N st) cm^{-1}; ^1H NMR (400 MHz, CD_3OD) δ 1.40 (tt, $J = J' = 7.2$ Hz, 2H, 4-H_2), 1.58 (s, 3H, 9'-CH_3), superimposed in part 1.60 (tt, $J = J' = 7.2$ Hz, 2H, 3-H_2), 1.92 (br d, $J = 18.4$ Hz, 1H, 10'-H_{endo}), superimposed in part 1.94 (dm, J =12.4 Hz, 1H, 13'-H_{syn}), 2.07 (dm, $J = 12.4$ Hz, 1H, 13'-H_{anti}), 2.14 (dt, $J = J' = 6.8$ Hz, 2H, 5-H_2), 2.20 (t, $J = 7.2$ Hz, 2H, 2-H_2), 2.45 (dd, $J = 18.4$ Hz, $J' = 4.8$ Hz, 1H, 10'-H_{exo}), 2.77 (m, 1H, 7'-H), 2.87 (br d, $J = 17.6$ Hz, 1H, 6'-H_{endo}), 3.21 (dd, $J = 17.6$ Hz, $J' = 5.6$ Hz, 1H, 6'-H_{exo}), 3.44 (m, 1H, 11'-H), 3.80 (s, 3H, 3''-OCH_3), 4.25 (d, J =6.0 Hz, 2H, CONHCH_2), 4.51 (br d, $J = 4.0$ Hz, 2H, 8-H_2), 4.85 (s, NH, $^+$NH, OH), 5.58 (br d, $J = 4.8$ Hz, 1H, 8'-H), 5.73 (dt, $J = 15.6$ Hz, $J' = 4.0$ Hz, 1H, 7-H), 5.80 (dt, $J = 15.6$

Hz, *J'* = 6.8 Hz, 1H, 6-H), 6.67–6.71 (complex signal, 2H, 5"-H, 6"-H), 6.84 (s, 1H, 2"-H), 7.50 (dd, *J* = 9.2 Hz, *J'* = 2.4 Hz, 1H, 2'-H), 7.74 (d, *J* = 2.4 Hz, 1H, 4'-H), 8.35 (m, 1H, CON*H*CH_2), 8.38 (d, *J* = 9.2 Hz, 1H, 1'-H); ^{13}C NMR (100.6 MHz, CD_3OD) δ: 23.5 (CH_3, 9'-CH_3), 26.3 (CH_2, C3), 27.3 (CH, C11'), 27.9 (CH, C7'), 29.3 (CH_2, C13'), 29.6 (CH_2, C4), 32.9 (CH_2, C5), 36.0 (CH_2, C6'), 36.2 (CH_2, C10'), 36.7 (CH_2, C2), 43.9 (CH_2, CONH*C*H2), 50.4 (CH_2, C8), 56.4 (CH_3, 3"-OCH_3), 112.5 (CH, C2"), 115.5 (C, C12a'), 116.1 (CH, C5"), 117.8 (C, C11a'), 119.1 (CH, C4'), 121.3 (CH, C6"), 125.1 (CH, C8'), 126.6 (CH, C2'), 126.8 (CH, C7), 129.7 (CH, C1'), 131.5 (C, C1"), 134.7 (C, C9'), 135.1 (CH, C6), 140.3 (C, C3'), 140.9 (C, C4a'), 146.8 (C, C4"), 148.9 (C, C3"), 151.3 (C, C5a'), 157.2 (C, C12'), 175.7 (C, C1); HRMS (ESI) calcd for ($C_{33}H_{38}{}^{35}ClN_3O_3$ + H^+): 560.2674, found 560.2671. Anal. ($C_{33}H_{38}ClN_3O_3 \cdot HCl \cdot 2H_2O$) C, H, N.

(*E*)-10-[(3-Chloro-6,7,10,11-tetrahydro-9-methyl-7,11-methanocycloocta[*b*]quinolin-12-yl)amino]-*N*-(4-hydroxy-3-methoxybenzyl)-6-decenamide (5h). It was prepared as described for **5g**. From alkenes **10h**[62] (613 mg, 1.74 mmol) and **9** (547 mg, 2.08 mmol), and after purification of the resulting mixture by column chromatography (40–60 μm silica gel, CH_2Cl_2/MeOH/50% aq. NH_4OH mixtures, gradient elution), hybrid **5h** (73 mg, 7% yield) was obtained on elution with CH_2Cl_2/MeOH/50% aq. NH_4OH 99.5:0.5:0.2; R_f 0.32 (CH_2Cl_2/MeOH/50% aq. NH_4OH 9:1:0.05).

5h·HCl: mp 129–130 °C; IR (KBr) ν 3500–2500 (max at 3253, 3061, 2997, 2926, 2857, 2795, O–H, N–H, N^+–H, and C–H st), 1651, 1635, 1598, 1583, 1568, 1558, 1515 (C=O, Ar–C–C, and Ar–C–N st) cm^{-1}; ^{1}H NMR (400 MHz, CD_3OD) δ 1.30 (tt, *J* = *J'* = 7.2 Hz, 2H, 4-H_2), 1.576 (s, 3H, 9'-CH_3), superimposed in part 1.582 (tt, *J* = *J'* = 7.2 Hz, 2H, 3-H_2), 1.93 (br d, *J* = 16.4 Hz, 1H, 10'-H_{endo}), superimposed in part 1.95 (dm, *J* = 12.0 Hz, 1H, 13'-H_{syn}), superimposed

1.92–1.99 (m, 2H, 9-H_2), superimposed 2.02–2.10 (m, 2H, 8-H_2), 2.07 (dm, *J* = 12.0 Hz, 13'-H_{anti}), 2.12 (dt, *J* = *J'* = 6.4 Hz, 2H, 5-H_2), 2.19 (t, *J* = 7.2 Hz, 2H, 2-H_2), 2.55 (dm, *J* = 16.4 Hz, 1H, 10'-H_{exo}), 2.76 (m, 1H, 7'-H), 2.86 (br d, *J* = 18.0 Hz, 1H, 6'-H_{endo}), 3.19 (dm, *J* = 18.0 Hz, 1H, 6'-H_{exo}), 3.44 (m, 1H, 11'-H), 3.81 (s, 3H, 3"-OCH_3), 3.96 (m, 2H, 10-H_2), 4.23 (m, 2H, CONHCH_2), 4.85 (s, NH, $^+$NH, OH), 5.36 (dt, *J* = 15.6 Hz, *J'* = 6.0 Hz, 1H) and 5.42 (dt, *J* = 15.6 Hz, *J'* = 5.6 Hz, 1H) (6-H, 7-H), 5.57 (m, 1H, 8'-H), 6.67–6.71 (complex signal, 2H, 5"-H, 6"-H), 6.83 (br s, 1H, 2"-H), 7.52 (br d, *J* = 8.8 Hz, 1H, 2'-H), 7.76 (br s, 1H, 4'-H), 8.29 (m, 1H, CON*H*CH_2), 8.34 (d, *J* = 8.8 Hz, 1H, 1'-H); ^{13}C NMR (100.6 MHz, CD_3OD) δ 23.5 (CH_3, 9'-CH_3), 26.5 (CH_2, C3), 27.3 (CH, C11'), 27.8 (CH, C7'), 29.3 (CH_2, C13'), 30.0 (CH_2, C4), 30.6 (CH_2), 30.9 (CH_2), 33.1 (CH_2) (C5, C8, C9), 36.0 (CH_2, C6'), 36.2 (CH_2, C10'), 36.9 (CH_2, C2), 43.9 (CH_2, CONH*C*H_2), 49.1 (CH_2, C10), 56.4 (CH_3, 3"-OCH_3), 112.4 (CH, C2"), 115.6 (C, C12a'), 116.0 (CH, C5"), 117.6 (C, C11a'), 119.1 (CH, C4'), 121.3 (CH, C6"), 125.1 (CH, C8'), 126.6 (CH, C2'), 129.4 (CH, C1'), 130.0 (CH) and 132.8 (CH) (C6, C7), 131.6 (C, C1"), , 134.5 (C, C9'), 140.2 (C, C3'), 140.9 (C, C4a'), 146.8 (C, C4"), 148.9 (C, C3"), 151.2 (C, C5a'), 157.0 (C, C12'), 175.8 (C, C1); HRMS (ESI) calcd for ($C_{35}H_{42}{}^{35}ClN_3O_3$ + H^+): 588.2987, found 588.2969. Anal. ($C_{35}H_{42}ClN_3O_3 \cdot HCl \cdot 1/2H_2O$) C, H, N.

***N*-[4-(*tert*-Butyldimethylsilyloxy)-3-methoxybenzyl]-3-butynamide (12).** To a solution of 3-methoxy-4-(*tert*-butyldimethylsilyloxy)benzylamine, **11**[65] (2.10 g, 7.83 mmol) in CH_2Cl_2 (40 mL), 3-butynoic acid (658 mg, 7.83 mmol) and EDC hydrochloride (1.18 g, 6.16 mmol) were successively added. The reaction mixture was stirred at rt for 2 h until complete consumption of the amine. The mixture was diluted with H_2O and extracted with CH_2Cl_2 (2 × 100 mL). The combined organic extracts were washed with H_2O, then with brine, dried over anhydrous $MgSO_4$, and concentrated under reduced pressure. The crude product was purified by column

chromatography (40–60 µm silica gel, cyclohexane/EtOAc 80:20 to 70:30 mixtures, gradient elution) to yield amide **12** (950 mg, 36% yield) as a yellow-orange solid and the corresponding allene derivative (430 mg, 16% yield) as an off-white solid. ^{1}H NMR (300 MHz, $CDCl_3$) δ 0.14 [s, 6H, OSi(C*H*$_3$)$_2$C(CH$_3$)$_3$], 0.98 [s, 9H, OSi(CH$_3$)$_2$C(C*H*$_3$)$_3$], 2.33 (t, *J* = 2.7 Hz, 1H, 4-H), 3.26 (d, *J* = 2.7 Hz, 2H, 2-H$_2$), 3.79 (s, 3H, 3'-OCH$_3$), 4.39 (d, *J* = 5.7 Hz, 2H, CONHC*H*$_2$), 6.67–6.85 (complex signal, 3H, 2´-H, 5´-H, 6'-H); ^{13}C NMR (75.4 MHz, $CDCl_3$) δ –4.5 [2CH$_3$, OSi(*C*H$_3$)$_2$C(CH$_3$)$_3$], 18.6 [C, OSi(CH$_3$)$_2$*C*(CH$_3$)$_3$], 25.8 [3CH$_3$, OSi(CH$_3$)$_2$C(*C*H$_3$)$_3$], 27.5 (CH$_2$, C2), 43.9 (CH$_2$, CONH*C*H$_2$), 55.6 (CH$_3$, 3'-OCH$_3$), 74.4 (CH, C4), 77.5 (C, C3), 111.9 (CH, C2'), 120.2 (CH, C5'), 121.0 (CH, C6'), 131.1 (C, C1'), 144.7 (C, C4'), 151.2 (C, C3'), 166.0 (C, C1); MS (ESI+) m/z = 334 $[M + H]^+$.

2-{1-[4-(12-Amino-3-chloro-6,7,10,11-tetrahydro-7,11-methanocycloocta[*b*]quinolin-9-yl)butyl]-1*H*-1,2,3-triazol-4-yl}-*N*-[4-(*tert*-butyldimethylsilyloxy)-3-methoxybenzyl]acetamide (14). To a solution of azide **13**[64] (50 mg, 136 µmol) and alkyne **12** (54 mg, 162 µmol) in acetonitrile (5.4 mL), CuI (26 mg, 136 µmol) was added. The reaction mixture was stirred with protection from light at rt for 12 h and concentrated at reduced presure. The resulting crude was purified by column chromatography (40–60 µm silica gel, CH_2Cl_2/MeOH 98:2 to 80:20 mixtures, gradient elution) to afford the hybrid **14** (76 mg, 80% yield) as a yellowish solid: ^{1}H NMR (200 MHz, CD_3OD) δ 0.10 [s, 6H, OSi(C*H*$_3$)$_2$C(CH$_3$)$_3$], 0.97 [s, 9H, OSi(CH$_3$)$_2$C(C*H*$_3$)$_3$], 1.29 (m, 2H, 9'-CH$_2$C*H*$_2$CH$_2$CH$_2$), 1.60 (complex signal, 2H, 9'-CH$_2$CH$_2$C*H*$_2$CH$_2$), 1.90–2.10 (complex signal, 5H, 9'-C*H*$_2$CH$_2$CH$_2$CH$_2$, 13'-H$_{syn}$, 13'-H$_{anti}$, 10'-H$_{endo}$), 2.38 (dd, *J* = 17.0 Hz, *J* = 3.3 Hz, 1H, 10'-H$_{exo}$), 2.77 (m, 1H, 7'-H), 2.87 (d, *J* = 18.0 Hz, 1H, 6'-H$_{endo}$), 3.17 (dd, *J* = 18.0 Hz, *J* = 6.0 Hz, 1H, 6'-H$_{exo}$), superimposed 3.30 (m, 1H, 11'-H), 3.67 (s, 2H, 2-H$_2$), 3.80 (s, 3H, 3"-OCH$_3$), 4.18 (t, *J* = 7.0 Hz, 2H, 9'-CH$_2$CH$_2$CH$_2$C*H*$_2$),

4.33 (s, 2H, CONHCH_2),5.58 (d, J = 4.5 Hz, 8'-H), 6.73 (complex signal, 2H, 5"-H, 6"-H), 6.88 (s, 1H, 2"-H), 7.49 (dd, J = 9.0 Hz, J = 1.5 Hz, 1H, 2'-H), 7.67 (s, 1H, triazole C5-H), 7.70 (d, J = 1.5 Hz, 1H, 4'-H), 8.27 (d, J = 9.0 Hz, 1H, 1'-H); ^{13}C NMR (75.4 MHz, CD_3OD) δ –4.5 [2CH_3, OSi(CH_3)$_2$C(CH_3)$_3$], 19.3 [C, OSi(CH_3)$_2$C(CH_3)$_3$], 24.9 (CH_2, 9'-$CH_2CH_2CH_2CH_2$), 26.2 [3CH_3, OSi(CH_3)$_2$C(CH_3)$_3$], 27.6 (CH_2, C10'), 28.4 (CH, C11'), 29.5 (CH_2, 9'-$CH_2CH_2CH_2CH_2$), 30.0 (CH, C7'), 33.7 (CH_2, C13'), 36.8 (CH_2, C2), 37.1 (CH_2, 9'-$CH_2CH_2CH_2CH_2$), 44.2 (CH_2, C6'), 50.9 (CH_2, CONHCH_2), 53.2 (CH_2, 9'-$CH_2CH_2CH_2CH_2$), 55.9 (CH_3, 3"-OCH_3), 99.4 (CH, C2"), 112.9 (C, C11a'), 115.4 (C, C12a'), 120.6 (CH, C5"), 121.0 (CH, C6"), 121.7 (CH, C1'), 124.4 (CH, C2'), 124.6 (CH, triazole C5), 125.9 (CH, C8'), 126.0 (C, triazole C4), 127.2 (CH, C4'), 133.5 (C, C1"), 137.8 (C, C3'), 139.5 (C, C9'), 141.1 (C, C4a'), 145.4 (C, C4"), 152.3 (C, C3"), 154.2 (C, C12'), 155.4 (C, C5a'), 171.8 (C, C1); MS (ESI+) (m/z) = 701 $[M + H]^+$.

2-{1-[4-(12-Amino-3-chloro-6,7,10,11-tetrahydro-7,11-methanocycloocta[*b*]quinolin-9-yl)butyl]-1*H*-1,2,3-triazol-4-yl}-*N*-[4-hydroxy-3-methoxybenzyl]acetamide (5i). To a solution of hybrid **14** (57 mg, 81.3 µmol) in CH_2Cl_2/MeOH 80:20 (3.2 mL), camphorsulfonic acid (0.4 mg, 1.72 µmol) was added. The reaction mixture was stirred with protection from light at rt for 24 h. Progress of the reaction was checked by HPLC. The resulting mixture was quenched with sat. aq. $NaHCO_3$ (10 mL) and extracted with CH_2Cl_2 (3 × 25 mL). The combined organic extracts were dried over anhydrous Na_2SO_4 and evaporated at reduced pressure. The crude product was purified by column chromatography (40–60 µm silica gel, EtOAc/MeOH/Et_3N 95:5:1 to 80:20:1 mixtures, gradient elution) to afford hybrid **5i** (35 mg, 73% yield) as an orange solid: ^{1}H NMR (200 MHz, CD_3OD) δ 1.30 (m, 2H, 9'-$CH_2CH_2CH_2CH_2$), 1.61 (m, 2H, 9'-$CH_2CH_2CH_2CH_2$), 1.87–2.10 (complex signal, 5H, 9'-$CH_2CH_2CH_2CH_2$, 10'-H_{endo}, 13'-H_{syn}, 13'-H_{anti}), 2.37 (dd, J =

17.0 Hz, *J* = 3.3 Hz, 10'-H_{exo}) 2.74 (m, 7'-H), 2.82 (d, *J* = 18.0 Hz, 6'-H_{endo}), 3.11 (dd, *J* = 18.0 Hz, *J* = 5.4 Hz, 6'-H_{exo}), superimposed 3.30 (m, 1H, 11'-H), 3.66 (s, 2H, 2-H_2), 3.81 (s, 3H, 3"-OCH_3), 4.17 (t, *J* = 6.9 Hz, 2H, 9'-$CH_2CH_2CH_2CH_2$), 4.29 (s, 2H, CONHCH_2), 5.59 (d, *J* = 5.7 Hz, 8'-H), 6.71 (complex signal, 2H, 5"-H, 6"-H), 6.86 (s, 1H, 2"-H), 7.42 (dd, *J* = 9.1 Hz, *J* = 1.9 Hz, 1H, 2'-H), 7.63 (s, 1H, triazole C5-H), 7.67 (d, *J* = 1.9 Hz, 1H, 4'-H), 8.33 (d, *J* = 9.1 Hz, 1H, 1'-H); ^{13}C NMR (75.4 MHz, CD_3OD) δ 24.8 (CH_2, C6'), 25.4 (CH_2, 9'-$CH_2CH_2CH_2CH_2$), 27.5 (CH_2, C2), 28.1 (2CH, C7', C11'), 29.3 (CH_2, 9'-$CH_2CH_2CH_2CH_2$), 30.0 (CH_2, C10'), 33.6 (CH_2, C13'), 36.0 (CH_2, CONHCH_2), 37.0 (CH_2, 9'-$CH_2CH_2CH_2CH_2$), 50.8 (CH_2, 9'-$CH_2CH_2CH_2CH_2$), 56.4 (CH_3, 3"-OCH_3), 112.4 (CH, C2"), 115.4 (2C, C11a', C12a'), 116.1 (CH, triazole C5), 119.3 (CH, C5"), 121.3 (CH, C6"), 125.7 (CH, C1') (CH, C2'), 126.3 (CH, C8'), 127.7 (CH, C4'), 131.1 (C, C1"), 135.4 (C, triazole C4), 137.9 (C, C3'), 139.5 (C, C9'), 140.5 (C, C3"), 140.6 (C, C4"), 149.0 (C, C4a'), 153.0 (C, C12'), 156.7 (C, C5a'), 171.4 (C, C1); MS (ESI+) = (m/z) 587 $[M + H]^+$; HRMS (ESI) calcd for ($C_{32}H_{35}{}^{35}ClN_6O_3 + H^+$): 587.2532, found 587.2534.

AChE and BChE Inhibition Assays. Inhibition of human cholinesterases was evaluated spectrophotometrically by the method of Ellman *et al.*[66] An AChE stock solution was prepared by dissolving human recombinant AChE (E.C.3.1.1.7) lyophilized powder (Sigma, Italy) in 0.1 M phosphate buffer (pH = 8.0) containing 0.1% Triton X-100. A stock solution of human serum BChE (E.C. 3.1.1.8, Sigma, Italy) was prepared by dissolving the lyophilized powder in an aqueous solution of 0.1% gelatine. Stock solutions of the tested compounds (1 mM) were prepared and diluted in MeOH. Five increasing concentrations of each inhibitor were used, able to yield inhibition of enzymatic activity in the range of 20–80%. The assay solution consisted of 0.1 M phosphate buffer, pH 8.0, with the addition of 340 μM 5,5'-dithio-bis(2-nitrobenzoic acid),

0.02 unit/mL of human recombinant AChE, or BChE from human serum, and 550 μM substrate (acetylthiocholine iodide (ATCh) or butyrylthiocholine iodide (BTCh), respectively).

Assay solutions, with and without inhibitor, were preincubated at 37 ºC for 20 min, followed by addition of substrate. Control solutions containing all components except AChE or BChE were prepared in parallel to correct for non-enzymatic substrate hydrolysis. Initial rate assays were performed at 37 °C with a Jasco V-530 double beam Spectrophotometer: the rate of increase in absorbance at 412 nm was followed for 210 s. The velocities in the presence and absence of inhibitor were compared and the percentage inhibition was calculated. The percentage inhibition was plotted vs. the logarithm of the final inhibitor concentration. Linear regression and IC_{50} values were calculated using Microcal Origin 3.5 software (Microcal Software, Inc). Values are expressed as mean ± standard error of the mean (SEM) of at least two experiments, each performed in duplicate/triplicate.

Kinetic Analysis of AChE Inhibition. To assess the mechanism of action of hybrid **5c**, reciprocal plots of $1/v$ vs. 1/S (S = substrate) were constructed at relatively low substrate concentrations (0.113–0.566 mM) for inhibition of human recombinant AChE (Sigma, Milan). Four inhibitor concentrations were employed: 0.170, 0.341, 0.681, 1.363 nM. The plots were assessed by a weighted least-squares analysis that assumed the variance of the velocity (v) to be a constant percentage of v for the entire data set. Data analysis was performed with GraphPad Prism 4.03 software (GraphPad Software Inc.). The mechanism of inhibition was assessed by two independent experiments, each performed in triplicate.

Calculation of the inhibition constant, K_i, was performed by re-plotting slopes of lines from the Lineweaver–Burk plot vs. the inhibitor concentration, and K_i was determined as the intersection

on the negative x-axis. The K'_i value (dissociation constant for the enzyme–substrate–inhibitor complex) was determined by plotting the apparent $1/v_{max}$ vs. inhibitor concentration.[89]

Propidium Displacement Studies. The affinity of hybrid **5c** for the peripheral binding site of *Ee*AChE (type VI-S, Sigma, Italy) was determined using propidium iodide (P), a PAS-specific ligand, as previously described by Taylor *et al.*.[69,70] A shift in the excitation wavelength follows formation of the propidium/AChE complex.[69] Fluorescence intensity was monitored in a Jasco 6200 spectrofluorometer (Jasco Europe, Italy), using a 0.5 mL quartz cuvette at room temperature. *Ee*AChE (2 μM, assuming 82,000 kDa mass) was first incubated with 8 μM propidium iodide in 1 mM Tris-HCl, pH 8.0, at room temperature. An 8 mM stock solution of hybrid **5c** was prepared in MeOH. In the back-titration experiments, aliquots of inhibitor (4–64 μM final concentration) were added successively to the solution of the propidium/AChE complex, and fluorescence emission was monitored at 602 nm upon excitation at 535 nm. Blanks containing propidium alone, inhibitor plus propidium and *Ee*AChE were prepared, and fluorescence emission determined and subtracted. Raw data were processed following the method of Taylor and Lappi[69] to estimate the K_D value, assuming a dissociation constant value for propidium and *Ee*AChE of 0.7 μM.[90] Data analysis was performed with GraphPad Prism 4.03 software (GraphPad Software Inc.). Data are the average of three independent experiments.

The same experimental procedure was used in the attempt to also determine the affinity of capsaicin for PAS. A 8 mM stock solution of capsaicin was prepared in MeOH. In the back-titration experiments, aliquots of inhibitor (4–92 μM final concentration) were added successively to the solution of the propidium/AChE complex. However, fluorescence emission at 602 nm (λexc = 535 nm) of capsaicin blank solutions showed significant intensities which hampered an accurate quantitative determination of the affinity constant.

BACE-1 Inhibition Assay. BACE-1 (Sigma) inhibition studies were performed employing a peptide mimic of the APP sequence as substrate, methoxycoumarin-Ser-Glu-Val-Asn-Leu-Asp-Ala-Glu-Phe-Lys-dinitrophenyl (M-2420, Bachem, Germany). The following procedure was employed: 5 μL of test compound (or DMSO in the control well) were pre-incubated with 175 μL of enzyme (in 20 mM sodium acetate, pH 4.5, containing CHAPS 0.1% w/v) for 1 h at rt. The substrate (3 μM, final concentration) was then added and left to react for 15 min. The fluorescence signal was read at λ_{em} = 405 nm (λ_{exc} = 320 nm). The DMSO concentration in the final mixture was maintained below 5% (v/v) to preclude significant loss of enzyme activity. The background signal was measured in control wells containing all the reagents except BACE-1 and subtracted. The fluorescence intensities with and without inhibitor were compared and the percent inhibition due to the presence of test compounds was calculated by the following expression: $100 - (IF_i/IF_o \times 100)$, where IF_i and IF_o are the fluorescence intensities obtained for BACE-1 in the presence and absence of inhibitor, respectively. To demonstrate inhibition of BACE-1 activity, a peptidomimetic inhibitor (β-secretase inhibitor IV, Calbiochem) was serially diluted into the reaction wells (IC_{50} = 13.0 ± 0.1 nM). Values are expressed as mean ± standard deviation (SD) of two independent experiments, each performed in triplicate.

DPPH radical scavenging activity assay. Radical scavenging activity of the capsaicin–huprine hybrids was determined using the DPPH assay.[91,92] Four different concentrations of the compounds (3–100 μM), dissolved in DMSO, were incubated with a methanolic solution of DPPH (100 μM). The final concentration of DMSO was kept below 1%. After 30 min of incubation at rt in the dark, the absorbance at 517 nm was measured. The percentage inhibition for each concentration was calculated by comparison with the absorbance of the DPPH solution. Dose–response curves were plotted and IC_{50} values were calculated by the

software CurveExpert version 1.34 for Windows. Data are expressed as the mean ± SD of three experiments, each performed in duplicate.

Crystallization and Data Collection. *Tc*AChE[93] was concentrated to 12 mg/mL and crystallized using the hanging-drop vapor diffusion method. At rt, an equal volume (1 µL) of *Tc*AChE solution was mixed with a mother liquor solution composed of 50 mM MES, pH 5.8–6.2, 28–32% PEG 200. After 10-20 days, crystals were harvested and soaked for 12 h in a solution of the mother liquor complemented with specific compounds (1 mM). All data were collected at the European Synchrotron Radiation Facility (ESRF, Grenoble, France). Data collected on ESRF beamline ID30A1 were from crystals flash-frozen and stored in liquid nitrogen before the experiment. Data were collected on ESRF beamlines ID29 and ID23-2 from crystals directly flash-cooled in the stream of N_2 gas at 100 K.

Recombinant *h*BChE, purified after expression in insect cells,[94] was concentrated to 6 mg/mL in 20 mM Tris, pH 7.4. Using the hanging-drop vapor diffusion technique, crystals were obtained at rt by mixing of equal volumes of protein (2 µL) and of the reservoir solution (250 mM ammonium acetate, 20% polyethylene glycol 4000). Crystals were soaked for 12 h in the reservoir solution complemented with compounds at 1 mM. Cryoprotection of hBChE crystals was carried out via a short soak in mother liquor solution complemented with 20% glycerol, before being flash-cooled at 100 K in liquid nitrogen. Data were collected on ESRF beamline ID30A-3.

Data Processing and Refinement. Data were indexed and integrated using XDS, and intensity measurements were scaled and merged with XSCALE. Molecular replacement was carried out with PHASER to retrieve the phases. Models of hBChE from PDB entry 4TPK, and of *Tc*AChE from PDB entry 2XI4, were used as search models. Two subunits were placed in the asymmetric

unit of all complex structures, except for the *Tc*AChE–**5i** complex structure, for which a single subunit was found. Structures were refined by iterative reciprocal-space refinement with phenix.refine and real-space refinement using Coot. Reciprocal space refinement included refinement of atomic positions and individual isotropic temperature factors. All ligand topologies were generated with the PRODRG server, and their occupancies were refined during the last cycles of reciprocal-space refinement. The atomic coordinates and structure factors have been deposited in the protein data bank under accession codes 7ais, 7ait, 7aiu, 7aiv, 7aiw and 7aix for compounds **5b**, **5c**, **5d**, **5f**, **5h**, **5i** complexed with TcAChE and under accession code 7aiy for compound **5i** complexed with hBChE.

BBB Permeation Assay. The parallel artificial membrane permeation assay for blood–brain barrier permeation described by Di *et al.*[77] was used to assess the brain penetration of the HC hybrids. The *in vitro* permeability (P_e) of the synthesized hybrids and of fourteen commercial drugs through lipid extract of porcine brain membrane was determined using a mixture of phosphate-buffered saline (PBS)/EtOH 70:30. Assay validation was established by comparison of the experimental and reported P_e values for the commercial drugs (Table S3 of the Supporting Information), which showed a good correlation: P_e (exp) = 1.4974 P_e (lit) − 0.8434 (R^2 = 0. 9428). From this equation and taking into account the limits established by Di *et al.* for BBB permeation, the following ranges of permeability were established: compounds of high BBB permeation (CNS+): P_e (10^{-6} cm s^{-1}) > 5.1; compounds of low BBB permeation (CNS−): P_e (10^{-6} cm s^{-1}) < 2.1, and compounds of uncertain BBB permeation (CNS±): 5.1 > P_e (10^{-6} cm s^{-1}) > 2.1. Values are expressed as mean ± SD of three experiments, each performed in triplicate.

Biodistribution Studies in C57BL6 Mice. This study was carried out using 6-month-old female C57BL6 mice. Animals were housed in the Faculty of Pharmacy and Food Sciences of the

University of Barcelona, maintained under controlled light, temperature, and humidity conditions, with access to water and food ad libitum. Every possible effort was made to reduce the number of animals used and to minimize their suffering. Mice were treated in accordance with the European Community Council Directive 86/609/EEC and the procedures established by the Department d'Agricultura, Ramaderia i Pesca of the Generalitat de Catalunya.

Each compound was administered in triplicate and the recovery percentage using spiked standards was studied for each drug in order to normalise the results obtained. In addition, three animals treated with saline serum were used as a blank. Briefly, the drugs were administered intraperitoneally at a dose of 2 mg/kg day for two weeks, three times a week. Mice were weighted weekly and the equivalent volume was administered. Once the two-week-treatment was finished, 4 h after the last dose, the animals were sacrificed by cervical dislocation and the lungs, liver, kidney and brain, as well as a blood sample, were extracted. The plasma was extracted from the blood by centrifugation at 2000 r.p.m. at 4 ^{o}C for 20 min. The drugs were extracted from the tissues by adding MeOH/DMSO 75:25, followed by homogenization for 45 min. Then, 800 µL of the mixture were placed in an Eppendorf tube and 40 µL of an internal standard were added. After mixing on a vortex, 2 M NaOH (40 µL) was added and the samples were vortexed for a further 15 min. Then, 2 M HCl (40 µL) was added to each sample and the samples were vortexed for an additional 15 min. Finally, the samples were centrifuged at 14000 r.p.m for 15 min and the supernatant was removed and placed in an HPLC vial. The solvents were evaporated and the drug on the vial walls was dissolved in MeOH. The recovery procedure was carried out using the same methodology, but adding an initial known amount of drug. Finally, the samples were quantified using HPLC coupled with MS in a positive mode (HPLC/MS/MS). The mobile phases, used in a gradient described in Table S5 of the Supporting

Information, were acetonitrile with 0.1% formic acid (A) and H_2O with 0.1% formic acid (B). A Kinetex 2.6 μm C18 100A 50 × 2.1 mm column was employed.

For donepezil detection, diphenhydramine was used as the internal standard. The collision-induced transition m/z 380→91 was used to analyse donepezil in selected reaction monitoring mode based on the method of Xie and colleagues.[95]

Data were analyzed using one-way analysis of variance (ANOVA), followed by Tukey's post hoc test; ** $p < 0.01$; *** $p < 0.001$ were considered significant differences.

In Vivo Efficacy Studies. Animals, Drugs, and Treatment: AβPPswe/PS-1 double transgenic male mice, which express the mutant APPswe (K595N/M596L) and PSEN1ΔE9, the deletion of the exon 9 under the control of the mouse prion promoter, were obtained from the Jackson Laboratory (Bar Harbor, ME, Stock no 004462). Animals were maintained at the Animal Facility of the Pontificia Universidad Católica de Chile under sanitary barrier in ventilated racks and in closed colonies. Experimental procedures were approved by the Bioethical and Biosafety Committee of the Faculty of Biological Sciences of the Pontificia Universidad Católica de Chile with the ethical approval CBB-180703004. The inclusion/exclusion criteria for this study were the health of the animals after treatment. Thus, all the animals finishing the treatment correctly and remaining healthy were to be used to continue the analysis, whereas those showing signs of illness were to be excluded. For implementation of this inclusion/exclusion criterion we evaluated the weight of the animals and the lipid and hepatic parameters, accompanied by visual inspection. In fact, in this particular study it was not necessary to exclude any animal. To avoid suffering, the animals were reviewed by technical personnel every day to look for evidence of suffering (NIH tables of supervision). Also, we used isoflurane (4% for induction) before

removing the animals' brains. All the cognitive tests (training and experiments) and the slices experiments were performed in a double-blind manner, between the operator and the designer of the experiment.

The experimental design comprised 6 groups. Treatment started when groups of mice were 5 month-old (young mice) or 10 month-old (old mice). In both cases the treatment continued for 4 weeks, so that, at the end of the treatment, mice in the two groups were 6 and 11 month-old, respectively. Each set comprised 3 experimental groups: AβPPswe/PS-1 control, AβPPswe/PS-1 treated with **5i** and AβPPswe/PS-1 treated with **5c**. The treatment consisted of intraperitoneal injection (i.p.) of 2.0 mg/kg of either compound, with saline solution as vehicle, three times per week during 4 weeks. Transgenic control animals were injected only with the vehicle.

Large Open-Field (LOF) Test. A 120 × 120 cm transparent Plexiglas platform with 35-cm-high transparent walls was used to study locomotor and stress behavior in our mouse model. The open field, which measured 40 × 40 cm, was defined as the center area of the field. Data were collected using an automatic tracking system (HVS Imagen, UK). Each mouse was placed alone in the center of the open field, and its behavior was tracked for 20 min. At the end of the session, the mouse was returned to its home cage. The parameters measured included total time moving and number of times the mouse crossed the center area of the platform.[96,97]

Novel Object Recognition (NOR) and Novel Object Localization (NOL). The NOR and NOL tasks were performed as previously described.[98,99] Mice were habituated to the experimental room in the experimental cages for 3 consecutive days, for 30 min per day, and for 1 h on the testing day. The task occurred in a 120 × 120 cm transparent Plexiglas platform with 35-cm-high

transparent walls, which contained two identical objects placed at specific locations. For object familiarization, mice were allowed to explore the platform for 10 min. The animals were subsequently returned to their home cages for 1 h, followed by a 5-min exposure to a novel localization of one of the familiar objects (NOL). The mice were again returned to their home cages for 1 h and were subsequently exposed to a novel object (NOR) for 5 min. The mice had no observed baseline preference for the different objects. An object preference index was determined by calculating the time spent near the relocated/novel object divided by the cumulative time spent with both the familiar and relocated/novel objects. The cages were routinely cleaned with EtOH following testing/habituation of the mice.

Memory Flexibility Test. This test was performed as previously described,[78,100] and the pool conditions were the same as those of a Morris Water Maze.[97] Each animal was trained for one pseudo-random location of the platform per day, for 5 days, with a new platform location each day. Training was conducted for up to 10 trials per day, until the criterion of 3 successive trials with an escape latency of 20 s was achieved. When testing had been completed, the mouse was removed from the maze, dried and returned to its cage. Animals were tested for the next location on the following day. Data were collected using a video tracking system (HVS Imagen).

Detection and Quantification of Aβ. To determine the concentrations of Aβ peptides, two sandwich enzyme-linked immunosorbent assays (ELISAs) specific for Aβ40 and Aβ42 were used, as previously described.[101] Hippocampal and cortical homogenates of each animal were diluted to 1 μg/μL in homogenization buffer containing protease and phosphatase inhibitors. Diluted homogenate (100 μL) was prepared to measure Aβ40/Aβ42 levels according to the manufacturer's instructions. Plates were read at 450 nm and 590 nm on a Metertech 960 ELISA Analyzer.

To detect soluble Aβ oligomers using Western blot analysis, 100 μg of protein of the hippocampal and cortical total protein lysate was separated in a Tris–Tricine buffer system (0.2 M Tris, pH 8.9, as the anode buffer and 0.1 M Tris, 0.1 M Tricine, 0.1% SDS, pH 8.25, as the cathode buffer) and then transferred to a PVDF membrane. The membranes were incubated with the primary antibody anti Aβ-4G8 (Biolegend, San Diego, CA) and developed using an ECL kit (Luminata Forte Western HRP Substrate, Millipore Corporation, Burlington, MA). Data are expressed as mean values ± SEM of n = 7 animals in each group.

Electrophysiological Measurements. Mouse Brain Slice Preparation. A detailed description of the method for preparing the slices was recently published.[83] As mentioned above, all young and old double transgenic mice had been treated with vehicle, **5i** or **5c** for 4 weeks before they were used to prepare acute coronal brain slices. Every animal was killed by decapitation subsequent to anesthesia with isoflurane. The brain was quickly removed and placed in a beaker of cold artificial cerebrospinal artificial solution (ACSF), modified by replacing a part of the NaCl by sucrose. Its composition, in mM, was as follows: 85 NaCl, 75 sucrose, 3 KCl, 1.25 NaH_2PO_4, 25 $NaHCO_3$, 10 dextrose, 3.5 $MgSO_4$, 0.5 $CaCl_2$, 3 sodium pyruvate, 0.5 sodium L-ascorbate and 3 myo-inositol (305 mOsm, pH 7.4). Then, 350 μm coronal sections were cut with a vibratome in the same cold solution. After cutting, the slices were maintained for 1 h in the same solution, but at 36 °C. They were then transferred to 'recording solution', composed of (in mM): 126 NaCl, 3.5 KCl, 1.25 NaH_2PO_4, 25 $NaHCO_3$, 10 dextrose, 1 $MgSO_4$, 2 $CaCl_2$, 3 sodium pyruvate, 0.5 sodium L-ascorbate and 3 myo-inositol (305 mOsm, pH 7.4) at room temperature (22 °C), in which they were maintained until recording. The experiments were performed in recording solution that was maintained at 32–34 °C. Picrotoxin (25 μM) was applied to block the γ-aminobutyric acid ($GABA_A$)-mediated inhibitory field component. At least three brain slices

from each animal were used, which were considered as replicates. Thus, they were averaged to represent a single animal. Therefore, for the group of young mice we had a transgenic (Tg) control (n = 3 mice, three slices each), Tg treated with **5i** (n = 3 mice, three slices each) and Tg treated with **5c** (n = 3 mice, three slices each). The same number of animals and slices was used for the old mice. Thus, data represent the mean ± SEM from 9 slices out of 3 Tg control mice, 9 slices out of 3 Tg + **5i** mice, and 9 slices out of 3 Tg + **5c** mice.

Electrophysiology. Electrophysiological recordings were obtained by placing the slice in a recording chamber allocated on an upright infrared-differential interference contrast (IR-DIC) fluorescence microscope (Eclipse FNI, Nikon). Visualization of hippocampal circuits utilized a 40× water objective and a light-sensitive camera (TOPICA CCD Camera). To stimulate the Schaffer collaterals between CA3 and CA1, we used a bipolar concentric electrode (World Precision Instruments, Sarasota, FL, United States) connected to an ISO-Flex stimulus generator (A.M.P.I., Jerusalem, Israel). We recorded the evoked field excitatory postsynaptic potentials (fEPSPs) in the stratum radiatum of CA1, using a borosilicate glass electrode (World Precision Instruments, United States) of 0.5–1 MΩ, pulled on a P-97 Flaming/Brown Micropipette Puller (Sutter Instruments, United States), filled with the recording solution. The signals were recorded using a MultiClamp 700B amplifier (Axon CNS, Molecular Devices LLC, United States), and digitally sampled at 30 kHz using a Digidata-1440A interface (Axon CNS, Molecular Devices). All analyses were done offline, using pClamp 10.3 (Molecular Devices LLC, United States).

Several experimental protocols were applied to study the effects of the two target compounds. We obtained the input-output curve to establish the relationship between the stimulus intensity and the extent of the evoked response. To do that, the fEPSP slopes measurements (measured in mV/ms) at increasing levels of current intensity were plotted. The amount of current required to

evoke 60% of the maximum slope value was used to perform other protocols in the same slice. To evaluate synaptic plasticity in the slices, we performed long-term potentiation (LTP) experiments. Two pulses of 5 ms duration (R1 and R2) separated by 50 ms were applied with the stimulus generator every 15 s. The fEPSP slope of the first pulse (R1) was averaged during 15 to 20 min once a baseline was obtained. Then, a theta burst stimulation (TBS), consistent of 5 bursts at 100 Hz every 20 s, was applied. After TBS, the same two pulses separated by 50 ms were applied during at least 60 min, considered to be an LTP induction period. Every slope measurement (R1) obtained during the post-TBS period was compared to the averaged slope measurements obtained before TBS, during the basal period. The data thus obtained represent the degree of potentiation. They were plotted as the relative value of the fEPSP slope as a function of time, and compared among the groups. To evaluate the efficacy of synaptic strength before and after LTP induction, we studied the correlation between the fiber volley (FV) amplitudes and their corresponding fEPSP slopes and compared them among groups.

The results are expressed as the means ± standard errors. The data were analyzed by one-way and two-way analysis of variance (ANOVA), followed by Bonferroni's post hoc test; the threshold for statistical significance was $p < 0.05$, with a 95% confidence interval (CI). Statistical analyses were performed using Prism software (GraphPad, United States).

Immunofluorescence Determination of Hippocampal Levels of Oxidative Stress Markers. After the treatment had been terminated, the mouse brains were removed on ice, and one hemisphere was fixed by immersion in 4% paraformaldehyde (PFA) for 7 days at 4 °C. It was then placed in 30% sucrose in PBS at 4 °C overnight and sliced into 30-µm-thick coronal sections using a cryostat (Leitz, 1900) at −20 °C. The slices were washed three times in ice-cold PBS and then permeabilized for 30 min with 0.2% Triton X-100 in PBS. After several rinses in

ice-cold PBS, the samples were incubated in blocking solution (0.2 % bovine serum albumin in PBS) for 1 h at room temperature, followed by overnight incubation at 4 °C with primary antibodies. The primary antibodies included rabbit anti-GFAP (Dako, Denmark, USA) and rabbit anti-4-HNE (Abcam, Cambridge, UK). After primary antibody incubation, the slices were extensively washed with PBS and then incubated with Alexa-conjugated secondary antibodies (Molecular Probes, Carlsbad, CA) for 2 h at 37 °C. Nuclear staining was performed by treating the slices with Hoechst (Sigma-Aldrich). All the inmunofluorecence samples were obtained using slices from the midbrain region (bregma -3,-5) The slices were subsequently mounted on slides using mounting medium and photographs of each slice were taken using a Zeiss LSM 5 Pascal confocal microscope. Four or five slices from each animal were stained, and three animals were examined for each condition. The photographs were analyzed by separating the channels and then measuring the fluorescence intensity, normalized by the area in every 8-bit (black and white) photograph vs the control condition using the average of all the determinations, using NIH ImageJ software.

Statistical Analysis. All in vivo experiments were performed at least 3 times, with triplicates for each condition in each experimental run. The results are expressed as means ± standard errors. Data were analyzed by one-way analysis of variance (ANOVA), followed by Bonferroni's post hoc test; $*p \leq 0.05$ and $**p \leq 0.01$ were considered significant differences. Statistical analyses were performed using Prism software (GraphPad, USA). For testing normality, we employed the SPSS Statistics software (IBM, USA), using the numerical method.

ASSOCIATED CONTENT

Supporting Information. Additional data of the crystal structures of target compounds in complex with *Tc*AChE and hBChE, PAMPA-BBB, biodistribution, hippocampal Aβ levels, and electrophysiological studies, copies of ^{1}H and ^{13}C NMR spectra, elemental analysis and HPLC data, and PDB files of the crystal structures of the complexes of compounds **5b**, **5c**, **5d**, **5f**, **5h**, and **5i** with *Tc*AChE and of compound **5i** with hBChE. This material is available free of charge via the Internet at http://pubs.acs.org.

AUTHOR INFORMATION

Corresponding Authors

* **Diego Muñoz-Torrero** – *Laboratory of Medicinal Chemistry (CSIC Associated Unit), Faculty of Pharmacy and Food Sciences, and Institute of Biomedicine (IBUB), University of Barcelona (UB), E-08028 Barcelona, Spain*; orcid.org/0000-0002-8140-8555; Phone: (+34) 934024533; E-mail: dmunoztorrero@ub.edu

* **Pierre-Yves Renard** – *Normandie University, UNIROUEN, INSA Rouen, CNRS, COBRA (UMR 6014), 76000 Rouen, France*; orcid.org/0000-0001-9094-9778; Phone: (+33) 235522476; E-mail: pierre-yves.renard@univ-rouen.fr

* **Jacques-Philippe Colletier** – *Institut de Biologie Structurale, Université Grenoble Alpes, CEA, CNRS UMR 5075, F-38054 Grenoble, France*; orcid.org/0000-0003-1819-4686; Phone: (+33) 457428515; E-mail: colletier@ibs.fr

* **Nibaldo C. Inestrosa** – *Center of Aging and Regeneration UC (CARE-UC), Departamento de Biología Celular y Molecular, Facultad de Ciencias Biológicas, Pontificia Universidad Católica*

de Chile, Av. Libertador Bernardo O'Higgins 340, P.O. Box 114, 8331150-Santiago, and Centro de Excelencia en Biomedicina de Magallanes (CEBIMA), Universidad de Magallanes, Punta Arenas, Chile; orcid.org/0000-0003-3118-9726; Phone: (+56-2) 223542724; E-mail: ninestrosa@bio.puc.cl

Author Contributions

▽ These authors contributed equally. The manuscript was written through contributions of all authors. All authors have given approval to the final version of the manuscript.

Notes

The authors declare no competing financial interest.

ACKNOWLEDGMENTS

This work was supported by Ministerio de Ciencia, Innovación y Universidades (MCIU), Agencia Estatal de Investigación (AEI) and FEDER (SAF2017-82771-R, SAF2014-57094-R), Generalitat de Catalunya (GC) (2017SGR106), the Agence Nationale de la Recherche (ANR) (project Multi-Click, grant number ANR-12-BS07-0008-01), the France Alzheimer Foundation (grant FA-AAP-2013-65-101349 to J.-P.C.), the Italian Ministry of Education, University and Research – MIUR, the Basal Center of Excellence in Aging and Regeneration (CONICYT-AFB 170005 to N.C.I.), FONDECYT (no. 11160651 to P.C.), and MIADES T010131, MIADES T010132 to N.C.I. We also thank the Sociedad Química y Minera de Chile (SQM) for the special grants "The role of K+ on Hypertension and Cognition" and "The role of Lithium in Human Health and Disease". Fellowships from GC to E.V., from ANR to M.C.-B., from Lifelong

Learning Programme/Erasmus to M.Ri., and from and from Leonardo da Vinci Project Unipharma-Graduates 5 to M.Re., and the support of the Vice-Chancellor for Research of the Shiraz University of Medical Sciences to O.F. are gratefully acknowledged.

ABBREVIATIONS

Aβ, β-amyloid peptide; ACh, acetylcholine; AChE, acetylcholinesterase; AD, Alzheimer's disease; APP, amyloid precursor protein; ATCh, acetylthiocholine iodide; BBB, blood–brain barrier; BACE-1, β-site APP cleaving enzyme 1 or β-secretase; BChE, butyrylcholinesterase; BTCh, butyrylthiocholine iodide; CAS, catalytic anionic site; CNS, central nervous system; CuAAC, copper-catalyzed azide–alkyne cycloaddition; *Ee*AChE, electric eel acetylcholinesterase; hAChE, human acetylcholinesterase; hBChE, human butyrylcholinesterase; MCI, mild cognitive impairment; MTDLs, multitarget-directed ligands; PAMPA-BBB, parallel artificial membrane permeation assay; PAS, peripheral anionic site; PBS, phosphate-buffered saline; *Tc*AChE, *Torpedo californica* acetylcholinesterase.

PDB ID CODES

The coordinates and structure factors corresponding to the complexes of compounds **5b**, **5c**, **5d**, **5f**, **5h**, and **5i** with *Tc*AChE and of compound **5i** with hBChE have been deposited in the Protein Data Bank under accession codes 7ais, 7ait, 7aiu, 7aiv, 7aiw, 7aix, and 7aiy, respectively. The Authors will release the atomic coordinates and experimental data upon article publication.

REFERENCES

(1) Alzheimer's Disease International. 2019. World Alzheimer Report 2019: Attitudes to Dementia. London: Alzheimer's Disease International.

(2) Sharma, A. K.; Taneja, G.; Khanna, D.; Rajput, S. K. Reactive oxygen species: friend or foe? *RSC Adv.* **2015**, *5*, 57267–57276.

(3) Rodrigues, R.; Petersen, R. B.; Perry, G. Parallels between major depressive disorder and Alzheimer's disease: Role of oxidative stress and genetic vulnerability. *Cell. Mol. Neurobiol.* **2014**, *34*, 925–949.

(4) Bachurin, S. O.; Bovina, E. V.; Ustyugov, A. A. Drugs in clinical trials for Alzheimer's disease: The major trends. *Med. Res. Rev.* **2017**, 37, 1186–1225.

(5) Hu, H.; Chen, Z.; Xu, X.; Xu, Y. Structure-based survey of the binding modes of BACE1 inhibitors. *ACS Chem. Neurosci.* **2019**, *10*, 880–889

(6) Doody, R. S.; Thomas, R. G.; Farlow, M.; Iwatsubo, T.; Vellas, B.; Joffe, S.; Kieburtz, K.; Raman, R.; Sun, X.; Aisen, P. S.; Siemers, E.; Liu-Seifert, H.; Mohs, R. Phase 3 trials of solanezumab for mild-to-moderate Alzheimer's disease. *N. Engl. J. Med.* **2014,** *370*, 311–321.

(7) Pimplikar, S. W. Reassessing the amyloid cascade hypothesis of Alzheimer's disease. *Int. J. Biochem. Cell Biol.* **2009**, *41*, 1261–1268.

(8) Rosini, M.; Simoni, E.; Milelli, A.; Minarini, A.; Melchiorre. C. Oxidative stress in Alzheimer's disease: Are we connecting the dots? *J. Med. Chem.* **2014**, *57*, 2821–2831.

(9) Deardorff, W. J.; Feen, E.; Grossberg, G. T. The use of cholinesterase inhibitors across all stages of Alzheimer's disease. *Drugs Aging* **2015,** *32*, 537–547.

(10) Hutton, M.; Lendon, C. L.; Rizzu, P.; Baker, M.; Froelich, S.; Houlden, H.; Pickering-Brown, S.; Chakraverty, S.; Isaacs, A.; Grover, A.; Hackett, J.; Adamson, J.; Lincoln, S.; Dickson, D.; Davies, P.; Petersen, R. C.; Stevens, M.; de Graaff, E.; Wauters, E.; van Baren, J.; Hillebrand, M.; Joosse, M.; Kwon, J. M.; Nowotny, P.; Che, L. K.; Norton, J.; Morris, J. C.; Reed, L. A.; Trojanowski, J.; Basun, H.; Lannfelt, L.; Neystat, M.; Fahn, S.; Dark, F.; Tannenberg, T.; Dodd, P. R.; Hayward, N.; Kwok, J. B.; Schofield, P. R.; Andreadis, A.; Snowden, J.; Craufurd, D.; Neary, D.; Owen, F.; Oostra, B. A.; Hardy, J.; Goate, A.; van Swieten, J.; Mann, D.; Lynch, T.; Heutink, P. Association of missense and 5'-splice-site mutations in tau with the inherited dementia FTDP-17. *Nature* **1998,** *393*, 702–705.

(11) Geula, C.; Mesulam, M. M.; Saroff, D. M.; Wu, C. K. Relationship between plaques, tangles, and loss of cortical cholinergic fibers in Alzheimer disease. *J. Neuropathol. Exp. Neurol.* **1998,** *57*, 63–75.

(12) Campanari, M. L.; Garcia-Ayllon, M. S.; Blazquez-Llorca, L.; Luk, W. K.; Tsim, K.; Saez-Valero, J. Acetylcholinesterase protein level is preserved in the Alzheimer's brain. *J. Mol. Neurosci.* **2014,** *53*, 446–453.

(13) Darvesh, S.; Cash, M. K.; Reid, G. A.; Martin, E.; Mitnitski, A.; Geula, C. Butyrylcholinesterase is associated with β-amyloid plaques in the transgenic APPSWE/PSEN1dE9 mouse model of Alzheimer disease. *J. Neuropathol. Exp. Neurol.* **2012,** *71*, 2–14.

(14) Alvarez, A.; Alarcon, R.; Opazo, C.; Campos, E. O.; Munoz, F. J.; Calderon, F. H.; Dajas, F.; Gentry, M. K.; Doctor, B. P.; De Mello, F. G.; Inestrosa, N. C. Stable complexes involving acetylcholinesterase and amyloid-β peptide change the biochemical properties of the enzyme and increase the neurotoxicity of Alzheimer's fibrils. *J. Neurosci.* **1998,** *18*, 3213–3223.

(15) Inestrosa, N. C.; Alvarez, A.; Pérez, C. A.; Moreno, R. D.; Vicente, M.; Linker, C.; Casanueva, O. I.; Soto, C.; Garrido, J. Acetylcholinesterase accelerates assembly of amyloid-β-peptides into Alzheimer's fibrils: possible role of the peripheral site of the enzyme. *Neuron* **1996**, *16*, 881–891.

(16) Alvarez, A.; Opazo, C.; Alarcon, R.; Garrido, J.; Inestrosa, N. C. Acetylcholinesterase promotes the aggregation of amyloid-β-peptide fragments by forming a complex with the growing fibrils. *J. Mol. Biol.* **1997,** *272*, 348–361.

(17) Greenblatt, H. M.; Dvir, H.; Silman, I.; Sussman, J. L. Acetylcholinesterase: a multifaceted target for structure-based drug design of anticholinesterase agents for the treatment of Alzheimer's disease. *J. Mol. Neurosci.* **2003,** *20*, 369–383.

(18) Greig, N. H.; Utsuki, T.; Ingram, D. K.; Wang, Y.; Pepeu, G.; Scali, C.; Yu, Q. S.; Mamczarz, J.; Holloway, H. W.; Giordano, T.; Chen, D.; Furukawa, K.; Sambamurti, K.; Brossi, A.; Lahiri, D. K. Selective butyrylcholinesterase inhibition elevates brain acetylcholine, augments learning and lowers Alzheimer beta-amyloid peptide in rodent. *Proc. Natl. Acad. Sci. U. S. A.* **2005**, *102*, 17213–17218.

(19) Li, Q.; Xing, S.; Chen, Y.; Liao, Q.; Xiong, B.; He, S.; Lu, W.; Liu, Y.; Yang, H.; Li, Q.; Feng, F.; Liu, W.; Chen, Y.; Sun, H. Discovery and biological evaluation of a novel

highly potent selective butyrylcholinsterase inhibitor. *J. Med. Chem.* **2020**, *63*, 10030–10044.

(20) Brus, B.; Kosak, U.; Turk, S.; Pislar, A.; Coquelle, N.; Kos, J.; Stojan, J.; Colletier, J. P.; Gobec, S. Discovery, biological evaluation, and crystal structure of a novel nanomolar selective butyrylcholinesterase inhibitor. *J. Med. Chem.* **2014,** *57*, 8167–8179.

(21) Knez, D.; Brus, B.; Coquelle, N.; Sosic, I.; Sink, R.; Brazzolotto, X.; Mravljak, J.; Colletier, J. P.; Gobec, S. Structure-based development of nitroxoline derivatives as potential multifunctional anti-Alzheimer agents. *Bioorg. Med. Chem.* **2015,** *23*, 4442–4452.

(22) Fernández-Bachiller, M. I.; Pérez, C.; Monjas, L.; Rademann, J.; Rodríguez-Franco, M. I. New tacrine–4-oxo-4*H*-chromene hybrids as multifunctional agents for the treatment of Alzheimer's disease, with cholinergic, antioxidant, and β-amyloid-reducing properties. *J. Med. Chem.* **2012**, *55*, 1303–1317.

(23) Fernández-Bachiller, M. I.; Pérez, C.; Campillo, N. E.; Páez, J. A.; González-Muñoz, G. C.; Usán, P.; García-Palomero, E.; López, M. G.; Villarroya, M.; García, A. G.; Martínez, A.; Rodríguez-Franco, M. I. Tacrine-melatonin hybrids as multifunctional agents for Alzheimer's disease, with cholinergic, antioxidant, and neuroprotective properties. *ChemMedChem* **2009**, *4*, 828–841.

(24) Nachon, F.; Carletti, E.; Ronco, C.; Trovaslet, M.; Nicolet, Y.; Jean, L.; Renard, P.-Y. Crystal structures of human cholinesterases in complex with huprine W and tacrine: elements of specificity for anti-Alzheimer's drugs targeting acetyl- and butyryl-cholinesterase. *Biochem. J.* **2013**, *453*, 393–399.

(25) Cavalli, A.; Bolognesi, M. L.; Minarini, A.; Rosini, M.; Tumiatti, V.; Recanatini, M.; Melchiorre, C. Multi-target-directed ligands to combat neurodegenerative diseases. *J. Med. Chem.* **2008**, *51*, 347–372.

(26) Mesiti, F.; Chavarria, D.; Gaspar, A.; Alcaro, S.; Borges, F. The chemistry toolbox of multitarget-directed ligands for Alzheimer's disease. *Eur. J. Med. Chem.* **2019**, *181*, 111572.

(27) Wang, T.; Liu, X.; Guan, J.; Ge, S.; Wu, M.-B.; Lin, J.; Yang, L. Advancement of multi-target drug discoveries and promising applications in the field of Alzheimer's disease. *Eur. J. Med. Chem.* **2019**, *169*, 200–223.

(28) Gontijo, V. S.; Viegas, F. P. D.; Ortiz, C. J. C.; de Freitas Silva, M.; Damasio, C. M.; Rosa, M. C.; Campos, T. G.; Couto, D. S.; Tranches Dias, K. S.; Viegas Jr., C. Molecular hybridization as a tool in the design of multi-target directed drug candidates for neurodegenerative diseases. *Curr. Neuropharmacol.* **2020**, *18*, 348–407.

(29) Gabr, M. T.; Brogi, S. MicroRNA-based multitarget approach for Alzheimer's disease: Discovery of the first-in-class dual inhibitor of acetylcholinesterase and MicroRNA-15b biogenesis. *J. Med. Chem.* **2020**, *63*, 9695–9704.

(30) Malek, R.; Arribas, R. L.; Palomino-Antolin, A.; Totoson, P.; Demougeot, C.; Kobrlova, T.; Soukup, O.; Iriepa, I.; Moraleda, I.; Diez-Iriepa, D.; Godyń, J.; Panek, D.; Malawska, B.; Głuch-Lutwin, M.; Mordyl, B.; Siwek, A.; Chabchoub, F.; Marco-Contelles, J.; Kiec-Kononowicz, K.; Egea, J.; de los Ríos, C.; Ismaili, L. New dual small molecules for Alzheimer's disease therapy combining histamine H_3 receptor (H3R) antagonism and

calcium channels blockade with additional cholinesterase inhibition. *J. Med. Chem.* **2019**, *62*, 11416–11422.

(31) Scheiner, M.; Dolles, D.; Gunesch, S.; Hoffmann, M.; Nabissi, M.; Marinelli, O.; Naldi, M.; Bartolini, M.; Petralla, S.; Poeta, E.; Monti, B.; Falkeis, C.; Vieth, M.; Hübner, H.; Gmeiner, P.; Maitra, R.; Maurice, T.; Decker, M. Dual-acting cholinesterase–human cannabinoid receptor 2 ligands show pronounced neuroprotection in vitro and overadditive and disease-modifying neuroprotective effects in vivo. *J. Med. Chem.* **2019**, *62*, 9078–9102.

(32) Xu, A.; He, F.; Zhang, X.; Li, X.; Ran, Y.; Wei, C.; James Chou, C.; Zhang, R.; Wu, J. Tacrine-hydroxamate derivatives as multitarget-directed ligands for the treatment of Alzheimer's disease: design, synthesis, and biological evaluation. *Bioorg. Chem.* **2020**, *98*, 103721.

(33) Duarte, Y.; Fonseca, A.; Gutiérrez, M.; Adasme-Carreño, F.; Muñoz-Gutierrez, C.; Alzate-Morales, J.; Santana, L.; Uriarte, E.; Álvarez, R.; Matos, M. J. Novel coumarin-quinoline hybrids: design of multitarget compounds for Alzheimer's disease. *Chemistry Select* **2019**, *4*, 551–558.

(34) Lalut, J.; Payan, H.; Davis, A.; Lecoutey, C.; Legay, R.; Sopkova-de Oliveira Santos, J.; Claeysen, S.; Dallemagne, P.; Rochais, C. Rational design of novel benzisoxazole derivatives with acetylcholinesterase inhibitory and serotoninergic 5-HT4 receptors activities for the treatment of Alzheimer's disease. *Sci. Rep.* **2020**, *10*, 3014.

(35) Pérez-Areales, F. J.; Turcu, A. L.; Barniol-Xicota, M.; Pont, C.; Pivetta, D.; Espargaró, A.; Bartolini, M.; De Simone, A.; Andrisano, V.; Pérez, B.; Sabate, R.; Sureda, F. X.;

Vázquez, S.; Muñoz-Torrero, D. A novel class of multitarget anti-Alzheimer benzohomoadamantane–chlorotacrine hybrids modulating cholinesterases and glutamate NMDA receptors. *Eur. J. Med. Chem.* **2019**, *180*, 613–626.

(36) Estrada-Valencia, M.; Herrera-Arozamena, C.; Pérez, C.; Viña, D.; Morales-García, J. A.; Pérez-Castillo, A.; Ramos, E.; Romero, A.; Laurini, E.; Pricl, S.; Rodríguez-Franco, M. I. New flavonoid – *N*,*N*-dibenzyl(*N*-methyl)amine hybrids: Multi-target-directed agents for Alzheimer´s disease endowed with neurogenic properties. *J. Enzyme Inhib. Med. Chem.* **2019**, *34*, 712–727.

(37) Pérez-Areales, F. J.; Garrido, M.; Aso, E.; Bartolini, M.; De Simone, A.; Espargaró, A.; Ginex, T.; Sabate, R.; Pérez, B.; Andrisano, V.; Puigoriol-Illamola, D.; Pallàs, M.; Luque, F. J.; Loza, M. I.; Brea, J.; Ferrer, I.; Ciruela, F.; Messeguer, A.; Muñoz-Torrero, D. Centrally active multitarget anti-Alzheimer agents derived from the antioxidant lead CR-6. *J. Med. Chem.* **2020**, 63, 9360–9390.

(38) Patel, D. V.; Patel, N. R.; Kanhed, A. M.; Patel, S. P.; Sinha, A.; Kansara, D. D.; Mecwan, A. R.; Patel, S. B.; Upadhyay, P. N.; Patel, K. B.; Shah, D. B.; Prajapati, N. K.; Murumkar, P. R.; Patel, K. V.; Yadav, M. R. Novel multitarget directed triazinoindole derivatives as anti-Alzheimer agents. *ACS Chem. Neurosci.* **2019**, *10*, 3635–3661.

(39) Nepovimova, E.; Korabecny, J.; Dolezal, R.; Babkova, K.; Ondrejicek, A.; Jun, D.; Sepsova, V.; Horova, A.; Hrabinova, M.; Soukup, O.; Bukum, N.; Jost, P.; Muckova, L.; Kassa, J.; Malinak, D.; Andrs, M.; Kuca, K. Tacrine–trolox hybrids: A novel class of centrally active, nonhepatotoxic multi-target-directed ligands exerting anticholinesterase and antioxidant activities with low in vivo toxicity. *J. Med. Chem.* **2015**, *58*, 8985–9003.

(40) Yang, Z.; Song, Q.; Cao, Z.; Yu, G.; Liu, Z.; Tan, Z.; Deng, Y. Design, synthesis and evaluation of flurbiprofen-clioquinol hybrids as multitarget-directed ligands against Alzheimer's disease. *Bioorg. Med. Chem.* **2020**, *28*, 115374.

(41) Barraza-Garza, G.; Pérez-León, J. A.; Castillo-Michel, H.; de la Rosa, L. A.; Martinez-Martinez, A.; Cotte, M.; Alvarez-Parrilla, E. Antioxidant effect of phenolic compounds (PC) at different concentrations in IEC-6 cells: A spectroscopic analysis. *Spectrochim. Acta A Mol. Biomol. Spectrosc.* **2020**, *227*, 117570.

(42) Lu, M.; Chen, C.; Lan, Y.; Xiao, J.; Li, R.; Huang, J.; Huang, Q.; Cao, Y.; Ho, C.-T. Capsaicin–The major bioactive ingredient of chili peppers: Bio-efficacy and delivery systems. *Food Funct.* **2020**, 11, 2848–2860.

(43) Chaudhary, A.; Gour, J. K.; Rizvi, S. I. Capsaicin has potent anti-oxidative effects *in vivo* through a mechanism which is non-receptor mediated. *Arch. Physiol. Biochem.* **2019**, 1–7.

(44) Yancheva, D.; Stoyanov, S.; Anichina, K.; Nikolova, S.; Velcheva, E.; Stamboliyska, B. Combined infrared spectroscopic and computational study on simpler capsaicin derivatives and their anion intermediates in the scavenging of free radicals. *Chem. Phys.* **2020**, *535*, 110763.

(45) Dairam, A.; Fogel, R.; Daya, S.; Limson, J. L. Antioxidant and iron-binding properties of curcumin, capsaicin, and S-allylcysteine reduce oxidative stress in rat brain homogenate. *J. Agric. Food Chem.* **2008**, *56*, 3350–3356.

(46) Du, Y.; Fu, M.; Huang, Z.; Tian, X.; Li, J.; Pang, Y.; Song, W.; Tian Wang, Y.; Dong, Z. TRPV1 activation alleviates cognitive and synaptic plasticity impairments through inhibiting AMPAR endocytosis in APP23/PS45 mouse model of Alzheimer's disease. *Aging Cell* **2020**, *19*, e13113.

(47) Chen, L.; Huang, Z.; Du, Y.; Fu, M.; Han, H.; Wang, Y.; Dong, Z. Capsaicin attenuates amyloid-β-induced synapse loss and cognitive impairments in mice. *J. Alzheimers Dis.* **2017**, *59*, 683–694.

(48) Woo, M.; Kim, M.; Song, Y. Bioactive compounds in Kimchi improve the cognitive and memory functions impaired by amyloid beta. *Nutrients* **2018**, *10*, 1554.

(49) Woo, M.; Noh, J. S.; Cho, E. J.; Song, Y. O. Bioactive compounds of Kimchi inhibit apoptosis by attenuating endoplasmic reticulum stress in the brain of amyloid β-injected mice. *J. Agric. Food Chem.* **2018**, *66*, 4883–4890.

(50) Liu, C.-H.; Bu, X.-L.; Wang, J.; Zhang, T.; Xiang, Y.; Shen, L.-L.; Wang, Q.-H.; Deng, B.; Wang, X.; Zhu, C.; Yao, X.-Q.; Zhang, M.; Zhou, H.-D.; Wang, Y.-J. The associations between a capsaicin-rich diet and blood amyloid-β levels and cognitive function. *J. Alzheimers Dis.* **2016**, *52*, 1081–1088.

(51) Jiang, X.; Jia, L.-W.; Li, X.-H.; Cheng, X.-S.; Xie, J.-Z.; Ma, Z.-W.; Xu, W.-J.; Liu, Y.; Yao, Y.; Du, L.-L.; Zhou, X.-W. Capsaicin ameliorates stress-induced Alzheimer's disease-like pathological and cognitive impairments in rats. *J. Alzheimer's Dis.* **2013**, *35*, 91–105.

(52) Camps, P.; El Achab, R.; Morral, J.; Muñoz-Torrero, D.; Badia, A.; Baños, J. E.; Vivas, N. M.; Barril, X.; Orozco, M.; Luque, F. J. New tacrine−huperzine a hybrids (huprines): Highly potent tight-binding acetylcholinesterase inhibitors of interest for the treatment of Alzheimer's disease. *J. Med. Chem.* **2000**, *43*, 4657–4666.

(53) Camps, P.; Cusack, B.; Mallender, W. D.; El Achab, R.; Morral, D.; Muñoz-Torrero, D.; Rosenberry, T. L. Huprine X is a novel high-affinity inhibitor of acetylcholinesterase that is of interest for treatment of Alzheimer's disease. *Mol. Pharmacol.* **2000**, *57*, 409–417.

(54) Alcalá, M. del M.; Vivas, N. M.; Hospital, S.; Camps, P.; Muñoz-Torrero, D.; Badia, A. Characterisation of the anticholinesterase activity of two new tacrine–huperzine A hybrids. *Neuropharmacol.* **2003**, *44*, 749–755.

(55) Muñoz-Torrero, D.; Camps, P. Huprines for Alzheimer's disease drug development. *Expert Opin. Drug Discov.* **2008**, *3*, 65–81.

(56) Viayna, E.; Sola, I.; Bartolini, M.; De Simone, A.; Tapia-Rojas, C.; Serrano, F. G.; Sabaté, R.; Juárez-Jiménez, J.; Pérez, B.; Luque, F. J.; Andrisano, V.; Clos, M. V.; Inestrosa, N. C.; Muñoz-Torrero, D. Synthesis and multitarget biological profiling of a novel family of rhein derivatives as disease-modifying anti-Alzheimer agents. *J. Med. Chem.* **2014**, *57*, 2549–2567.

(57) Galdeano, C.; Viayna, E.; Sola, I.; Formosa, X.; Camps, P.; Badia, A.; Clos, M. V.; Relat, J.; Ratia, M.; Bartolini, M.; Mancini, F.; Andrisano, V.; Salmona, M.; Minguillón, C.; González-Muñoz, G. C.; Rodríguez-Franco, M. I.; Bidon-Chanal, A.; Luque, F. J.; Muñoz-Torrero, D. Huprine–tacrine heterodimers as anti-amyloidogenic compounds of

potential interest against Alzheimer's and prion diseases. *J. Med. Chem.* **2012**, *55*, 661–669.

(58) Viayna, E.; Gómez, T.; Galdeano, C.; Ramírez, L.; Ratia, M.; Badia, A.; Clos, M. V.; Verdaguer, E.; Junyent, F.; Camins, A.; Pallàs, M.; Bartolini, M.; Mancini, F.; Andrisano, V.; Arce, M. P.; Rodríguez-Franco, M. I.; Bidon-Chanal, A.; Luque, F. J.; Camps, P.; Muñoz-Torrero, D. Novel huprine derivatives with inhibitory activity toward β-amyloid aggregation and formation as disease-modifying anti-Alzheimer drug candidates. *ChemMedChem* **2010***, 5*, 1855–1870.

(59) Ronco, C.; Foucault, R.; Gillon, E.; Bohn, P.; Nachon, F.; Jean, L.; Renard, P.-Y. New huprine derivatives functionalized at position 9 as highly potent acetylcholinesterase inhibitors. *ChemMedChem* **2011**, *6*, 876–888.

(60) Ronco, C.; Carletti, E.; Colletier, J.-P.; Weik, M.; Nachon, F.; Jean, L.; Renard, P.-Y. Huprine derivatives as sub-nanomolar human acetylcholinesterase inhibitors: From rational design to validation by X-ray crystallography. *ChemMedChem* **2012**, *7*, 400–405.

(61) Carr, J. L.; Wease, K. N.; Van Ryssen, M. P.; Paterson, S.; Agate, B.; Gallagher, K. A.; Brown, C. T. A.; Roderick, H. S.; Conway, S. J. In vitro photo-release of a TRPV1 agonist. *Bioorg. Med. Chem. Lett.* **2006**, *16*, 208–212.

(62) Pérez-Areales, F. J.; Di Pietro, O.; Espargaró, A.; Vallverdú-Queralt, A.; Galdeano, C.; Ragusa, I. M.; Viayna, E.; Guillou, C.; Clos, M. V.; Pérez, B.; Sabaté, R.; Lamuela-Raventós, R. M.; Luque, F. J.; Muñoz-Torrero, D. Shogaol–huprine hybrids: dual antioxidant and anticholinesterase agents with β-amyloid and tau anti-aggregating properties. *Bioorg. Med. Chem.* **2014**, *22*, 5298–5307.

(63) Hong, S. H.; Sanders, D. P.; Lee, C. W.; Grubbs, R. H. Prevention of undesirable isomerization during olefin metathesis. *J. Am. Chem. Soc.* **2005**, *127*, 17160–17161.

(64) Oukoloff, K.; Chao, S.; Cieslikiewicz-Bouet, M.; Mougeot, R.; Jean, L.; Renard, P.-Y. Improved access to huprine derivatives functionalized at position 9. *Eur. J. Org. Chem.* **2016,** 2016, 1337–1343.

(65) Cole, A. G.; Metzger, A.; Brescia, M.-R.; Qin, L.-Y.; Appell, K. C.; Brain, C. T.; Hallet, A.; Ganju, P.; Denholm, A. A.; Wareing, J. R.; Ritchie, T. J.; Drake, G. M.; Bevan, S. J.; MacGloinn, A.; McBryde, A.; Patel, V.; Oakley, P. J.; Nunez, X.; Gstach, H.; Schneider, P.; Baldwin, J. J.; Dolle, R. E.; McDonald, E.; Henderson, I. Sulfonamido-aryl ethers as bradykinin B1 receptor antagonists. *Bioorg. Med. Chem. Lett.* **2009**, *19*, 119–122.

(66) Ellman, G. L.; Courtney, K. D.; Andres, V., Jr.; Featherstone, R. M. A new and rapid colorimetric determination of acetylcholinesterase activity. *Biochem. Pharmacol.* **1961**, *7*, 88–95.

(67) Khorana, N.; Markmee, S.; Ingkaninan, K.; Ruchirawat, S.; Kitbunnadaj, R.; Pullagurla, M. R. Evaluation of a new lead for acetylcholinesterase inhibition. *Med. Chem. Res.* **2009**, *18*, 231–241.

(68) Cornish-Bowden, A. A simple graphical method for determining the inhibition constants of mixed, uncompetitive and non-competitive inhibitors. *Biochem. J.* **1974**, *137*, 143−144.

(69) Taylor, P.; Lappi, S. Interactions of fluorescent probes with acetylcholinesterase. The site and specificity of propidium binding. *Biochemistry* **1975**, *14*, 1989–1997.

(70) Taylor, P.; Lwebuga-Mukasa, J.; Lappi, S.; Rademacher J. Propidium – A fluorescent probe for a peripheral anionic site on acetylcholinesterase. *Mol. Pharmacol.* **1974**, *10*, 703–708.

(71) Dvir, H.; Wong, D. M.; Harel, M.; Barril, X.; Orozco, M.; Luque, F. J.; Muñoz-Torrero, D.; Camps, P.; Rosenberry, T. L.; Silman, I.; Sussman, J. L. 3D Structure of *Torpedo californica* acetylcholinesterase complexed with huprine X at 2.1 Å resolution: Kinetic and molecular dynamics correlates. *Biochemistry* **2002**, *41*, 2970–2981.

(72) Savini, L.; Gaeta, A.; Fattorusso, C.; Catalanotti, B.; Campiani, G.; Chiasserini, L.; Pellerano, C.; Novellino, E.; McKissic, D.; Saxena, A. Specific targeting of acetylcholinesterase and butyrylcholinesterase recognition sites. Rational design of novel, selective, and highly potent cholinesterase inhibitors. *J. Med. Chem.* **2003**, *46*, 1–4.

(73) Elsinghorst, P. W.; Cieslik, J. S.; Mohr, K.; Tränkle, C.; Gütschow, M. First gallamine–tacrine hybrid: Design and characterization at cholinesterases and the M_2 muscarinic receptor. *J. Med. Chem.* **2007**, *50*, 5685–5695.

(74) Rosenberry, T.; Brazzolotto, X.; Macdonald, I.; Wandhammer, M.; Trovaslet-Leroy, M.; Darvesh, S.; Nachon, F. Comparison of the binding of reversible inhibitors to human butyrylcholinesterase and acetylcholinesterase: A crystallographic, kinetic and calorimetric study. *Molecules* **2017**, *22*, 2098.

(75) Di Pietro, O.; Juárez-Jiménez, J.; Muñoz-Torrero, D.; Laughton, C. A.; Luque, F. J. Unveiling a novel transient druggable pocket in BACE-1 through molecular simulations:

conformational analysis and binding mode of multisite inhibitors. *PLoS ONE* **2017**, *12*, e0177683.

(76) Huang, D.; Ou, B.; Prior, R. L. The chemistry behind antioxidant capacity assays. *J. Agric. Food Chem.* **2005**, *53*, 1841–1856.

(77) Di, L.; Kerns, E. H.; Fan, K.; McConnell, O. J.; Carter, G. T. High throughput artificial membrane permeability assay for blood–brain barrier. *Eur. J. Med. Chem.* **2003**, *38*, 223–232.

(78) Chen, G.; Chen, K. S.; Knox, J.; Inglis, J.; Bernard, A.; Martin, S. J.; Justice, A.; McConlogue, L.; Games, D.; Freedman, S. B.; Morris, R. G. M. A learning deficit related to age and β-amyloid plaques in a mouse model of Alzheimer's disease. *Nature* **2000**, *408*, 975–979.

(79) Selkoe, D. J. Alzheimer's disease is a synaptic failure. *Science* **2002**, *298*, 789–791.

(80) Tanzi, R. E. The synaptic Aβ hypothesis of Alzheimer disease. *Nat. Neurosci.* **2005**, *8* (8), 977–979.

(81) Mango, D.; Saidi, A.; Cisale, G. Y.; Feligioni, M.; Corbo, M.; Nisticò, R. Targeting synaptic plasticity in experimental models of Alzheimer's disease. *Front. Pharmacol.* **2019**, *10*, 778.

(82) Trinchese, F.; Liu, S.; Battaglia, F.; Walter, S.; Mathews, P. M.; Arancio, O. Progressive age-related development of Alzheimer-like pathology in APP/PS1 mice. *Ann. Neurol.* **2004**, *55*, 801–814.

(83) Cisternas, P.; Oliva, C. A.; Torres, V. I.; Barrera, D. P.; Inestrosa, N. C. Presymptomatic treatment with andrographolide improves brain metabolic markers and cognitive behavior in a model of early-onset Alzheimer's disease. *Front. Cell. Neurosci.* **2019**, *13*, 295.

(84) Zhang, J.-H.; Yu, L.-J.; Yang, H.; Hui, Z.; Jiang, S.; Chen, L.; Zhao, Y.; Wang, S.-L.; Liu, Y.; Xu, Y. Huatuo Zaizao pill ameliorates cognitive impairment of APP/PS1 transgenic mice by improving synaptic plasticity and reducing Aβ deposition. *BMC Complement Altern. Med.* **2018**, *18*, 167.

(85) Serrano, F. G.; Tapia-Rojas, C.; Carvajal, F. J.; Hancke, J.; Cerpa, W.; Inestrosa, N. C. Andrographolide reduces cognitive impairment in young and mature AβPPswe/PS-1 mice. *Mol. Neurodegener.* **2014**, *9*, 61.

(86) Perluigi, M.; Coccia, R.; Butterfield, D. A. 4-Hydroxy-2-nonenal, a reactive product of lipid peroxidation, and neurodegenerative diseases: A toxic combination illuminated by redox proteomics studies. *Antioxid. Redox Signal.* **2012**, *17*, 1590–1609.

(87) Kamphuis, W.; Middeldorp, J.; Kooijman, L.; Sluijs, J. A.; Kooi, E.-J.; Moeton, M.; Freriks, M.; Mizee, M. R.; Hol, E. M. Glial fibrillary acidic protein isoform expression in plaque related astrogliosis in Alzheimer's disease. *Neurobiol. Aging* **2014**, *35*, 492–510.

(88) Nordberg, A.; Ballard, C.; Bullock, R.; Darreh-Shori, T.; Somogyi, M. A review of butyrylcholinesterase as a therapeutic target in the treatment of Alzheimer's disease. *Prime Care Companion CNS Disord.* **2013**, *15*, PCC.12r01412.

(89) Silverman R. B. The Organic Chemistry of Enzyme-Catalyzed Reactions. Academic Press, San Diego, 2002.

(90) Nunes-Tavares, N.; Nery da Matta, A.; Batista e Silva, C. M.; Araújo, G. M.; Louro S. R., Hassón-Voloch, A. Inhibition of acetylcholinesterase from Electrophorus electricus (L.) by tricyclic antidepressants. *Int. J. Biochem. Cell Biol.* **2002**, *34*, 1071–1079.

(91) Brand-Williams, W.; Cuvelier, M. E.; Berset, C. Use of a free radical method to evaluate antioxidant activity. *LWT-Food Sci. Technol.* **1995**, *28*, 25–30.

(92) Garrido, J.; Gaspar, A.; Garrido, E. M.; Miri, R.; Tavakkoli, M.; Pourali, S.; Saso, L.; Borges, F.; Firuzi, O. Alkyl esters of acids with improved antioxidant activity and lipophilicity protect PC12 cells against oxidative stress. *Biochimie* **2012**, *94*, 961–967.

(93) Sussman, J. L.; Harel, M.; Frolow, F.; Varon, L.; Toker, L.; Futerman, A. H.; Silman, I. Purification and crystallization of a dimeric form of acetylcholinesterase from *Torpedo californica* subsequent to solubilization with phosphatidylinositol-specific phospholipase C. *J. Mol. Biol.* **1988**, *203*, 821–823.

(94) Brazzolotto, X.; Wandhammer, M.; Ronco, C.; Trovaslet, M.; Jean, L.; Lockridge, O.; Renard, P.-Y.; Nachon, F. Human butyrylcholinesterase produced in insect cells: huprine-based affinity purification and crystal structure. *FEBS J.* **2012**, *279*, 2905–2916.

(95) Xie, Z.; Liao, Q.; Xu, X.; Yao, M.; Wan, J.; Liu, D. Rapid and sensitive determination of donepezil in human plasma by liquid chromatography/tandem mass spectrometry: Application to a pharmacokinetic study. *Rapid Commun. Mass Spectrom.* **2006**, *20*, 3193–3198.

(96) Walsh, R. N.; Cummins, R. A. The open-field test: A critical review. *Psychol. Bull.* **1976**, *83*, 482–504.

(97) Cisternas, P.; Lindsay, C. B.; Salazar, P.; Silva-Alvarez, C.; Retamales, R. M.; Serrano, F. G.; Vio, C. P.; Inestrosa, N. C. The increased potassium intake improves cognitive performance and attenuates histopathological markers in a model of Alzheimer's disease. *Biochim. Biophys. Acta* **2015**, *1852*, 2630–2644.

(98) Bevins, R. A.; Besheer, J. Object recognition in rats and mice: A one-trial non-matching-to-sample learning task to study "recognition memory." *Nat. Protoc.* **2006**, *1*, 1306–1311.

(99) Vargas, J. Y.; Fuenzalida, M.; Inestrosa, N. C. In vivo activation of Wnt signaling pathway enhances cognitive function of adult mice and reverses cognitive deficits in an Alzheimer's disease model. *J. Neurosci.* **2014**, *34*, 2191–2202.

(100) Salazar, P.; Cisternas, P.; Codocedo, J. F.; Inestrosa, N. C. Induction of hypothyroidism during early postnatal stages triggers a decrease in cognitive performance by decreasing hippocampal synaptic plasticity. *Biochim. Biophys. Acta Mol. Basis Dis.* **2017**, *1863*, 870–883.

(101) Rivera, D. S.; Lindsay, C.; Codocedo, J. F.; Morel, I.; Pinto, C.; Cisternas, P.; Bozinovic, F.; Inestrosa, N. C. Andrographolide recovers cognitive impairment in a natural model of Alzheimer's disease (*Octodon degus*). *Neurobiol. Aging* **2016**, *46*, 204–220.

Table of Content (TOC) Graphic